1-29-2009

Modeling Arctic sea ice using the material-point method and an elastic-decohesive rheology

Kara Peterson

Follow this and additional works at: https://digitalrepository.unm.edu/math_etds

Kara Peterson

Candidate

Mathematics and Statistics

Department

This dissertation is approved, and it is acceptable in quality
and form for publication on microfilm:

Approved by the dissertation Committee:

Deborah Sulsky   , Chairperson

Howard Schreyer

Pedro Embid

Santiago Simanca

Accepted:

Dean, Graduate School

Date

Modeling Arctic Sea Ice Using the Material-Point Method and an Elastic-Decohesive Rheology

by

Kara Peterson

M.S., University of Colorado, 1994
B.S., New Mexico State University, 1991

DISSERTATION

Submitted in Partial Fulfillment of the
Requirements for the Degree of

Doctor of Philosophy
Mathematics

The University of New Mexico

Albuquerque, New Mexico

December, 2008

Dedication

For Dion, Sophie, and Theo

Acknowledgments

Modeling Arctic Sea Ice Using the Material-Point Method and an Elastic-Decohesive Rheology

by

Kara Peterson

ABSTRACT OF DISSERTATION

Submitted in Partial Fulfillment of the
Requirements for the Degree of

Doctor of Philosophy
Mathematics

The University of New Mexico

Albuquerque, New Mexico

December, 2008

Modeling Arctic Sea Ice Using the Material-Point Method and an Elastic-Decohesive Rheology

by

Kara Peterson

M.S., University of Colorado, 1994

B.S., New Mexico State University, 1991

PhD., Mathematics, University of New Mexico, 2008

Abstract

Sea ice has an important effect on global climate by reducing the heat transfer between the atmosphere and ocean and by reflecting incoming solar radiation. Additionally, sea ice can be an important navigational concern. For both of these reasons accurate and efficient models for sea ice are required. Current models have a number of limitations. In particular, the constitutive models used generally treat ice as isotropic when in fact the main observational features of ice are anisotropic leads and ridges. Also, the equations are typically solved using Eulerian methods that generate numerical errors when solving the transport equations for sea ice parameters related to ice thickness. To address these limitations the approach advocated here is to use an elastic-decohesive constitutive model for the ice and solve with the material-point method (MPM). MPM is a numerical method that uses two descriptions of the continuum to combine the best features of Lagrangian and Eulerian methods.

Unconnected Lagrangian material points carry mass, velocity, stress, and other internal variables throughout the calculation. The material points model advection naturally, allow the determination of a sharp ice boundary, and can handle large deformations. The momentum equation is solved on a background grid to keep the computational work linear in the number of material points. The elastic-decohesive constitutive model is an anisotropic model that allows for explicit representation of leads in the sea ice. This is combined with an energy conserving thermodynamic model and an ice thickness distribution for a complete sea ice model. Calculations of ice deformation for a region in the Beaufort Sea are used to illustrate the model.

Contents

Contents

Contents

List of Figures

xiii

List of Tables

Chapter 1

Introduction

Although sea ice covers only a small area of the world's oceans it plays an important role in the global climate. In particular, ice reduces the heat transfer between the ocean and atmosphere and causes a large amount of incoming solar energy to be reflected back to space [41]. Additionally, sea ice influences ocean circulation by increasing the salinity of the nearby water when ice freezes and decreasing the salinity when ice melts. [26]. With concerns growing about global warming there is renewed interest in having an accurate model of sea ice so that the effect of these coupling mechanisms can be better understood. On a more local scale, warming of the Arctic has important implications for shipping and transportation and ice models that accurately forcast ice boundary locations are needed [10].

Sea ice is composed of a series of floes or large sections of intact ice separated by water or thin ice. The floe diameters can range from tens of meters to several kilometers in the interior of the Arctic [15]. The floes are driven by surface winds, ocean currents and Coriolis forces. The interacting floes can separate forming leads which uncover open water, or converge to close leads and form pressure ridges. The ice grows and melts seasonally in response to incoming solar radiation and thermal radiation from the atmosphere. These processes result in an average thickness of ice in the Arctic between 2 and 4 meters, where the distribution includes new ice only centimeters thick up to mechanically deformed or ridged ice up to tens of meters thick [30]. A complete model of sea ice must include the dynamics of the interacting floes and the thermodynamic processes of freezing and melting.

The standard models used today for sea ice were largely developed during the 1970's. Improvements have been made since then to make them more computationally efficient and to include more detailed physics, but there are still limitations in the current models. For example, the constitutive models in particular were developed to represent sea ice on scales of 100 kilometers, for which it was natural to assume that ice is isotropic since the leads and ridges in the ice are fairly random over 100

kilometers [9]. However, since the models have been developed the resolution in the calculations has become finer. On scales of the order of 5 kilometers the assumption of isotropy is probably not justified. Another disadvantage in the current methods is in the numerical framework used to solve the equations. A large portion of the sea ice modeling done today uses finite difference methods formulated in an Eulerian frame to solve the mechanical and thermodynamical equations. The formulation of the sea ice problem contains multiple transport equations that must be solved for quantities such as ice fractional area, which can lead to numerical diffusion due to the discretization of the nonlinear convective term and which in turn can limit the accuracy.

To overcome these disadvantages this work will use an elastic-decohesive constitutive model, which explicitly predicts the formation and evolution of leads. This model is inherently anisotropic and may more accurately describe the behavior of the sea ice. This constitutive model and the other dynamic and thermodynamic equations are solved in the framework of the Material Point Method (MPM), a particle-in-cell method. This method uses both a Lagrangian set of material points and a background grid where the momentum equation is solved. Because the equations are solved in a Lagrangian framework in MPM, the nonlinear convective term does not appear and the numerical dissipation or dispersion seen with Eulerian methods is avoided, which makes it a natural method to use for transport problems.

The next chapter describes the history of ice modeling and provides an overview of the primary ice models currently in use. Chapter 3 contains a derivation of the governing equations for sea ice in a finite strain setting that will be used in the new MPM elastic-decohesive model and Chapter 4 describes their numerical implementation. In Chapter 5 the satellite data used in the modeling effort are discussed and a kinematic representation of cracks is derived. Chapter 6 illustrates the model with some numerical examples and Chapter 7 summarizes the results and describes future

work.

Chapter 2

Previous Modeling

2.1   History

At the end of the 19th century the Arctic was largely unexplored and debate still raged over whether the central Arctic contained open sea, numerous islands surrounded by shallow water, or a large land mass connected to Greenland [49]. The drift of the wreckage of a ship that sailed through the Bering Straight, the *Jeanette*, suggested to some observers that the Arctic must contain mostly open water and that ocean currents determined the path of the drift. Based on this evidence, Fridtjof Nansen (Figure 2.1a), a Norwegian explorer and scientist, advocated building a ship strong enough to withstand the crushing pressure of the Arctic ice. This ship could then be frozen into the ice and allowed to drift to the North Pole. The *Fram* or forward in Norwegian, was the ship Nansen commissioned for this purpose. The *Fram* carried Nansen and his expedition team across the Arctic from 1893 to 1896 and is shown in Figure 2.1b embedded in the ice during the expedition. The ship did not quite reach the Pole, but did drift as far as 84° 4' N latitude and Nansen and his team made it as far as 86° 6' N latitude on skis. This was the closest to the Pole anyone had reached at that time. A popular account of this voyage can be found in Nansen's book *Farthest North* [1]. More importantly, the scientific results recorded on the journey were published in six volumes as the Norwegian North Polar Expedition Scientific Results [32].

During this expedition, the ocean currents and winds were meticulously documented. The data showed that the *Fram* drifted between 20 and 45 degrees to the right of the wind direction. Nansen believed this was due to the effects of the rotation of the Earth. The data on this drift were provided to a Swedish graduate student, Vagn Walfrid Ekman, who proposed a mathematical basis for the observation. In his theoretical model, the discrepancy between the drift direction and the wind direction can be explained in terms of the effects of frictional forces in the ocean and Coriolis forces. This model predicts a fixed angle between the water drag vector and the ice
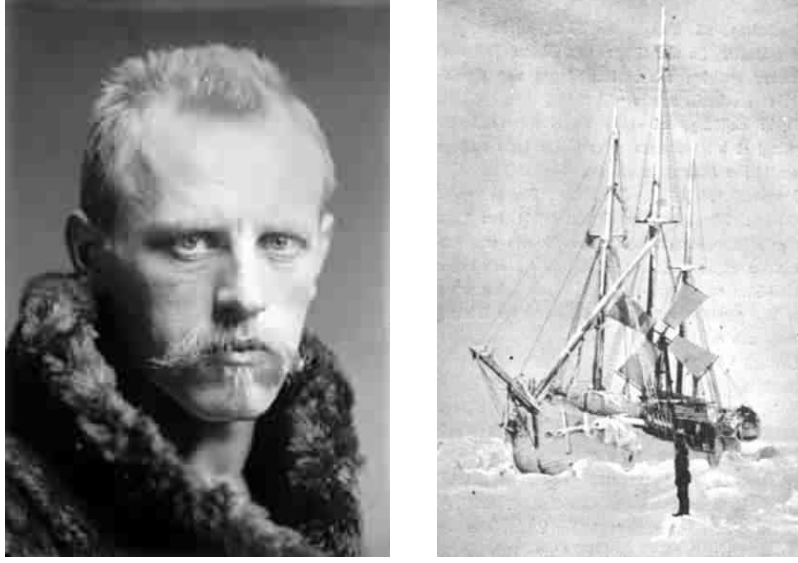
Figure 2.1: Fridtjof Nansen (Bain Collection Library of Congress LC-B2-705-3) and the Fram in Ice March 1894 [1]

velocity at the water-ice interface of 45 degrees [49]. The angle of the water drag vector is predicted to change with depth, a phenomenon known as the Ekman spiral because of the path the vector takes with increasing depth. This model is applicable to general ocean flows and was a major contribution to oceanography.

Based on the data from Nansen's *Fram* expedition, the first so-called free-drift models of sea ice were developed. This model can be written as

$$\mathbf{t}_a + \mathbf{t}_w + \mathbf{f}_c = 0 \tag{2.1}$$

where $\mathbf{t}_a$ is the force due to the atmospheric winds, $\mathbf{t}_w$ is the drag due to the ocean currents, and the Coriolis force, $\mathbf{f}_c$, has the following form

$$\mathbf{f}_c = 2(\rho h)\omega \sin\phi(\mathbf{e_3} \times \mathbf{v}) \tag{2.2}$$

where ω is the magnitude of the Earth's rotation, ϕ is the latitude, $\mathbf{e}_3$ is unit vector in the vertical direction, and $\mathbf{v}$ is the ice velocity. The atmospheric and ocean drag

terms, $\mathbf{t}_a$ and $\mathbf{t}_w$, are prescribed as a function of $\mathbf{v}$ and with the Coriolis term Equation (2.1) can be solved for the ice drift velocity, $\mathbf{v}$. Here the Earth is assumed spherical and in a local coordinate system fixed with respect to the Earth, the vertical direction is the radial direction and the horizontal directions are in a local tangent plane to the surface. Note that a steady-state flow is assumed in this balance by neglecting the ice acceleration or inertial term and the ice internal forces are neglected as well.

The assumption that the Ekman layer begins at the ice water interface results in an ice velocity direction that is farther away from the wind direction in terms of angle than is observed in the *Fram* expedition data. Therefore, much of the early work on sea ice dynamics focused on the forms of $\mathbf{t}_a$ and $\mathbf{t}_w$. In particular, work was done in including the effects of a boundary layer between the ice and the Ekman layer [8].

Because of lingering discrepancies between the purely free drift model predictions and data, internal force terms, $\mathbf{F}^{int}$ were added to the balance equation as

$$\mathbf{t}_a + \mathbf{t}_w + \mathbf{f}_c + \mathbf{F}^{int} = 0 \tag{2.3}$$

Sverdrup in 1928 included a simple internal force term proportional to the ice velocity and in the opposite direction [8]. Later authors, such as Campbell in 1965 [8], felt that the ice would be better modeled as a highly viscous fluid and so used an internal force proportional to $\Delta \mathbf{v}$ where Δ is the two-dimensional in-plane Laplacian operator.

During this same time, research was moving forward in the area of sea ice thermo-dynamics. The thermodynamic work focused on trying to relate the growth rate of ice to the fluxes from the atmosphere and ocean. For example, in 1961 Untersteiner [52] described the heat budget of the Arctic and in 1971 Maykut and Untersteiner [30] developed a one-dimensional thermodynamic model of an ice column that solved the heat equation in the ice interior with a balance of fluxes at the atmosphere and

ocean surfaces to determine the change in ice thickness.

In 1970 a large effort known as the Arctic Ice Dynamics Joint Experiment (AID-JEX) began. Between 1970 and 1978 the members of the AIDJEX program worked to develop a complete model of ice dynamics and thermodynamics on spatial scales of 100 km and temporal scales of one day [9]. Under this effort, the full dynamic momentum equation was solved including the intertial term and internal force term as

$$\mathbf{t}_a + \mathbf{t}_w + \mathbf{f}_c + \mathbf{F}^{int} = \rho h \dot{\mathbf{v}}. \tag{2.4}$$

Here the superimposed dot indicates a material derivative, $\partial/\partial t + \mathbf{v} \cdot \nabla$.

One of the main priorities of the AIDJEX effort was measuring deformation in the ice pack and using these deformations to develop a realistic function for the ice internal forces [53]. To this end, an elastic-plastic constitutive law for the ice was derived. Additionally, under AIDJEX, a method for coupling the one-dimensional thermodynamical heat equation to the balance of momentum equation was proposed. The coupling was done with an ice thickness distribution model developed by Thorndike and Maykut [50]. The ice thickness distribution includes the assumption that ice over an area on the order of the spatial resolution of 100 km is of variable thickness. The distribution of ice thickness then changes with time due to thermodynamic melt or growth of ice and due to the mechanical deformation of ice. This framework introduced under AIDJEX, illustrated in Figure 2.2, is still the sea ice modeling framework used today.

In 1979 after the completion of the AIDJEX program, an alternative constitutive law due to Hibler was published that treats the ice as a viscous-plastic material [17]. Hibler's model also included a simplified two-category ice thickness distribution. The majority of current sea ice dynamic and thermodynamic models use the AIDJEX framework with the viscous-plastic constitutive model due to Hibler. In the following
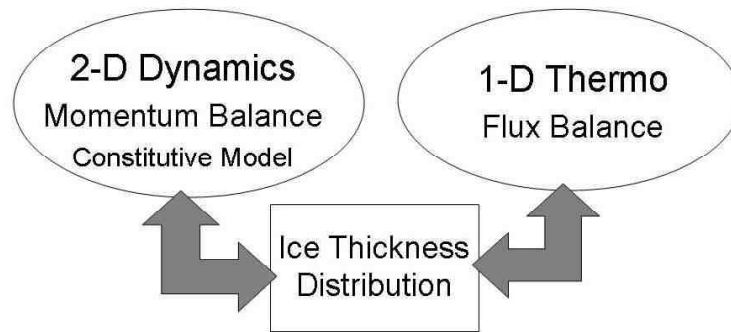
Figure 2.2: Sea Ice Model Framework

sections, details of the components of the standard model are discussed.

2.2 Sea Ice Governing Equations: Dynamics

As shown in Figure 2.2, the sea ice dynamic model consists of the balance of momentum equation, from which the ice velocity or displacement can be determined, and a constitutive model that relates the velocity gradient or displacement gradient to the internal stress. Although the AIDJEX program proposed an elastic-plastic constitutive model, the majority of sea ice models use the viscous-plastic formulation due to Hibler [17]. Therefore, a description of the viscous-plastic model is given here. The following two sections describe the dynamics in more detail. Note that mass conservation comes into the sea ice model through an assumption of incompressibility, which results in a volume conservation restriction on the dynamic part of the ice thickness distribution. The coordinate system used for the sea ice model is assumed to be fixed with respect to the Earth and for most cases is assumed to be Cartesian.
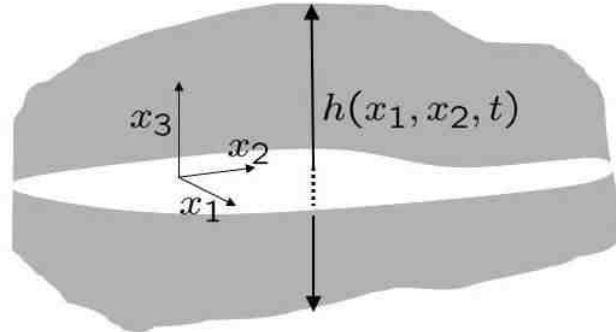
Figure 2.3: Ice Column

2.2.1   Momentum Equation for Sea Ice

The main mechanical equation governing the behavior of sea ice is the balance of linear momentum equation, which is a statement of Newton's Third Law: the forces acting on a body are equal to its mass times its acceleration. Because sea ice has a small thickness to area ratio, the momentum equation is solved in two dimensions in the plane of the ice with an evolving thickness parameter that tracks deformations in the third dimension. The horizontal coordinates (x_1, x_2) are assumed to be in the plane of the ice and the vertical coordinate x_3 is out of the plane as shown in Figure 2.3. Gray and Morland showed that this equation can be derived by integrating the full three-dimensional momentum equation through the ice thickness and applying suitable assumptions [15]. The two-dimensional depth integrated momentum equation can be written as

$$(\rho h)\dot{\mathbf{v}} = \mathbf{F}^{int} + \mathbf{F}^{ext} \tag{2.5}$$

where ρ is the ice density, which can depend on position and time, but is taken to be constant in the standard model, $h(x_1, x_2, t)$ is the ice thickness, $\mathbf{v}(x_1, x_2, t)$ is

the two-dimensional ice velocity, and the superimposed dot represents the material derivative. The internal forces acting on the ice are due to the divergence of the depth-integrated stress tensor, $\mathbf{N}(x_1, x_2, t)$ and can be written as $\mathbf{F}^{int} = \nabla \cdot \mathbf{N}$. The external forces acting on the ice are the air drag, $\mathbf{t}_a$, the water drag, $\mathbf{t}_w$, and the Coriolis force, $\mathbf{f}_c$. The air and water drag terms are generally formulated in a quadratic form as

$$\mathbf{t}_a = c_a \rho_a \|\mathbf{v}_a\| Q_a \mathbf{v}_a$$
$$\mathbf{t}_w = c_w \rho_w \|(\mathbf{v} - \mathbf{v}_w)\| Q_w (\mathbf{v} - \mathbf{v}_w)$$

$$(2.6)$$

where c_a is the air drag coefficient, ρ_a is the air density, $\mathbf{v}_a$ is the air velocity, Q_a is the rotation matrix for the air turning angle, c_w is the water drag coefficient, ρ_w is the water density, $\mathbf{v}_w$ is the water velocity, Q_w is the rotation matrix for water turning angle, and $\|\cdot\|$ is the Euclidean norm. The rotation matrices are included to account for the effects of the Ekman spiral given that the wind velocity and ocean velocity used in the balance are generally measured away from the ice surface. An additonal external force often included in ice modeling is due to gradients in the sea surface height and is written as $\rho h \mathbf{g} \nabla H$, where $\mathbf{g}$ is the acceleration due to gravity and H is the sea surface dynamic height. This term is smaller than the others in magnitude [15].

After putting all these pieces together the momentum equation for sea ice can be written as [17]

$$(\rho h)\dot{\mathbf{v}} = c_a \rho_a \|\mathbf{v}_a\| Q_a \mathbf{v}_a + c_w \rho_w \|(\mathbf{v} - \mathbf{v}_w)\| Q_w (\mathbf{v} - \mathbf{v}_w)$$
$$- 2(\rho h)\omega \sin\phi(\mathbf{e_3} \times \mathbf{v}) - \rho h g \nabla H + \nabla \cdot \mathbf{N}.$$

$$(2.7)$$

The unknowns in this equation are the ice thickness, the ice velocity, and the depth integrated stress. Therefore, to close this equation a thermodynamic model for $h(x_1, x_2, t)$ is needed as well as a constitutive model to relate changes in $\mathbf{N}$ to changes in $\mathbf{v}$. A description of the constitutive model follows.

2.2.2   Viscous-Plastic Constitutive Model

In the viscous-plastic model due to Hibler [17],[16], ice behavior is based on a rigid plastic model. The plastic behavior is defined by a yield curve in depth integrated stress space and associated flow rules for the strain rate. The original viscous-plastic model uses an elliptical yield curve in principal depth integrated stress space of the form

$$F(N_1, N_2) = \left(\frac{N_1 + N_2 + P}{P}\right)^2 + \left(\frac{N_2 - N_1}{P}e\right)^2 - 1 \tag{2.8}$$

where N_1 and N_2 are the principal components of the depth integrated stress, e is the eccentricity of the elliptical yield curve and P is a measure of ice strength. The ice is constrained in stress space to lie on the curve where $F = 0$, which defines the plastic regime. In Hibler's original formulation, P, is taken to be

$$P = P^* h e^{-C(1-A)} \tag{2.9}$$

where $h = \hat{h}A$ is the average thickness over an area, A is the compactness or fractional area covered by ice, $\hat{h}$ is the thickness of the ice in the area, and C and P^* are constants. Equations for h and A are needed to close the system and are discussed below in the section on ice thickness modeling. When using the full ice thickness distribution P is related to the ridging function, which is also defined in the ice thickness distribution section. Note that the thickness h in this equation is the same as the average thickness used in the momentum equation. A plot of the original viscous-plastic yield curve is shown in Figure 2.4 and labeled plastic.

The two-dimensional strain rate tensor, $\dot{\varepsilon}(x_1, x_2, t)$ is defined as the symmetric part of the velocity gradient, which is equal to $1/2(\nabla\mathbf{v} + \nabla\mathbf{v}^T)$. The viscous-plastic constitutive law can be derived from the yield curve assuming a normal flow rule for strain rate as shown here in terms of the principal components of depth integrated
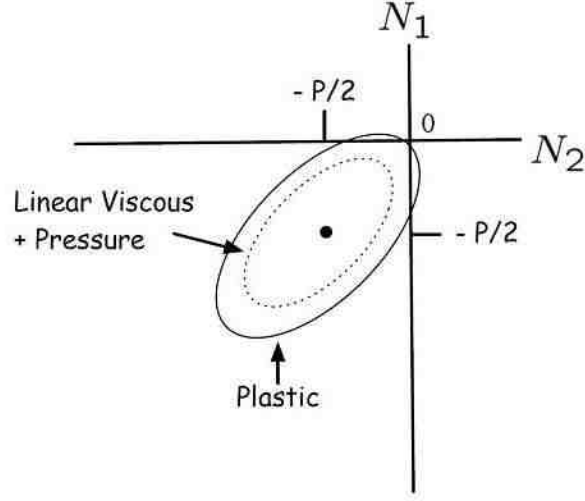
Figure 2.4: Yield curve in principal depth-integrated stress space for viscous-plastic model.

stress

$$\dot{\varepsilon}_1 = \gamma \frac{\partial F}{\partial N_1} = \frac{\gamma}{P^2} \left(2\left(N_1 + N_2 + P\right) - 2(N_2 - N_1)e^2 \right)$$
$$\dot{\varepsilon}_2 = \gamma \frac{\partial F}{\partial N_2} = \frac{\gamma}{P^2} \left(2\left(N_1 + N_2 + P\right) + 2(N_2 - N_1)e^2 \right)$$

(2.10)

where γ is the plastic evolution parameter, which satisfies $\gamma F = 0$. That is, the yield function is equal to zero when plastic deformation is occuring and $\gamma > 0$, and in the viscous regime when $F < 0$, γ is equal to 0. Using this property and solving for γ from the above flow rules results in

$$\gamma = \frac{P}{4}\Delta = \frac{P}{4} \left(\left(\dot{\varepsilon}_1^2 + \dot{\varepsilon}_2^2\right)\left(1 - \frac{1}{e^2}\right) + 2\dot{\varepsilon}_1\dot{\varepsilon}_2 \left(1 - \frac{1}{e^2}\right) \right)^{1/2}.$$

(2.11)

By solving for the depth integrated stresses as a function of strain rate, the constitutive law can be written as

$$\mathbf{N} = 2\eta\dot{\boldsymbol{\varepsilon}} + (\zeta - \eta)\text{tr}(\dot{\boldsymbol{\varepsilon}})\mathbf{I} + \frac{P\mathbf{I}}{2}$$

(2.12)

where ζ is the bulk modulus, η is the shear modulus, and $\mathbf{I}$ is the two-dimensional identity tensor. Both ζ and η are functions of the strain rate, $\dot{\varepsilon}$, and can be written as

$$\zeta = \frac{P}{2\Delta} \qquad \eta = \frac{\zeta}{e^2} = \frac{P}{2\Delta e^2}. \tag{2.13}$$

In terms of general components of the strain rate, Δ is defined as

$$\Delta = \left((\dot{\varepsilon}_{11}^2 + \dot{\varepsilon}_{22}^2)(1 + e^{-2}) + 4\dot{\varepsilon}_{12}^2 e^{-2} + 2\dot{\varepsilon}_{11}\dot{\varepsilon}_{22}(1 + e^{-2}) \right)^{1/2}. \tag{2.14}$$

The rigid plastic model is closed by assuming that Equation 2.12 holds inside the yield surface, as well as on it. In this formulation the viscosity coefficients, ζ and η, can become arbitrarily large as the strain rate goes to zero. To remove this possibility, limiting values are set for the strain rates in the original formulation such that, $\zeta_{max} = 2.5 \times 10^8 P$, and $\eta_{max} = \zeta_{max}/e^2$ [17]. When the limiting values are approached the ice behaves as a linearly viscous fluid undergoing slow creep. For small strain rates when the ice is approximately rigid, the stress lies on an elliptical surface concentric with the original yield surface in principal stress space as shown in Figure 2.5. This formulation results in a nonzero stress state for a zero strain rate. Later authors including Ip *et al.*[21] and Geiger *et al.*[12] modified this property so that a zero strain rate results in a zero stress state. This is accomplished by calculating ζ as the minimum of $P/2\Delta$ and ζ_{max}, then the ice strength term is recalculated as $P = 2\Delta\zeta$, which forces the yield curve to go through the origin in all cases. Figure 2.5 shows this modification to the yield curve.

Another method of regularizing the constitutive equation is due to Hunke and Dukowicz [19], who included an elastic component to control the behavior in the limit of infinite viscosity. This elastic component was introduced for numerical rather than physical reasons. The viscous plastic constitutive model for strain rate as a function of depth integrated stress is

$$\dot{\varepsilon} = \frac{1}{2\eta}\mathbf{N} + \frac{\eta - \zeta}{4\eta\zeta}\left(\mathrm{tr}\mathbf{N} + \frac{P}{4\zeta}\right)\mathbf{I}. \tag{2.15}$$
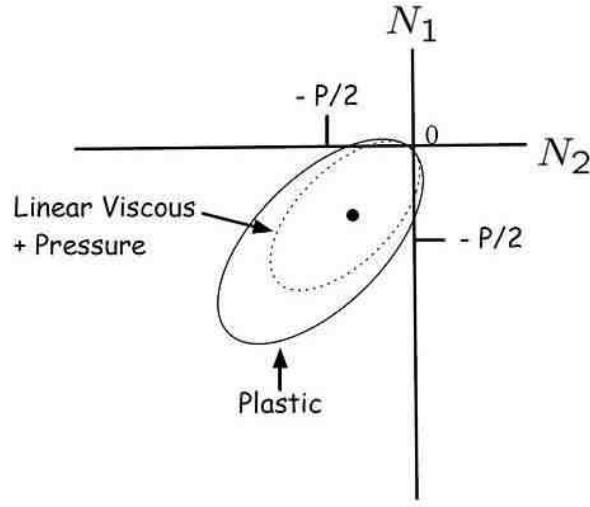
Figure 2.5: Modified yield curve in principal depth integrated stress space for viscous-plastic model

A simple linear elastic relationship can be written as $\dot{\mathbf{N}} = E\dot{\varepsilon}$ where E is an elastic parameter not to be confused with the full elastic tensor. Combining this with the viscous-plastic constitutive model results in

$$\dot{\varepsilon} = \frac{1}{2\eta}\mathbf{N} + \frac{\eta - \zeta}{4\eta\zeta}\left(\text{tr}\mathbf{N} + \frac{P}{4\zeta}\right)\mathbf{I} + \frac{1}{E}\dot{\mathbf{N}}. \tag{2.16}$$

In the limit as $\eta, \zeta \to \infty$ the simple elastic equation is recovered and in the steady state limit the viscous-plastic relationship is recovered.

Other variations on this model generally use the standard viscous-plastic constitutive law with restrictions on ζ and η to generate other yield curve shapes. For example, Ip *et al.* [21] use the standard Hibler constitutive law with four different yield criteria in prinicipal stress space, an elliptical yield curve, a square yield curve, a Mohr-Coulomb surface, and a cavitating fluid surface. Note that the constitutive law is no longer associative when used with other yield surfaces.

Related to the shape of the yield curve is the issue of stability. Gray and Killworth

[14] showed that for regions of tensile stress when the material is behaving as a viscous fluid, the model in linearly unstable and, therefore, ill-posed. Their suggestion for improving the behavior of the model is to restrict the yield curve to the third quadrant of principal stress space. However, for many applications the original elliptic yield curve is still used.

Numerically, the momentum balance and viscous-plastic constitutive model are generally solved using finite difference approximations. Because of the nonlinear viscous terms iterative techniques are often employed. For example, Hibler [17] iteratively solves the system using successive overrelaxation. The advantage of the elastic-viscous-plastic version of the model is that the equations can be solved explicitly. However, subcycling the constitutive terms is still often required [19]. Several authors have also investigated the use of finite elements [39], [31], or particle-in-cell methods [10], [36] for solving the sea ice equations.

2.3 Governing Equations: Ice Thickness Distribution

The average thickness used in the momentum equation and in the pressure calculation for the viscous-plastic model comes from the ice thickness distribution, which is a formalism that defines the variation of ice thickness in an area. A model for the thickness distribution of sea ice was proposed by Thorndike and Maykut [50] under the AIDJEX project and later expanded by Thorndike *et al.* [51]. This model consists of an evolution equation for the ice thickness distribution due to the combined effects of mechanical forcing and thermodynamic growth. To define the ice thickness distribution, first consider a region of ice with total area, $R(\mathbf{x}, t)$, that contains a partial area, $A(h, \mathbf{x}, t)$ with ice of thickness less than h. Then the cumula-

tive ice thickness distribution $G(h, \mathbf{x}, t)$ can be defined as A/R and the ice thickness distribution $g(h, \mathbf{x}, t)$ can be interpreted as $\partial G/\partial h$ where

$$\int_0^h g(h, \mathbf{x}, t)dh = G(h, \mathbf{x}, t) = \frac{A(h, \mathbf{x}, t)}{R(\mathbf{x}, t)}. \tag{2.17}$$

The ice thickness distribution can be seen to satisfy

$$\int_0^\infty g(h, \mathbf{x}, t)dh = 1. \tag{2.18}$$

The evolution equation for g, can be written as

$$\frac{\partial g}{\partial t} = -\frac{\partial}{\partial h}(fg) - \nabla \cdot (\mathbf{v}g) + \psi \tag{2.19}$$

where $\mathbf{v}(x_1, x_2, t)$ is the two-dimensional velocity of the ice, $f = dh/dt$ is the rate of thermodynamic change in thickness, and ψ is a source term that accounts for the redistribution of ice due to ridging. This evolution equation can be understood by considering each term on the right-hand side separately. The first term ($\frac{\partial}{\partial h}(fg)$) is the form expected for a transport equation in thickness space where $f = dh/dt$ is analogous to a velocity in horizontal space. The second term is the corresponding transport term in horizontal space. The final term on the right-hand side (ψ) redistributes ice of a given thickness to ice of a different thickness due to ridging or opening. A number of different forms have been proposed for this final term, but all must satisfy the following two constraints. The first constraint is conservation of area which can be written as

$$\int_0^\infty \psi dh = \nabla \cdot \mathbf{v}. \tag{2.20}$$

and the second constraint is conservation of volume

$$\int_0^\infty h\psi dh = 0. \tag{2.21}$$

A third constraint due to Rothrock [35] is often used, which relates the dissipation due to the plastic deformation of the ice to the change in potential energy of the ice

due to ridging and can be written as

$$\hat{\rho}\hat{g}\int_0^\infty h^2\psi dh = \mathbf{N} : \dot{\boldsymbol{\varepsilon}} \tag{2.22}$$

where

$$\hat{\rho} = \rho\frac{(\rho - \rho_w)}{\rho_w} \tag{2.23}$$

for a water density, ρ_w, and gravitational acceleration $\hat{g}$.

Thorndike *et. al.* [51] assumed the following form for the redistribution function

$$\psi = |\dot{\varepsilon}|(\alpha_0(\theta)\delta(h) + \alpha_r(\theta)w_r) \tag{2.24}$$

where $|\dot{\varepsilon}| = \sqrt{\dot{\varepsilon}_I^2 + \dot{\varepsilon}_{II}^2}$ is the strain rate magnitude and $\theta = \text{atan}(\dot{\varepsilon}_{II}/\dot{\varepsilon}_I)$ for

$$\begin{aligned}
\dot{\varepsilon}_I &= \nabla \cdot \mathbf{v} = \frac{\partial v_1}{\partial x_1} + \frac{\partial v_2}{\partial x_2} \\
\dot{\varepsilon}_{II} &= \sqrt{\left(\frac{\partial v_1}{\partial x_1} - \frac{\partial v_2}{\partial x_2}\right)^2 + \left(\frac{\partial v_1}{\partial x_2} + \frac{\partial v_2}{\partial x_1}\right)^2}.
\end{aligned} \tag{2.25}$$

In this equation contributions for opening and closing modes are combined. The first term containing the Dirac delta function increases the distribution of g at $h = 0$ due to the opening of leads in the ice. The second term contains a ridging function w_r, which controls how ice is redistributed in converging conditions. Using the constraints defined above, the coefficients of the redistribution term can be derived for the viscous-plastic model as

$$\alpha_r(\theta) = \frac{1}{2}\left(\cos^2\theta + \frac{\sin^2(\theta)}{e^2}\right)^{1/2} - \frac{1}{2}\cos(\theta) \tag{2.26}$$

and

$$\alpha_0(\theta) = \frac{1}{2}\left(\cos^2\theta + \frac{\sin^2(\theta)}{e^2}\right)^{1/2} + \frac{1}{2}\cos(\theta) \tag{2.27}$$

where e is the ellipticity of the yield curve.

The ridging function, $w_r(h)$ is defined as

$$w_r(h, \mathbf{x}, t) = \frac{-a(h, \mathbf{x}, t) + n(h, \mathbf{x}, t)}{N} \tag{2.28}$$

where $a(h, \mathbf{x}, t)$ is the distribution of ice participating in ridging, $n(h, \mathbf{x}, t)$ is the distribution of the newly ridged ice, and N is a normalization factor equal to

$$N(\mathbf{x}, t) = \int_0^\infty (a(h, \mathbf{x}, t) - n(h, \mathbf{x}, t))dh. \tag{2.29}$$

The ice that participates in ridging is calculated as $a(h, \mathbf{x}, t) = b(h, \mathbf{x}, t)g(h, \mathbf{x}, t)$ where $b(h, \mathbf{x}, t)$ is a function that weighs the distribution toward the thinnest ice. The original formulation in [51] used

$$b(h, \mathbf{x}, t) = \frac{2}{G^*} \left(1 - \frac{G(h, \mathbf{x}, t)}{G^*} \right) \quad \text{for } 0 \le G(h, \mathbf{x}, t) \le G^* \tag{2.30}$$

where $G(h, \mathbf{x}, t)$ is the cumulative ice distribution defined in Equation 2.22 and $G^* = 0.15$. For this form of $b(h, \mathbf{x}, t)$, $a(h, \mathbf{x}, t)$ is equal to zero when $G(h) = G^*$. This cutoff creates a problem when the open water fraction is close to G^*. The ice strength term can then change abruptly, which can lead to calculational instabilities [28]. Therefore, Lipscomb *et al.*, [28], recommend the exponential form

$$b(h, \mathbf{x}, t) = \frac{\exp(-G(h, \mathbf{x}, t)/a^*)}{a^*[1 - \exp(-1/a^*)]} \tag{2.31}$$

where $a^* = 0.05$. With this function all the ice participates in ridging, but the participating ice is weighed toward the thin end of the distribution.

The newly ridged ice distribution is calculated as

$$n(h, \mathbf{x}, t) = \int_0^\infty a(\tilde{h}, \mathbf{x}, t)\gamma(\tilde{h}, h)d\tilde{h} \tag{2.32}$$

where the function $\gamma(\tilde{h}, h)$ determines how the ice ridged from thickness $\tilde{h}$ is redistributed to another thickness, h. The original formulation from Thorndike *et. al.*, suggested

$$\gamma(\tilde{h}, h) = \frac{1}{k}\delta(h - k\tilde{h}) \tag{2.33}$$

which moves ice from thickness $\tilde{h}$ to thickness $k\tilde{h}$ and $k = 5$ is generally used. Hibler [18] introduced another form for γ that redistributes ice of thickness, $\tilde{h}$, uniformly over a thickness range $(2\tilde{h}, 2\sqrt{H^*\tilde{h}})$ and is of the form

$$\gamma(\tilde{h}, h) = \frac{1}{2(H^* - \tilde{h})} \quad \text{for } 2\tilde{h} \le h \le 2\sqrt{H^*\tilde{h}} \tag{2.34}$$

where $H^* = 100$. Another form of γ was proposed by Lipscomb *et al.* [28] based on experimental observations from Amundrud *et al.* [2]. This function is

$$\gamma(\tilde{h}, h) = \frac{\lambda(\tilde{h})}{k(\tilde{h})}\exp\left(-\frac{(h - H_{min}(\tilde{h}))}{\lambda(\tilde{h})}\right) \quad \text{for } H_{min}(\tilde{h}) \le h < \infty \tag{2.35}$$

where $\lambda(\tilde{h}) = 4\sqrt{\tilde{h}}$, $H_{min}(\tilde{h}) = \min(2\tilde{h}, \tilde{h} + 1)$, and $k(\tilde{h}) = \tilde{h}/(H_{min}(\tilde{h}) + \lambda(\tilde{h}))$.

Numerically, this model is implemented by first dividing the thickness distribution into discrete bins defined by thickness bounds (H_{n-1}, H_n) such that

$$g_n(\mathbf{x}, t) = \int_{H_{n-1}}^{H_n} g(h, \mathbf{x}, t)dh. \tag{2.36}$$

A fractional volume can be associated with each bin defined by

$$v_n(\mathbf{x}, t) = \int_{H_{n-1}}^{H_n} hg(h, \mathbf{x}, t)dh. \tag{2.37}$$

such that the average thickness in a bin is calculated as $h_n = v_n/g_n$. The one-dimensional thermodynamic equation must be solved for each thickness bin for a column of ice equal to the average thickness. Then an average thickness over all bins is calculated for each element and used in the momentum balance equation.

Other authors have further modified the model, such as Zhang and Rothrock, who include a term for lateral melting in the ice thickness distribution evolution and combine that with an enthalpy distribution equation to conserve both ice mass and thermal energy [56]. The standard form of this model uses fixed thickness bins, but Bitz *et al.* [6] use a Lagrangian formulation for the ice thickness distribution in thickness space.

A simpler ice thickness model is the two-level model due to Hibler and used with the original viscous-plastic rheology [17]. The two levels consist of open water and ice, which are represented by an average thickness, $h(\mathbf{x}, t)$, which includes both ice and open water, and a compactness, $A(\mathbf{x}, t)$. The conservation equations for the thickness and compactness consist of both dynamic and thermodynamic terms as shown below

$$
\begin{aligned}
\dot{h} &= -(\nabla \cdot \mathbf{v})h + S_h \\
\dot{A} &= -(\nabla \cdot \mathbf{v})A + S_A
\end{aligned}
\tag{2.38}
$$

where $\mathbf{v}(\mathbf{x}, t)$ is the velocity, and S_h and S_A are thermodynamic source terms. The change in the ice thickness and concentration due to dynamic effects is contained in the velocity divergence term. As expected, positive divergence results in a decrease in the average ice thickness and compactness. The thermodynamic terms are defined by

$$
S_h = f\left(\frac{h}{A}\right)A + (1 - A)f(0)
\tag{2.39}
$$

$$
S_A = \begin{cases} (f(0)/h_0)(1 - A), & \text{if } f(0) > 0 \\ 0, & \text{if } f(0) < 0 \end{cases} + \begin{cases} 0, & \text{if } S_h > 0 \\ (A/2\bar{h})S_h & \text{if } S_h < 0 \end{cases}
\tag{2.40}
$$

where $f = dh/dt$ is the ice growth rate defined by the thermodynamic model.

2.4 Governing Equations: Thermodynamics

The original thermodynamic model for a column of sea ice of a given thickness was developed by Maykut and Untersteiner [30]. It consists of a one-dimensional diffusion equation for the ice temperature with an internal heat source and flux conditions for the ice interactions with the atmosphere at the top and the ocean at the bottom. The governing equation for the temperature can be written as

$$
(\rho c)\frac{\partial T}{\partial t} = \frac{\partial}{\partial x_3}k\frac{\partial T}{\partial x_3} + \kappa I_0 e^{-\kappa x_3}
\tag{2.41}
$$

where ρ is the ice density, $c(x_3, T)$ is the specific heat, $T(x_3, t)$ is the temperature in $^\circ C$, $k(x_3, T)$ is the thermal conductivity, κ is the extinction coefficient, I_0 is the solar radiation that penetrates the upper surface, and x_3 is the vertical coordinate. The vertical temperature distribution in a column of sea ice is dependent on ice salinity due to brine pockets that act as thermal reservoirs [30]. The coefficients k and c in fact are assumed to depend on x_3 through the salinity. In the original model developed by Maykut and Untersteiner [30] the variable forms for the thermal conductivity and specific heat are given as

$$k(S, T) = k_0 + \frac{\beta S(x_3)}{T} \tag{2.42}$$

$$c(S, T) = c_0 + \frac{\gamma S(x_3)}{T^2} \tag{2.43}$$

where $S(x_3)$ is the salinity as a function of vertical coordinate, k_0 is the conductivity of fresh ice, c_0 is the specific heat of fresh ice, and β and γ are constant parameters. Note that T is equal to zero only for the case of melting fresh ice. If the ice has a nonzero salinity then the melting temperature of the ice is negative and bounded away from zero. In the case where fresh ice is melting both the salinity, $S(x_3)$, and temperature, T, approach zero so that in the limit $c(S, T)$ approaches c_0, the heat capacity of fresh ice, and $k(S, T)$ approaches k_0, the conductivity of fresh ice.

A fixed temperature boundary condition is used at the ice-ocean interface with temperature T_{bot} set at -1.8$^\circ C$, the freezing temperature of ocean water. The boundary conditions at the ice-atmosphere interface are more complicated due to the variety of fluxes impinging on the ice surface. The net flux at the top boundary can be written as

$$F_{net} = (1 - \alpha)F_r - I_0 + F_L - \epsilon_L \sigma T_0^4 + F_s + F_l + \left(k(S(z), T(z)) \frac{\partial T}{\partial z} \right) \Big|_{z_{top}} \tag{2.44}$$

where α is the surface albedo, F_r is the incoming short-wave solar radiation, I_0 is flux of radiative energy through the surface into the ice, F_L is the flux of long-wave

radiation from the clouds and atmosphere, ϵ_L is the long-wave emissivity, σ is the Stefan-Boltzmann constant, T_0 is the surface temperature of the ice in Kelvin, F_s is the flux of sensible heat, and F_l is the flux of latent heat. If $F_{net}(T_0 = 0°C) < 0$, then the surface temperature, T_0 is calculated by solving $F_{net} = 0$. If $F_{net}(T_0 = 0°C) \geq 0$, the surface temperature is set to the melting temperature $(0°C)$.

If $F_{net}(T_0 = 0°C) \geq 0$, the change in thickness due to melting at the top surface is calculated as

$$F_{net}(T_0 = 0°C) = -q(S(z_{top}), T_0)\dot{\hat{h}} \tag{2.45}$$

where $q(S(z_{top}), T_0)$ is the energy per unit volume required to melt the top surface ice and $\hat{h}(x_1, x_2, t)$ is the ice thickness. Similarly, the change in thickness at the bottom surface of the ice due to melting or freezing is calculated as a function of the ocean flux (F_w) as

$$\left(k(S, T)\frac{\partial T}{\partial z} \right)\bigg|_{z_{bot}} - F_w = q(S(z_{bot}), T_{bot})\dot{\hat{h}} \tag{2.46}$$

where $q(S(z_{bot}), T_{bot})$ is the energy per unit volume required to melt the bottom surface of ice and $k = k(S(z_{bot}), T(z_{bot}))$ is the thermal conductivity at the bottom surface. When combining this with the ice thickness distribution equation, $\hat{h}$ is interpreted as the average ice thickness for a given thickness category.

The numerical implementation of this model is expensive computationally due primarily to the dependence of k and c on the salinity. Therefore, Semtner [41] proposed a simple three-layer model without salinity dependent coefficients as an alternative. Semtner's model includes a layer of snow with thickness h_s, two layers of ice with total ice thickness, h_I, and a linear temperature profile assumed through the ice and snow layers. This model has been updated by Winton, who uses a variable heat capacity to more accurately include the salinity of the upper ice layer [54]. More recently, Bitz and Lipscomb proposed a numerical model that follows the original Maykut and Untersteiner model more closely [7]. The Bitz and Lipscomb

version includes a vertical salinity profile and specific heat and conductivity equations dependent on the salinity similar to those above. In addition, this model is energy and enthalpy preserving.

In the following chapter the version of the governing equations that will be used in this effort is derived and the assumptions required to obtain it are highlighted.

Chapter 3

Derivation of Governing Equations

3.1   Introduction

The basic structure of the sea ice models discussed in the previous chapter will be used for the new sea ice model proposed here. The equations used for the dynamic and thermodynamic pieces of the model can be derived starting from the fully coupled three-dimensional conservation equations with suitable assumptions. The purpose of this chapter is to go through this derivation in a finite deformation setting where the difference between the reference and current configurations is important and to highlight the various assumptions that are needed to obtain the more tractable two-dimensional and one-dimensional equations. General references used for the continuum mechanics and constitutive model derivation are Malvern [29], Simo and Hughes [42], and Belytschko *et al.* [5]. Malvern is additionally a general reference for the energy equation and thermodynamics. More specific references are provided in the text.

3.2   Problem Geometry

Consider a region of ice, $\mathcal{B} \subset \mathbb{R}^3$, with boundary $\partial\mathcal{B}$. This region of ice deforms with time under the action of a mapping $\boldsymbol{\varphi} : \mathcal{B} \times [0, T] \to \mathbb{R}^3$ such that the current configuration of the ice region is $\boldsymbol{\varphi}(\mathcal{B}, t) \subset \mathbb{R}^3$. This motion is illustrated in Figure 3.1. Now consider a coordinate system that is fixed with respect to the Earth. Consider first a coordinate system with origin at the center of the Earth. As shown in Figure 3.2, it will be assumed that $\mathcal{B}$ is a patch of ice on the surface of the Earth with dimension small enough so that over $\mathcal{B}$ the surface of the Earth has negligible curvature. Now rotate the coordinates so that $\mathbf{e}_3$ is in the direction normal to $\mathcal{B}$, which can be treated as the local vertical direction. Also assume that $X_3 = 0$ corresponds to the surface of the ice.
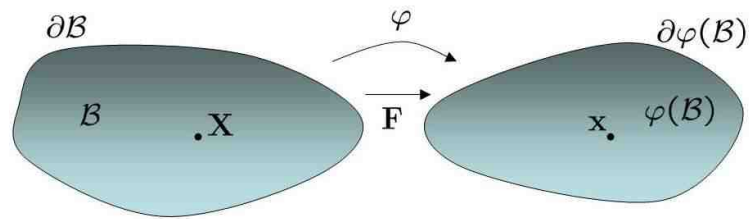
Figure 3.1: Evolution of Three-Dimensional Ice Region

Using this system, coordinates $\mathbf{X} = (X_1, X_2, X_3) \in \mathcal{B}$, and $\mathbf{x} = (x_1, x_2, x_3) \in \varphi(\mathcal{B})$ can be defined for the reference and current configuration. The deformation gradient associated with the motion is defined as $\mathbf{F} = \text{Grad}_{\mathbf{X}} = \partial\varphi/\partial\mathbf{X}$.

If the mass change due to thermodynamics is neglected, the set of admissible

(a)   (b)
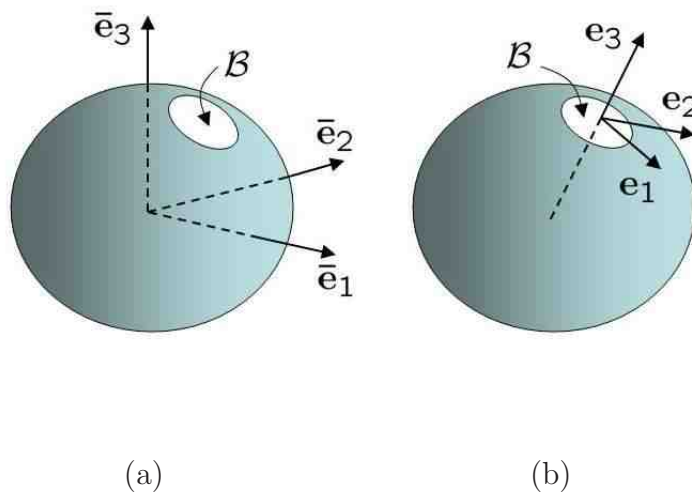
Figure 3.2: Coordinates of ice region with (a) origin at center of the Earth (b) origin rotated and translated to be at center of ice region.

configurations of the body is

$$\mathbb{S} = \left\{ \boldsymbol{\varphi} : \mathcal{B} \times [0, T] \to \mathbb{R}^3 \text{ s.t. } \det\mathbf{F} > 0 \text{ and } \boldsymbol{\varphi}|_{\partial\mathcal{B}_u} = \overline{\boldsymbol{\varphi}} \right\} \tag{3.1}$$

where $\partial\mathcal{B}_u$ is the portion of boundary where displacement is specified and $\overline{\boldsymbol{\varphi}}$ is the prescribed displacement. It is assumed that the boundary can be decomposed into regions where displacement is specified, $\partial\mathcal{B}_u$, and traction is specified, $\partial\mathcal{B}_T$, and that the regions satisfy $\partial\mathcal{B}_u \cap \partial\mathcal{B}_T = \emptyset$ and $\overline{\partial\mathcal{B}_u \cup \partial\mathcal{B}_T} = \partial\mathcal{B}$.

In the case of sea ice, the thickness to diameter ratio is very small, with thicknesses on the order of at most tens of meters and diameters on the order of hundreds of kilometers. The goal of the derivation of the governing equations will be to integrate the dynamic equations in the vertical direction and using suitable assumptions to derive the two-dimensional equations that define the ice deformation in the horizontal plane. With this task in mind, assume that a reference plane in $\mathcal{B}$ can be defined as $\mathcal{B}_2 = \{\mathbf{X} \in \mathcal{B} \text{ s.t. } X_3 = 0\}$ as shown in Figure 3.3. Each point, $(X_1, X_2) \in \mathcal{B}_2$ can be associated with a thickness, $h_0(X_1, X_2)$. This horizontal slice also evolves in time under the action of a mapping, $\boldsymbol{\varphi}_2 : \mathcal{B}_2 \times [0, T] \to \mathbb{R}^2$, with associated deformation gradient $\mathbf{F}_2 = \mathrm{Grad}\boldsymbol{\varphi}_2$. This two-dimensional mapping is related to the full three-dimensional mapping by $\boldsymbol{\varphi}_2 = \boldsymbol{\varphi}|_{X_3=0}$.

For a given column of ice, assume also that a top and bottom surface can be defined with an associated normal direction at each point. If the top surface of the ice is defined as $X_3 = Z_t(X_1, X_2)$, an outward normal to the surface is

$$\widetilde{\mathbf{N}}_t = \left(\frac{-\partial Z_t}{\partial X_1}, \frac{-\partial Z_t}{\partial X_2}, 1 \right). \tag{3.2}$$

The unit normal to the surface can then be calculated as $\mathbf{N}_t = \widetilde{\mathbf{N}}_t / \|\widetilde{\mathbf{N}}_t\|$ where

$$\|\widetilde{\mathbf{N}}_t\| = \sqrt{\left(\frac{\partial Z_t}{\partial X_1} \right)^2 + \left(\frac{\partial Z_t}{\partial X_2} \right)^2 + 1}. \tag{3.3}$$

Similarly, if the bottom surface is defined as $X_3 = Z_b(X_1, X_2)$, the corresponding
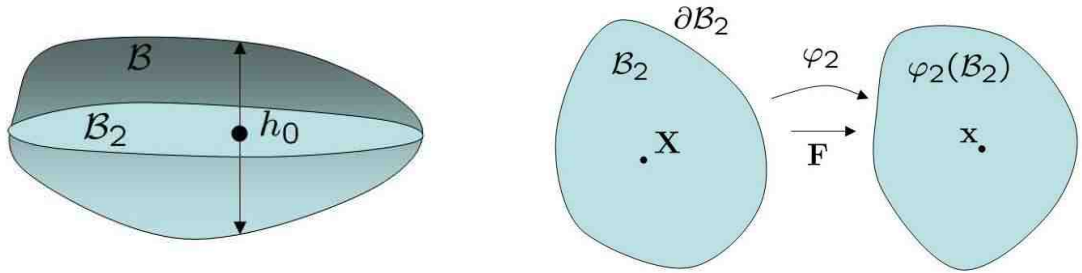
Figure 3.3: Evolution of two-dimensional ice region

normal direction is

$$\widetilde{\mathbf{N}}_b = \left(\frac{\partial Z_b}{\partial X_1}, \frac{\partial Z_b}{\partial X_2}, -1 \right). \tag{3.4}$$

The unit surface normal can then be calculated as $\mathbf{N}_b = \widetilde{\mathbf{N}}_b/\|\widetilde{\mathbf{N}}_b\|$ where $\|\widetilde{\mathbf{N}}_b\|$ is defined analogously to $\|\widetilde{\mathbf{N}}_t\|$. At any point, (X_1, X_2), in the ice cross-section, $\mathcal{B}_2$, the ice thickness can be defined as $h_0(X_1, X_2) = Z_t(X_1, X_2) - Z_b(X_1, X_2)$.

The top and bottom surfaces of the ice column will evolve in time due to dynamic and thermodynamic effects. Assume that at a time, t, the top and bottom surfaces are defined as $z_t(x_1, x_2, t)$ and $z_b(x_1, x_2, t)$, where $z_t(x_1, x_2, t) = z(\boldsymbol{\varphi}_2(X_1, X_2), t)$ and $z_b(x_1, x_2, t) = z_b(\boldsymbol{\varphi}_2(X_1, X_2), t)$. Then the thickness at time, t, will be $h(x_1, x_2, t) = z_t(x_1, x_2, t) - z_b(x_1, x_2, t)$. Using this definition of the geometry of the problem the following sections derive equations for the conservation of mass, momentum and energy.

3.3   Conservation of Mass

Given an arbitrary subdomain in the reference configuration, $\Omega_0 \subset \mathcal{B}$, and current configuration, $\Omega(t) = \boldsymbol{\varphi}(\Omega_0)$, mass conservation can be written as

$$\int_{\Omega_0} \rho_0(\mathbf{X})d\Omega = \int_{\Omega(t)} \rho(\mathbf{x}, t)d\Omega \tag{3.5}$$

where $\rho_0 : \mathcal{B} \to \mathbb{R}$ is the ice density per unit original volume and $\rho : \boldsymbol{\varphi}(\mathcal{B}) \times [0, T] \to \mathbb{R}$ is the ice density per unit current volume. Here thermodynamic changes in mass are neglected for now. Using a coordinate transformation the second integral becomes

$$\int_{\Omega_0} \rho_0(\mathbf{X})d\Omega = \int_{\Omega_0} \rho(\boldsymbol{\varphi}(\mathbf{X}, t))\mathcal{J}d\Omega \tag{3.6}$$

where $\mathcal{J} = \det\mathbf{F}$. If $\Omega_0 \subset \mathcal{B}$ is an arbitrary subregion and the integrands are continuous, then the standard local expression for mass conservation in material coordinates is obtained as

$$\rho_0 = \rho\mathcal{J}. \tag{3.7}$$

In sea ice modeling, the ice is generally assumed to be incompressible. Under this assumption mass conservation reduces to $\mathcal{J} = 1$ or $\rho = \rho_0$.

Now consider a column of ice as described in the previous section. Define arbitrary horizontal cross-sections $\Omega_{0,2} \subset \mathcal{B}_2$ and $\Omega_2(t) = \boldsymbol{\varphi}_2(\Omega_{0,2})$. For this column, mass conservation can be written as

$$\int_{\Omega_{0,2}} \int_{Z_b(X_1,X_2)}^{Z_t(X_1,X_2)} \rho_0(\mathbf{X})dX_3 d\Omega = \int_{\Omega_2(t)} \int_{z_b(x_1,x_2,t)}^{z_t(x_1,x_2,t)} \rho(\mathbf{x}, t)dx_3 d\Omega \tag{3.8}$$

where z_b and z_t are equations for the top and bottom surface of the ice column at time t. Assuming that ρ_0 is independent of X_3 and ρ is independent of x_3, integrating through the thickness results in

$$\int_{\Omega_{0,2}} \rho_0(X_1, X_2)h_0(X_1, X_2)d\Omega = \int_{\Omega_2(t)} \rho(x_1, x_2, t)h(x_1, x_2, t)d\Omega. \tag{3.9}$$

Changing variables using the two-dimensional mapping $\boldsymbol{\varphi}_2$, gives

$$\int_{\Omega_{0,2}} \rho_0(X_1, X_2) h_0(X_1, X_2) d\Omega = \int_{\Omega_{0,2}} \rho(\boldsymbol{\varphi}_2(X_1, X_2), t) h(\boldsymbol{\varphi}_2(X_1, X_2), t) J d\Omega \quad (3.10)$$

where $J = \det\mathbf{F}_2$. If $\Omega_{0,2}$ is an arbitrary subregion and the integrands are continuous, one obtains the local expression

$$\rho_0 h_0 = \rho h J. \tag{3.11}$$

Assuming that the ice behaves as an incompressible material $\rho_0 = \rho$, and therefore $h_0 = hJ$. Note that although $\mathcal{J} = 1$ for the assumption of incompressibility, J is not equal to one in general.

In the case of sea ice, mass is not truly conserved since it can be lost through melting and gained through freezing. To treat this system rigorously, a full model of ice and water would need to be implemented. If it is assumed that ice mass can only be gained or lost at the top and bottom surfaces of the ice region defined by z_t and z_b, then the thermodynamics will affect the ice thickness, but not the deformation of the horizontal region $\mathcal{B}_2$. In this case, the thermodynamic effects on the ice mass can be treated approximately in the evolution equations for ice thickness. Taking the material time derivative of Equation 3.11 with the assumption of incompressibility

$$\begin{aligned} \frac{d(hJ)}{dt} &= J\dot{h} + h\dot{J} = J\dot{h} + J\text{div}_{\mathbf{x}}\mathbf{v} = 0 \\ &\Rightarrow \dot{h} + h\text{div}_{\mathbf{x}}\mathbf{v} = 0 \end{aligned} \tag{3.12}$$

where $\text{div}_{\mathbf{x}}$ is the two-dimensional divergence operator in the coordinates defined by the current configuration and $\mathbf{v} = (v_1, v_2)$ is the in-plane velocity in the current configuration. Note that the material velocity defined as $\mathbf{V}(\mathbf{X}, t) = \dot{\boldsymbol{\varphi}}$ is related to the velocity defined in the current frame $\mathbf{v}(\mathbf{x}, t) = d\mathbf{x}/dt = \partial(\boldsymbol{\varphi}(\mathbf{X}, t))/\partial t = \dot{\boldsymbol{\varphi}}$. If it is assumed that thermodynamic effects can cause melt or growth of ice at the top and bottom of the ice column, the equation becomes

$$\dot{h} + h\text{div}_{\mathbf{x}}\mathbf{v} = \frac{dh_t}{dt} + \frac{dh_b}{dt} \tag{3.13}$$

where dh_t/dt and dh_b/dt are obtained from the balance of fluxes at the top and bottom surface of the column of ice.

In practice, rather than using this equation for ice thickness in a numerical model for sea ice, an ice thickness distribution is used. The following section contains a derivation of the ice thickness distribution.

3.4   Ice Thickness Distribution

In the case of sea ice modeling, conservation of mass is expressed through the ice thickness distribution developed by Thorndike *et al.* [50] [51]. Instead of considering a point mass, the ice thickness distribution is defined over a finite volume of ice. Consider a small column of ice in the three-dimensional ice pack, whose cross-section $(\Omega_{\mathbf{x}})$ surrounds a point $\mathbf{x} = (x_1, x_2)$ in the current configuration. This column has cross-sectional area

$$R(\mathbf{x}, t) = \int_{\Omega_{\mathbf{x}}(t)} d\Omega \tag{3.14}$$

that evolves with time based on the horizontal motion of the ice. Within this area the ice thickness, h, will vary. Note that although R is not a point quantity it is spatially varying in the sense that the small region $\Omega_{\mathbf{x}}$ over which it is defined varies with $\mathbf{x}$.

Let $A(h, \mathbf{x}, t)$ be the area of ice within $R(\mathbf{x}, t)$ of thickness less than h at time t. Then

$$R(\mathbf{x}, t) = \int_0^\infty \frac{\partial A}{\partial h}(h, \mathbf{x}, t)dh. \tag{3.15}$$

In the ice pack a maximum thickness, $h_{max} < \infty$, will exist such that $\partial A/\partial h = 0$ for $h > h_{max}$ and therefore the integral above is equal to $A(h_{max}, \mathbf{x}, t) - A(0, t)$. The

definition of A implies that $A(0, t) = 0$ and therefore $R(t) = A(h_{max}, \mathbf{x}, t)$. In this framework the partial area of open water is

$$\lim_{h \to 0+} A(h, \mathbf{x}, t). \tag{3.16}$$

$A(h, \mathbf{x}, t)$ can be normalized to consider the fractional area of ice in $R(\mathbf{x}, t)$ thinner than h, $G(h, \mathbf{x}, t) = A(h, \mathbf{x}, t)/R(\mathbf{x}, t)$. The function $G(h, \mathbf{x}, t)$ is the cumulative thickness distribution function with $G(h_{max}, \mathbf{x}, t) = 1$. Then, $\partial G/\partial h = g(h, \mathbf{x}, t)$ can be interpreted as a corresponding probability density function, with

$$\int_0^\infty g(h, \mathbf{x}, t)dh = 1. \tag{3.17}$$

Using these definitions, equations for the evolution of G or g with time can be derived. Both thermodynamics and ice motion contribute to the changes in G, but their effects can be considered separately.

First consider the motion of the two-dimensional ice region $\Omega_\mathbf{x}(t)$, which evolves from an initial state $\Omega_\mathbf{x}(0) \subset \mathcal{B}_2$. The motion of the region is characterized by the two-dimensional mapping $\boldsymbol{\varphi}_2$, which takes points from the reference configuration, $(X_1, X_2) \in \Omega_\mathbf{x}(0)$ and maps them to the current configuration, $(x_1, x_2) \in \Omega_\mathbf{x}(t)$.

The change in area of the region with time can be derived by transforming the integral in the current configuration to the equivalent integral in the reference configuration, as shown below

$$\begin{aligned}
\dot{R} &= \frac{d}{dt} \int_{\Omega_\mathbf{x}(t)} d\Omega = \frac{d}{dt} \int_{\Omega_\mathbf{x}(0)} J d\Omega_0 \\
&= \int_{\Omega_\mathbf{x}(0)} \frac{dJ}{dt} d\Omega_0 = \int_{\Omega_\mathbf{x}(0)} \mathrm{div}_\mathbf{x} \mathbf{v} J d\Omega_0 \\
&= \int_{\Omega_\mathbf{x}} \mathrm{div}_\mathbf{x} \mathbf{v} d\Omega
\end{aligned} \tag{3.18}$$

where $\mathrm{div}_\mathbf{x} \mathbf{v}$ is the divergence of the ice horizontal velocity with respect to the current coordinate system. For an infinitesimal region where $\mathrm{div}_\mathbf{x} \mathbf{v}$ is nearly constant

$$\dot{R} = \mathrm{div}_\mathbf{x} \mathbf{v} \int_{\Omega_\mathbf{x}(t)} d\Omega = (\mathrm{div}_\mathbf{x} \mathbf{v}) R(\mathbf{x}, t). \tag{3.19}$$

Now consider changes in the cumulative distribution function by taking the material derivative of $G(h, \mathbf{x}, t)$ to obtain

$$\dot{G} = \frac{d(A/R)}{dt} = \frac{1}{R}\dot{A} - \frac{A}{R^2}\dot{R}$$
$$= \frac{1}{R}\dot{A} - G\mathrm{div}_{\mathbf{x}}\mathbf{v}. \tag{3.20}$$

It is left to define $\dot{A}$, which will determine how the thickness is redistributed with ice motion. For now set

$$\frac{1}{R}\dot{A} = \Psi. \tag{3.21}$$

Then

$$\dot{G} = \Psi - (\mathrm{div}_{\mathbf{x}}\mathbf{v})G \tag{3.22}$$

and the corresponding equation for g obtained by differentiating Equation 3.22 with respect to h is

$$\dot{g} = \psi - (\mathrm{div}_{\mathbf{x}}\mathbf{v})g. \tag{3.23}$$

Now assume the changes in $G(h, \mathbf{x}, t)$ are entirely due to thermodynamics. Also assume that the growth rate of ice, $f(h, t) = dh/dt$, is known. In fact, the growth rate will be calculated from the thermodynamical model discussed in Section 3.6. Note that the growth rate involves the material derivative of h, which can be seen from Equation 3.13. Therefore, given $f(h, t)$, ice of thickness h at time t for the point that started at coordinate $\mathbf{X} = (X_1, X_2)$ will approximately grow or melt to ice of thickness $h + f(h, t)\Delta t$ at time $t + \Delta t$. If a function $\hat{G}(h, \mathbf{X}, t)$ is defined such that $G(h, \mathbf{x}, t) = G(h, \boldsymbol{\varphi}(\mathbf{X}), t) = \hat{G}(h, \mathbf{X}, t)$, then this relationship can be expressed as

$$\hat{G}(h, \mathbf{X}, t) = \hat{G}(h + f\Delta t, \mathbf{X}, t + \Delta t) + O(\Delta t^2). \tag{3.24}$$

Expanding this about $\hat{G}(h, \mathbf{X}, t + \Delta t)$ gives

$$\hat{G}(h, \mathbf{X}, t) = \hat{G}(h, \mathbf{X}, t + \Delta t) + f(h, t)\Delta t \frac{\partial \hat{G}}{\partial h} + O(\Delta t^2) \tag{3.25}$$

which can be rewritten as

$$\frac{\hat{G}(h, \mathbf{X}, t + \Delta t) - \hat{G}(h, \mathbf{X}, t)}{\Delta t} = -f\frac{\partial \hat{G}}{\partial h} + O(\Delta t). \tag{3.26}$$

Taking the limit as Δt goes to zero,

$$\frac{\partial \hat{G}}{\partial t} = -f\frac{\partial \hat{G}}{\partial h} \tag{3.27}$$

Then transforming back to G gives

$$\dot{G} = -f\frac{\partial G}{\partial h} \tag{3.28}$$

and

$$\dot{g} = -\frac{\partial}{\partial h}(fg). \tag{3.29}$$

Combining the mechanical and thermodynamical contributions leads to the final governing equations for the thickness distribution

$$\begin{aligned}\dot{G} &= -f\frac{\partial G}{\partial h} - (\text{div}_\mathbf{x}\mathbf{v})G + \Psi \\ \dot{g} &= -\frac{\partial}{\partial h}(fg) - (\text{div}_\mathbf{x}\mathbf{v})g + \psi.\end{aligned} \tag{3.30}$$

A reasonable function for Ψ and therefore $\psi = \partial\Psi/\partial h$ can be derived by considering constraints on the ice redistribution. The first constraint to consider is a balance for the total change in area. This can be written as

$$\begin{aligned}\dot{R} &= \frac{d}{dt}\int_0^\infty \frac{\partial A}{\partial h}dh = \int_0^\infty \frac{\partial}{\partial h}(R(t)\Psi)\,dh \\ &= R(t)\int_0^\infty \frac{\partial\Psi}{\partial h}dh\end{aligned} \tag{3.31}$$

which implies that in $\Omega_\mathbf{x}$

$$\int_0^\infty \psi dh = \frac{1}{R(t)}\dot{R} = \text{div}_\mathbf{x}\mathbf{v}. \tag{3.32}$$

If additional ice is only formed from thermodynamic growth and the ice is modeled as an incompressible material the redistribution function is constrained by the fact that ice volume is conserved. The fractional volume of ice in the region is

$$V(\mathbf{x}, t) = \int_0^\infty h \frac{\partial A}{\partial h} dh \tag{3.33}$$

The change in volume can then be calculated as

$$\begin{aligned}
\dot{V} &= \int_0^\infty h \frac{\partial}{\partial h} \left(\dot{A} \right) dh \\
&= \int_0^\infty h \frac{\partial}{\partial h} (R(t)\Psi) dh \\
&= R(t) \int_0^\infty h \frac{\partial \Psi}{\partial h} dh.
\end{aligned} \tag{3.34}$$

Since the change in volume must be equal to 0 for the redistribution, the following constraint on Ψ and therefore ψ is obtained

$$\int_0^\infty h \frac{\partial \Psi}{\partial h} dh = \int_0^\infty h\psi dh = 0. \tag{3.35}$$

The standard redistribution function is derived by considering opening ($\mathrm{div}_\mathbf{x}\mathbf{v} > 0$) and closing ($\mathrm{div}_\mathbf{x}\mathbf{v} < 0$) modes separately. In the case of opening, new water is created, and therefore the change in area contributes to the cumulative distribution function A for all h, which implies that

$$\dot{A} = \dot{R} = R\mathrm{div}_\mathbf{x}\mathbf{v} \quad \text{for } \mathrm{div}_\mathbf{x}\mathbf{v} > 0. \tag{3.36}$$

Then for an opening mode where $\mathrm{div}_\mathbf{x}\mathbf{v} > 0$, Ψ is equal to $H(h)\mathrm{div}_\mathbf{x}\mathbf{v}$, where

$$H(h) = \begin{cases} 1 & h \geq 0 \\ 0 & h < 0 \end{cases}. \tag{3.37}$$

Taking the derivative with respect to h leads to $\partial\Psi/\partial h = \delta(h)\mathrm{div}_\mathbf{x}\mathbf{v}$.

In the case of closing a more complicated function is necessary. Similar to the standard model [50] assume ψ is of the form

$$\psi = \delta(h)\langle \mathrm{div}_\mathbf{x}\mathbf{v} \rangle + w_r \langle -\mathrm{div}_\mathbf{x}\mathbf{v} \rangle \tag{3.38}$$

where the velocity divergence terms are area opening and closing rates for the deformation and the McCauly bracket is defined as

$$\langle x \rangle = \begin{cases} x \text{ for } x \geq 0 \\ 0 \text{ for } x < 0 \end{cases} \tag{3.39}$$

The closing rate is multiplied by a redistribution function, w_r, which has the following form

$$w_r = \frac{n(h, \mathbf{x}, t) - a(h, \mathbf{x}, t)}{N(\mathbf{x}, t)} \tag{3.40}$$

as shown in Equation 2.28. Recall that $a(h, \mathbf{x}, t)$ is the distribution of ice participating in ridging, $n(h, \mathbf{x}, t)$ is the distribution of the newly ridged ice, and $N(\mathbf{x}, t)$ is a normalization factor. The ice that participates in ridging is defined as $a(h, \mathbf{x}, t) = b(h, \mathbf{x}, t) g(h, \mathbf{x}, t)$ where $b(h)$ is a function that weighs the distribution toward the thinnest ice. Following Lipscomb *et. al.*, [28], an exponential form is used as shown below

$$b(h, \mathbf{x}, t) = \frac{\exp(-G(h, \mathbf{x}, t)/a^*)}{a^*[1 - \exp(-1/a^*)]} \tag{3.41}$$

where $a^* = 0.05$. The newly ridged ice distribution is calculated as

$$n(h, \mathbf{x}, t) = \int_0^\infty a(\tilde{h}, \mathbf{x}, t) \gamma(\tilde{h}, h) d\tilde{h} \tag{3.42}$$

where the following exponential form of the weighting function, $\gamma(\tilde{h}, h)$, is used

$$\gamma(\tilde{h}, h) = \frac{\lambda(\tilde{h})}{k(\tilde{h})} \exp\left(-\frac{(h - H_{min}(\tilde{h}))}{\lambda(\tilde{h})}\right) \text{ for } H_{min}(\tilde{h}) \leq h < \infty \tag{3.43}$$

for $\lambda(\tilde{h}) = 4\sqrt{\tilde{h}}$, $H_{min}(\tilde{h}) = \min(2\tilde{h}, \tilde{h} + 1)$, and $k(\tilde{h}) = \tilde{h}/(H_{min}(\tilde{h}) + \lambda(\tilde{h}))$ [28].

Given a closing mode where $\text{div}_{\mathbf{x}}\mathbf{v} < 0$, the area conservation constraint on ψ from Equation 3.32 can be written in terms of w_r as

$$\int_0^\infty w_r \langle -\text{div}_{\mathbf{x}}\mathbf{v} \rangle dh = \text{div}_{\mathbf{x}}\mathbf{v} \tag{3.44}$$

which implies that

$$\int_0^\infty w_r dh = -1.$$

(3.45)

Therefore, $N(\mathbf{x}, t)$ must be defined as

$$N(\mathbf{x}, t) = \int_0^\infty (a(h, \mathbf{x}, t) - n(h, \mathbf{x}, t)) dh.$$

(3.46)

A simplified expression for $N(\mathbf{x}, t)$ can be found using the above functions for $n(h, \mathbf{x}, t)$ and $a(h, \mathbf{x}, t)$. First, expand N by incorporating the definition of n

$$N = \int_0^\infty \left(a(h, \mathbf{x}, t) - \int_0^\infty a(\tilde{h}, \mathbf{x}, t)\gamma(\tilde{h}, h)d\tilde{h} \right) dh.$$

(3.47)

Then changing the order of integration for the second integral gives

$$N = \int_0^\infty a(h, \mathbf{x}, t)dh - \int_0^\infty \left(\int_0^\infty a(\tilde{h}, \mathbf{x}, t)\gamma(\tilde{h}, h)dh \right) d\tilde{h}$$

(3.48)

For the γ given in Equation (3.43) this becomes

$$N = \int_0^\infty a(h, \mathbf{x}, t)dh - \int_0^\infty \left(\int_{H_{min}(\tilde{h}}^\infty a(\tilde{h}, \mathbf{x}, t)\frac{\lambda(\tilde{h})}{k(\tilde{h})}\exp\left(-\frac{h - H_{min}(\tilde{h})}{\lambda(\tilde{h})} \right) dh \right) d\tilde{h}.$$

(3.49)

Now, integrating the second term over h results in

$$N = \int_0^\infty a(h, \mathbf{x}, t)dh - \int_0^\infty \frac{a(\tilde{h}, \mathbf{x}, t)}{k(\tilde{h})} \left(-\exp\left(-\frac{h - H_{min}(\tilde{h})}{\lambda(\tilde{h})} \right) \right) \Bigg|_{H_{min}}^\infty d\tilde{h}$$

(3.50)

which becomes

$$N = \int_0^\infty a(h, \mathbf{x}, t)dh - \int_0^\infty \frac{a(\tilde{h})}{k(\tilde{h})}d\tilde{h}$$
$$= \int_0^\infty a(h, \mathbf{x}, t) \left(1 - \frac{1}{k(h)} \right) dh.$$

(3.51)

Finally, the evolution equation for g can be written as

$$\dot{g} = -(\text{div}_\mathbf{x}\mathbf{v})g - \frac{\partial(fg)}{\partial h} + \delta(h)\langle\text{div}_\mathbf{x}\mathbf{v}\rangle$$
$$+ \frac{-a(h, \mathbf{x}, t) + \int_0^\infty a(\tilde{h}, \mathbf{x}, t)\gamma(\tilde{h}, h)d\tilde{h}}{\int_0^\infty a(h, \mathbf{x}, t)(1 - 1/k(h))dh}\langle-\text{div}_\mathbf{x}\mathbf{v}\rangle.$$

(3.52)

Note that one problem with the form of the equation for $g(h, \mathbf{x}, t)$ derived above is that it does not inherently maintain positive g. Given that $g(h, \mathbf{x}, t)$ is a distribution, negative values are unphysical, but g can become negative for certain values of ψ regardless of the functional form of ψ.

Solving the ice thickness distribution evolution equation provides an average thickness defined over the area $\Omega_{\mathbf{x}}$, which can be calculated as

$$h(\mathbf{x}, t) = \frac{\int_0^\infty \tilde{h} g(\tilde{h}, \mathbf{x}, t) d\tilde{h}}{\int_0^\infty g(\tilde{h}, \mathbf{x}, t) d\tilde{h}}. \tag{3.53}$$

This average thickness is then used in the momentum equation discussed in the following section.

3.5   Balance of Momentum

The derivation here for the two-dimensional momentum equation for sea ice generalizes the derivation in Gray and Morland [15] for the small strain case. The balance of momentum equation is a formulation of Newton's Second law, which states that force is equal to mass times acceleration. For an arbitrary subregion, Ω_0 of a body $\mathcal{B}$, the forces acting on it can be divided into body forces per unit mass, $\mathbf{B} : \Omega_0 \times [0, T] \to \mathbb{R}^3$, and surface tractions, $\mathbf{T} : \Omega_0 \times [0, T] \to \mathbb{R}^3$. Using this division of forces the balance of momentum can be expressed in material coordinates as

$$\int_{\Omega_0} \rho_0 \dot{\mathbf{V}}_I d\Omega = \int_{\Omega_0} \rho_0 \mathbf{B} d\Omega + \int_{\partial \Omega_0} \mathbf{T} dS \tag{3.54}$$

where $\mathbf{V}_I$ is the inertial velocity of the body.

In the case of sea ice, the coordinate system of interest is fixed with respect to the Earth as discussed in Section 3.1. Therefore, the coordinate system is noninertial as a result of the Earth's rotation. Using the mapping $\boldsymbol{\varphi}$ defined in Section 3.2 the velocity in the rotating frame, $\mathbf{V}_R$, is defined as $\mathbf{V}_R = \dot{\boldsymbol{\varphi}}$ in material coordinates.

The inertial velocity can be determined as a function of the rotating velocity by considering a change of coordinates from the inertial to the rotating frame. For a more detailed look at deriving the Coriolis force resulting from the change of coordinates see Pedlosky [34].

Now consider a position vector $\mathbf{X}$. The mapping $\boldsymbol{\varphi}$ takes $\mathbf{X}$ into a position vector in the current configuration, $\mathbf{x}$, and can be written in components as $\varphi_1\mathbf{e}_1 + \varphi_2\mathbf{e}_2 + \varphi_3\mathbf{e}_3$ where $\mathbf{e}_i$, $(i = 1, 2, 3)$, represent the unit vectors defining the Cartesian coordinate system fixed with respect to the Earth. The time derivative of $\boldsymbol{\varphi}$ in the rotating frame can be expressed as

$$\dot{\boldsymbol{\varphi}}_R = \dot{\varphi}_1\mathbf{e}_1 + \dot{\varphi}_2\mathbf{e}_2 + \dot{\varphi}_3\mathbf{e}_3. \tag{3.55}$$

In an inertial frame the time derivative of $\boldsymbol{\varphi}$ can be expressed as

$$\dot{\boldsymbol{\varphi}}_I = \dot{\boldsymbol{\varphi}}_R + \varphi_1\dot{\mathbf{e}}_1 + \varphi_2\dot{\mathbf{e}}_2 + \varphi_3\dot{\mathbf{e}}_3 \tag{3.56}$$

where the time derivatives of the coordinate basis functions from the rotating frame must be included. Assuming that the angular velocity of the Earth is a constant, $\boldsymbol{\omega}$, this can be written as

$$\begin{aligned}\dot{\boldsymbol{\varphi}}_I &= \dot{\boldsymbol{\varphi}}_R + \varphi_1(\boldsymbol{\omega} \times \mathbf{e}_1) + \varphi_2(\boldsymbol{\omega} \times \mathbf{e}_2) + \varphi_3(\boldsymbol{\omega} \times \mathbf{e}_3) \\ &= \dot{\boldsymbol{\varphi}}_R + \boldsymbol{\omega} \times \boldsymbol{\varphi}_R\end{aligned} \tag{3.57}$$

The velocity in the rotating frame is $\mathbf{V}_R = \dot{\boldsymbol{\varphi}}_R$ and therefore

$$\mathbf{V}_I = \mathbf{V}_R + \boldsymbol{\omega} \times \boldsymbol{\varphi}_R \tag{3.58}$$

The inertial acceleration, $\dot{\mathbf{V}}_I$, can be derived in the same manner as the inertial velocity, $\mathbf{V}_I$. Analogously to Equation 3.57, the inertial acceleration can be written as

$$\left(\dot{\mathbf{V}}_I\right) = \left(\dot{\mathbf{V}}_I\right)_R + \boldsymbol{\omega} \times \mathbf{V}_I. \tag{3.59}$$

Using the previous expression for $\mathbf{V}_I$, this leads to

$$
\begin{aligned}
\left(\dot{\mathbf{V}}_I\right)_I &= \left(\dot{\mathbf{V}}_R\right)_R + \boldsymbol{\omega} \times \dot{\boldsymbol{\varphi}}_R + \boldsymbol{\omega} \times \mathbf{V}_R + \boldsymbol{\omega} \times \boldsymbol{\omega} \times \boldsymbol{\varphi}_R \\
&= \left(\dot{\mathbf{V}}_R\right)_R + 2\boldsymbol{\omega} \times \mathbf{V}_R + \boldsymbol{\omega} \times \boldsymbol{\omega} \times \boldsymbol{\varphi}_R.
\end{aligned}
\tag{3.60}
$$

Substituting this form of the inertial acceleration the balance of momentum equation gives

$$
\int_{\Omega_0} \rho_0 \left(\dot{\mathbf{V}}_R + 2\boldsymbol{\omega} \times \mathbf{V} + \boldsymbol{\omega} \times \boldsymbol{\omega} \times \boldsymbol{\varphi}_R\right) d\Omega = \int_{\partial\Omega_0} \mathbf{T} dS + \int_{\Omega_0} \rho_0 \mathbf{B} d\Omega.
\tag{3.61}
$$

For a three-dimensional column of sea ice, the only body force acting on the ice is due to gravity, so set $\mathbf{B} = -\hat{g}\mathbf{e}_3$, where $\hat{g}$ is the acceleration due to gravity. In practice, the second term arising from the noninertial acceleration, the centripetal term, is absorbed into the gravitational field so that the revised body force is defined as $-\mathbf{g} = -\hat{g}\mathbf{e}_3 - \boldsymbol{\omega} \times \boldsymbol{\omega} \times \boldsymbol{\varphi}_R$.

Now the tractions in the reference frame can be related to the First Piola-Kirchhoff stress tensor by $\mathbf{PN} = \mathbf{T}$. Using this relationship and the divergence theorem, the surface integral term can be written as

$$
\int_{\partial\Omega_0} \mathbf{P} \cdot \mathbf{N} dS = \int_{\Omega_0} \mathrm{Div}_{\mathbf{X}} \mathbf{P} d\Omega
\tag{3.62}
$$

where $(\mathrm{Div}_{\mathbf{X}}\mathbf{P})_{ij} = \partial P_{ij}/\partial X_j$ is the divergence with respect to the coordinates in the reference configuration. The momentum equation then becomes

$$
\int_{\Omega_0} \rho_0 \left(\dot{\mathbf{V}} + 2\boldsymbol{\omega} \times \mathbf{V}\right) d\Omega = \int_{\Omega_0} (\mathrm{Div}_{\mathbf{X}}\mathbf{P} - \rho_0\mathbf{g}) d\Omega
\tag{3.63}
$$

where the R subscript has been dropped from the velocity.

Given that this holds for an arbitrary volume Ω_0 within $\mathcal{B}$ and the integrand is continuous, the local form of the momentum balance in three dimensions can be written as follows

$$
\rho_0\dot{\mathbf{V}} = \mathrm{Div}_{\mathbf{X}}\mathbf{P} - \rho_0\mathbf{g} - 2\boldsymbol{\omega} \times \mathbf{V}.
\tag{3.64}
$$

Now consider a region of sea ice with geometry as shown in Figure 3.3. In this case the momentum balance can be written as

$$\int_{\Omega_{0,2}} \int_{Z_b}^{Z_t} \rho_0 \left(\dot{\mathbf{V}} + 2\boldsymbol{\omega} \times \mathbf{V}\right) dX_3 d\Omega = \int_{\Omega_{0,2}} \int_{Z_b}^{Z_t} (\text{Div}_{\mathbf{X}}\mathbf{P} - \rho_0 g \mathbf{e}_3) dX_3 d\Omega. \quad (3.65)$$

Traction boundary conditions apply at the top and bottom surfaces of the ice. At the top surface, atmospheric winds create a traction $\mathbf{T}_t = \mathbf{P}(Z_t)\mathbf{N}_t$. This traction is assumed to be in a direction tangential to the surface so that $\mathbf{T}_t \cdot \mathbf{N}_t = 0$. At the bottom surface, the ocean current and hydrostatic water pressure create a traction $\mathbf{T}_b = \mathbf{P}(Z_b)\mathbf{N}_b$. The ocean current is assumed to be in a direction tangential to the surface. Additionally, the hydrostatic water pressure is assumed to be in a direction normal to the surface. Then $\mathbf{T}_b \cdot \mathbf{N}_b = \rho_w \mathbf{g} h_w$ is the hydrostatic water pressure, where the water thickness or height is defined as $h_w = Z_w - Z_b$ for a top water surface defined by Z_w.

The angular velocity of the Earth can be written in component form as $\boldsymbol{\omega} = \omega(\sin\phi\mathbf{e}_3 + \cos\phi\mathbf{e}_2)$ where ϕ is the latitude and $\omega = 0.729 \times 10^{-4}\text{rad s}^{-1}$ [15]. Using this, the Coriolis term can be written in component form as

$$2\boldsymbol{\omega} \times \mathbf{V} = 2\omega(\cos\phi V_3 - \sin\phi V_2)\mathbf{e}_1 + 2\omega\sin\phi V_1 \mathbf{e}_2 - 2\omega\cos\phi V_1 \mathbf{e}_3 \quad (3.66)$$

In the derivation of the two-dimensional momentum equation, first consider the $\mathbf{e}_1$ component of this equation, which can be written as

$$\int_{\Omega_{0,2}} \int_{Z_b}^{Z_t} \rho_0 \left(\dot{V}_1 + 2\omega(\cos\phi V_3 - \sin\phi V_2)\right) dX_3 d\Omega$$
$$= \int_{\Omega_{0,2}} \int_{Z_b}^{Z_t} \left(\frac{\partial P_{11}}{\partial X_1} + \frac{\partial P_{12}}{\partial X_2} + \frac{\partial P_{13}}{\partial X_3}\right) dX_3 d\Omega. \quad (3.67)$$

Define the depth integrated velocity as

$$\mathcal{W}_i(X_1, X_2, t) = \int_{Z_b}^{Z_t} V_i dX_3 \quad (3.68)$$

and the depth integrated stress as

$$\mathcal{N}_{ij}(X_1, X_2, t) = \int_{Z_b}^{Z_t} P_{ij} dX_3 \tag{3.69}$$

for $i = 1, 2, 3$ and $j = 1, 2$.

Note that

$$\int_{Z_b}^{Z_t} \frac{\partial P_{ij}}{\partial X_j} dX_3 = \frac{\partial}{\partial X_j} \int_{Z_b}^{Z_t} P_{ij} - \left(P_{ij} \frac{\partial Z_t}{\partial X_j} \right)\Big|_{Z_t} + \left(P_{ij} \frac{\partial Z_b}{\partial X_j} \right)\Big|_{Z_b}. \tag{3.70}$$

Then after integrating through the thickness the first component of the momentum balance becomes

$$\int_{\Omega_{0,2}} \rho_0 \left(\dot{\mathcal{W}}_1 + 2\omega(\cos\phi \mathcal{W}_3 - \sin\phi \mathcal{W}_2) \right) d\Omega =$$

$$\int_{\Omega_{0,2}} \left(\frac{\partial \mathcal{N}_{11}}{\partial X_1} - P_{11} \frac{\partial Z_t}{\partial X_1}\Big|_{Z_t} + P_{11} \frac{\partial Z_b}{\partial X_1}\Big|_{Z_b} \right) d\Omega$$

$$\int_{\Omega_{0,2}} \left(\frac{\partial \mathcal{N}_{12}}{\partial X_2} - P_{12} \frac{\partial Z_t}{\partial X_2}\Big|_{Z_t} + P_{12} \frac{\partial Z_b}{\partial X_2}\Big|_{Z_b} \right) d\Omega \tag{3.71}$$

$$+ \int_{\Omega_{0,2}} (P_{13}(Z_t) + P_{13}(Z_b)) \, d\Omega.$$

Rearranging terms results in

$$\int_{\Omega_{0,2}} \rho_0 \left(\dot{\mathcal{W}}_1 + 2\omega(\cos\phi \mathcal{W}_3 - \sin\phi \mathcal{W}_2) \right) d\Omega = \int_{\Omega_{0,2}} \left(\frac{\partial \mathcal{N}_{11}}{\partial X_1} + \frac{\partial \mathcal{N}_{12}}{\partial X_2} \right) d\Omega$$

$$+ \int_{\Omega_{0,2}} \left(P_{11} \frac{\partial Z_t}{\partial X_1}\Big|_{Z_t} - P_{12} \frac{\partial Z_t}{\partial X_2}\Big|_{Z_t} + P_{13}(Z_t) \right) d\Omega \tag{3.72}$$

$$+ \int_{\Omega_{0,2}} \left(P_{11} \frac{\partial Z_b}{\partial X_1}\Big|_{Z_b} - P_{12} \frac{\partial Z_b}{\partial X_2}\Big|_{Z_b} + P_{13}(Z_b) \right) d\Omega.$$

Note that

$$-P_{11} \frac{\partial Z_t}{\partial X_1}\Big|_{Z_t} - P_{12} \frac{\partial Z_t}{\partial X_2}\Big|_{Z_t} + P_{13}(Z_t) = P_{1j}(\widetilde{\mathbf{N}}_t)_j = \|\widetilde{\mathbf{N}}_t\|(T_t)_1 \tag{3.73}$$

and

$$P_{11} \frac{\partial Z_b}{\partial X_1}\Big|_{Z_b} + P_{12} \frac{\partial Z_b}{\partial X_2}\Big|_{Z_b} - P_{13}(Z_b) = P_{1j}(\widetilde{\mathbf{N}}_b)_j = \|\widetilde{\mathbf{N}}_b\|(T_b)_1. \tag{3.74}$$

Then the first component of the momentum balance equation becomes

$$\int_{\Omega_{0,2}} \rho_0 \left(\dot{\mathcal{W}}_1 + 2\omega(\cos\phi\mathcal{W}_3 - \sin\phi\mathcal{W}_2) \right) d\Omega =$$

$$\int_{\Omega_{0,2}} \left(\frac{\partial \mathcal{N}_{11}}{\partial X_1} + \frac{\partial \mathcal{N}_{12}}{\partial X_2} \right) d\Omega + \int_{\Omega_{0,2}} \left(\|\widetilde{\mathbf{N}}_t\|(T_t)_1 + \|\widetilde{\mathbf{N}}_b\|(T_b)_1 \right) d\Omega. \tag{3.75}$$

Similary, the second component of the momentum balance becomes

$$\int_{\Omega_{0,2}} \rho_0 \left(\dot{\mathcal{W}}_2 + 2\omega\sin\phi\mathcal{W}_1 \right) d\Omega =$$

$$\int_{\Omega_{0,2}} \left(\frac{\partial \mathcal{N}_{21}}{\partial X_1} + \frac{\partial \mathcal{N}_{22}}{\partial X_2} \right) d\Omega + \int_{\Omega_{0,2}} \left(\|\widetilde{\mathbf{N}}_t\|(T_t)_2 + \|\widetilde{\mathbf{N}}_b\|(T_b)_2 \right) d\Omega \tag{3.76}$$

and the third component can be written as

$$\int_{\Omega_{0,2}} \rho_0 \left(\dot{\mathcal{W}}_3 - 2\omega\cos\phi\mathcal{W}_1 \right) d\Omega =$$

$$\int_{\Omega_{0,2}} \left(\frac{\partial \mathcal{N}_{31}}{\partial X_1} + \frac{\partial \mathcal{N}_{32}}{\partial X_2} \right) d\Omega \tag{3.77}$$

$$+ \int_{\Omega_{0,2}} \left(\|\widetilde{\mathbf{N}}_t\|(\tau_t)_3 + \|\widetilde{\mathbf{N}}_b\|(\tau_b)_3 \right) d\Omega - \int_{\Omega_{0,2}} \rho_0 \mathbf{g} h_0 d\Omega.$$

If it is assumed that the ice is in isostatic equilibrium with the water then the force due to the hydrostatic pressure of the sea water balances the gravitational force on the ice resulting in a fixed proportion of ice floating above the water surface. In the case of ice and sea water the ratio of their densities, determines that about 10 percent of the ice will be above the water line. Given the assumption of isostatic equilibrium $V_3 = 0$ and therefore $\mathcal{W}_3 = 0$. Additionally the $\mathbf{e}_3$ component of the Coriolis force is generally negligible compared to the gravitational acceleration, and therefore will be dropped [15]. Then the third component of the momentum equation reduces to

$$\int_{\Omega_{0,2}} \left(\frac{\partial \mathcal{N}_{31}}{\partial X_1} + \frac{\partial \mathcal{N}_{32}}{\partial X_2} \right) d\Omega$$

$$+ \int_{\Omega_{0,2}} \left(\|\widetilde{\mathbf{N}}_t\|(T_t)_3 + \|\widetilde{\mathbf{N}}_b\|(T_b)_3 \right) d\Omega - \int_{\Omega_{0,2}} \rho_0 \mathbf{g} h_0 d\Omega = 0. \tag{3.78}$$

Now consider assumptions for the two in-plane components of the momentum balance. Suitable assumptions for these components will lead to the commonly used

two-dimensional form of the momentum balance for sea ice. Therefore, in addition to assuming that $V_3 = 0$, assume that the horizontal components of the velocity do not depend on X_3. Then

$$\mathcal{W}_\alpha = \int_{Z_b}^{Z_t} V_\alpha dX_3 = V_\alpha \int_{Z_b}^{Z_t} dX_3 = V_\alpha h_0 \tag{3.79}$$

for $\alpha = 1, 2$. Also assume that the horizontal components of the stress tensor do not depend on X_3 to obtain

$$\mathcal{N}_{\alpha,\beta} = \int_{Z_b}^{Z_t} P_{\alpha,\beta} dX_3 = P_{\alpha,\beta} \int_{Z_b}^{Z_t} dX_3 = P_{\alpha,\beta} h_0 \tag{3.80}$$

for $\alpha, \beta = 1, 2$. Next, assume that the surface gradients vary slowly such that

$$\left| \frac{\partial Z_t}{\partial X_1} \right|, \left| \frac{\partial Z_t}{\partial X_2} \right|, \left| \frac{\partial Z_b}{\partial X_1} \right|, \left| \frac{\partial Z_b}{\partial X_2} \right| < \epsilon \tag{3.81}$$

where $\epsilon \ll 1$. Then to leading order the top and bottom surface normals are $\mathbf{N}_t = (0, 0, 1)$ and $\mathbf{N}_b = (0, 0, -1)$. The boundary conditions on the top surface then reduce to

$$\mathbf{T}_t = P\mathbf{N}_t = \begin{pmatrix} P_{31}(Z_t) \\ P_{32}(Z_t) \\ P_{33}(Z_t) \end{pmatrix}. \tag{3.82}$$

The normal traction on the top surface is equal to zero, and therefore, if $\mathbf{N}_t = (0, 0, 1)$, $P_{33}(Z_t) = 0$. The tangential traction due to the atmospheric winds is in the horizontal plane with this assumption so define this (two-dimensional) horizontal traction as

$$\widetilde{\mathbf{T}}_t = \begin{pmatrix} P_{31}(Z_t) \\ P_{32}(Z_t) \end{pmatrix}. \tag{3.83}$$

Similarly, the tangential traction due to the ocean currents on the bottom surface of the ice can be written as

$$\widetilde{\mathbf{T}}_b = \begin{pmatrix} P_{31}(Z_b) \\ P_{32}(Z_b) \end{pmatrix}. \tag{3.84}$$

The normal traction on the bottom surface is $P_{33}(Z_b)$ which is equal to the hydrostatic water pressure $\rho_w \mathbf{g}(Z_w - Z_b) = \rho_w \mathbf{g} h_w$.

Using these additional assumptions the third component of the momentum balance can be written as

$$
\int_{\Omega_{0,2}} \left(\frac{\partial \mathcal{N}_{31}}{\partial X_1} + \frac{\partial \mathcal{N}_{32}}{\partial X_2} \right) d\Omega
$$
$$
+ \int_{\Omega_{0,2}} \rho_w \mathbf{g} h_w d\Omega - \int_{\Omega_{0,2}} \rho_0 \mathbf{g} h_0 d\Omega = 0.
\tag{3.85}
$$

The first and second components become

$$
\int_{\Omega_{0,2}} \rho_0 h_0 \left(\dot{V}_1 - 2\omega V_2 \sin \phi \right) d\Omega = \int_{\Omega_{0,2}} \left(\frac{\partial (h_0 P_{11})}{\partial X_1} + \frac{\partial (h_0 P_{12})}{\partial X_2} + T_{b,1} + T_{t,1} \right) d\Omega
$$
$$
\int_{\Omega_{0,2}} \rho_0 h_0 \left(\dot{V}_2 + 2\omega V_1 \sin \phi \right) d\Omega = \int_{\Omega_{0,2}} \left(\frac{\partial (h_0 P_{21})}{\partial X_1} + \frac{\partial (h_0 P_{22})}{\partial X_2} + T_{b,2} + T_{t,2} \right) d\Omega.
\tag{3.86}
$$

Combining these equations results in a balance equation for momentum in the horizontal plane

$$
\int_{\Omega_{0,2}} \rho_0 h_0 \left(h_0 \dot{\widetilde{\mathbf{V}}} - 2\omega \sin \phi (\mathbf{e}_3 \times \widetilde{\mathbf{V}}) \right) d\Omega = \int_{\Omega_{0,2}} \left(\mathrm{Div}_{\mathbf{X}} (h_0 \widetilde{\mathbf{P}}) + \widetilde{\mathbf{T}}_b + \widetilde{\mathbf{T}}_t \right) d\Omega
\tag{3.87}
$$

where a two-dimensional velocity is defined as $\widetilde{\mathbf{V}} = \dot{\boldsymbol{\varphi}}_2 = (V_1, V_2)$, and a two-dimensional stress tensor, $\widetilde{\mathbf{P}}$ is defined as

$$
\widetilde{\mathbf{P}} = \begin{bmatrix} P_{11} & P_{12} \\ P_{21} & P_{22} \end{bmatrix}.
\tag{3.88}
$$

In practice, quadratic drag laws are generally used for the forces due to the atmospheric winds, $\widetilde{\mathbf{T}}_t$, and the forces due to the ocean, $\widetilde{\mathbf{T}}_b$, and are defined as

$$
\widetilde{\mathbf{T}}_t = c_a \rho_a \|\mathbf{V}_a\| Q_a \mathbf{V}_a
$$
$$
\widetilde{\mathbf{T}}_b = c_w \rho_w \|(\widetilde{\mathbf{V}} - \mathbf{V}_w)\| Q_w (\widetilde{\mathbf{V}} - \mathbf{V}_w)
\tag{3.89}
$$

where c_a is the air drag coefficient, ρ_a is the air density, $\mathbf{V}_a(X_1, X_2, t)$ is the two-dimensional air velocity, Q_a is the rotation matrix for the air turning angle, c_w is the water drag coefficient, ρ_w is the water density, $\mathbf{V}_w(X_1, X_2, t)$ is the two-dimensional water velocity, and Q_w is the rotation matrix for water turning angle. The wind and water velocities are measured or obtained from atmospheric and ocean models.

3.6 Conservation of Energy

For the conservation of energy derivation, begin again with a region of ice, $\Omega_0 \subset \mathcal{B} \subset \mathbb{R}^3$. A derivation of the energy equation can be found in many texts, see for example Malvern [29], whose method is followed here. The power input is the rate at which the surface tractions, $\mathbf{T}$, and body forces, $\mathbf{B}$, are doing work on the region and can be expressed as

$$P_{in} = \int_{\partial\Omega_0} \mathbf{T} \cdot \mathbf{V}_I dS + \int_{\Omega_0} \rho_0 \mathbf{B} \cdot \mathbf{V}_I d\Omega. \tag{3.90}$$

Note that the velocity in this equation is the inertial velocity. The surface tractions are related to the stress tensor, $\mathbf{P}$, by $\mathbf{T} = \mathbf{PN}$, where $\mathbf{N}$ is the normal to the surface in the reference configuration. Therefore the term in the surface integral can be written as $(\mathbf{PN}) \cdot \mathbf{V}_I = (\mathbf{P}^T \mathbf{V}_I) \cdot \mathbf{N}$. Using this relationship and the divergence theorem the surface integral term becomes

$$\int_{\partial\Omega_0} (\mathbf{P}^T \mathbf{V}_I) \cdot \mathbf{N} dS = \int_{\Omega_0} \text{Div}_{\mathbf{X}} (\mathbf{P}^T \mathbf{V}_I) d\Omega. \tag{3.91}$$

In components the divergence is

$$\left(\text{Div}_{\mathbf{X}} (\mathbf{P}^T \mathbf{V}_I)\right)_{ij} = \frac{\partial(\mathbf{P}_{ji} V_{I,i})}{\partial X_j}. \tag{3.92}$$

Expanding this term results in

$$V_{I,i} \frac{\partial P_{ji}}{\partial X_j} + P_{ji} \frac{\partial V_{I,i}}{\partial X_j} = \left((\text{Div}_{\mathbf{X}} \mathbf{P}) \cdot \mathbf{V}_I + \mathbf{P} : \dot{\mathbf{F}}\right)_{ij} \tag{3.93}$$

where the notation $\mathbf{A} : \mathbf{B}$ signifies the inner product of two tensors and can be written in component form as $A_{ij}B_{ij}$ using the summation convention for repeated indices. Therefore the power input can be written as

$$P_{in} = \int_{\Omega_0} \left((\mathrm{Div}_{\mathbf{X}}\mathbf{P} + \rho_0\mathbf{B}) \cdot \mathbf{V}_I + \mathbf{P} : \dot{\mathbf{F}} \right) d\Omega \tag{3.94}$$

The momentum balance equation for the system as shown in Section 3.3 is

$$\int_{\Omega_0} \rho_0 \dot{\mathbf{V}}_I d\Omega = \int_{\Omega_0} (\mathrm{Div}_{\mathbf{X}}\mathbf{P} + \rho_0\mathbf{B})d\Omega \tag{3.95}$$

where the velocity in this equation is the inertial velocity. So substituting this into the equation for power input gives

$$\begin{aligned} P_{in} &= \int_{\Omega_0} \left(\rho_0 \dot{\mathbf{V}}_I \cdot \mathbf{V}_I + \mathbf{P} : \mathbf{F} \right) d\Omega \\ &= \frac{d}{dt} \int_{\Omega_0} \frac{1}{2}\rho_0 \mathbf{V}_I \cdot \mathbf{V}_I d\Omega + \int_{\Omega_0} \mathbf{P} : \dot{\mathbf{F}} d\Omega \end{aligned} \tag{3.96}$$

The heat input to the system is defined as the sum of the conduction through the surface and the contribution from a distributed heat source, R, and is written as

$$Q_{in} = - \int_{\partial\Omega_0} \mathbf{Q} \cdot \mathbf{N} dS + \int_{\Omega_0} \rho_0 R d\Omega \tag{3.97}$$

Using the divergence theorem on the first term results in

$$\int_{\partial\Omega_0} \mathbf{Q} \cdot \mathbf{N} dS = \int_{\Omega_0} \mathrm{Div}_{\mathbf{X}}\mathbf{Q} d\Omega \tag{3.98}$$

and the heat input becomes

$$Q_{in} = \int_{\Omega_0} \left(-\mathrm{Div}_{\mathbf{X}}\mathbf{Q} + \rho_0 R \right) d\Omega. \tag{3.99}$$

The first law of thermodynamics states that the change in total energy (E_{total}) of the system satisfies

$$\dot{E}_{total} = P_{in} + Q_{in} \tag{3.100}$$

The total energy of the system contains contributions from kinetic energy and internal energy. If the internal energy per unit volume of the undeformed region is $E(\mathbf{X}, t)$, then

$$\dot{E}_{total} = \frac{d}{dt} \int_{\Omega_0} \left(\frac{1}{2} \rho_0 \mathbf{V}_I \cdot \mathbf{V}_I + E \right) d\Omega \tag{3.101}$$

Equating this to the power and heat input gives

$$
\begin{aligned}
\frac{d}{dt} \int_{\Omega_0} \left(\frac{1}{2} \rho_0 \mathbf{V}_I \cdot \mathbf{V}_I + E \right) d\Omega = {} & \frac{d}{dt} \int_{\Omega_0} \frac{1}{2} \rho_0 \mathbf{V}_I \cdot \mathbf{V}_I d\Omega \\
& + \int_{\Omega_0} \left(\mathbf{P} : \dot{\mathbf{F}} - \mathrm{Div}_{\mathbf{X}} \mathbf{Q} + \rho_0 R \right) d\Omega.
\end{aligned}
\tag{3.102}
$$

Rearranging terms and cancelling the kinetic energy terms on both sides results in the following familiar form of the energy equation

$$\int_{\Omega_0} \left(\dot{E} - \mathbf{P} : \dot{\mathbf{F}} + \mathrm{Div}_{\mathbf{X}} \mathbf{Q} - \rho_0 R \right) d\Omega = 0. \tag{3.103}$$

If this holds true for an arbitrary region $\Omega_0 \subset \mathcal{B}$ and the functions in the integral are continuous, then the local form of the energy balance can be written as

$$\dot{E} - \mathbf{P} : \dot{\mathbf{F}} + \mathrm{Div}_{\mathbf{X}} \mathbf{Q} - \rho_0 R = 0. \tag{3.104}$$

In order to derive the thermodynamic heat equation used in sea ice modeling as well as the elastic-decohesive constitutive model, restrictions based on the second law of thermodynamics must be considered. The second law can be written as

$$\frac{d}{dt} \int_{\Omega_0} \eta \, d\Omega - \int_{\Omega_0} \rho_0 \frac{R}{T} d\Omega + \int_{\partial\Omega} \frac{\mathbf{Q} \cdot \mathbf{N}}{T} dA \geq 0 \tag{3.105}$$

where T is the temperature and η is the entropy per unit volume. Using the divergence theorem on the third integral gives

$$\frac{d}{dt} \int_{\Omega_0} \eta \, d\Omega - \int_{\Omega_0} \rho_0 \frac{R}{T} d\Omega + \int_{\Omega_0} \mathrm{Div}_{\mathbf{X}} \left(\frac{\mathbf{Q}}{T} \right) d\Omega \geq 0. \tag{3.106}$$

Expanding the final term and multiplying by T results in

$$\int_{\Omega_0} \left(T\dot{\eta} - \rho_0 R + \mathrm{Div}_{\mathbf{X}} \mathbf{Q} - \frac{\mathbf{Q}}{T} \cdot \mathrm{Grad}_{\mathbf{X}} T \right) d\Omega \geq 0. \tag{3.107}$$

The dissipation inequality can be obtained by substituting the energy conservation equation (first law) into the equation for the second law which gives

$$\int_{\Omega_0} \left(T\dot{\eta} - \dot{E} + \mathbf{P} : \dot{\mathbf{F}} - \frac{\mathbf{Q}}{T} \cdot \mathrm{Grad}_{\mathbf{X}}T \right) \geq 0 \tag{3.108}$$

Now introduce the Helmholtz free energy, which is defined as

$$A = \inf_{\eta}(E - T\eta). \tag{3.109}$$

Substituting the Helmholtz free energy into the dissipation inequality

$$\int_{\Omega_0} \left(-\dot{A} - \dot{T}\eta + \mathbf{P} : \dot{\mathbf{F}} - \frac{\mathbf{Q}}{T} \cdot \mathrm{Grad}_{\mathbf{X}}T \right) d\Omega \geq 0. \tag{3.110}$$

Given an appropriate form of A, the constitutive model can be derived from this dissipation inequality and the ice thermodynamic equation can be derived from the energy equation. In the case of sea ice, the mechanical and thermodynamic contributions to the internal energy are assumed to decompose additively. Therefore, assume that the Helmholtz free energy can be divided into mechanical and thermodynamic parts as $A = W(\mathbf{F}, \mathcal{I}) + V(T)$, where $\mathcal{I}$ is a set of internal variables related to the constitutive model. The function W must further be divided based on assumptions underlying the elastic-decohesive constitutive model. However, before the final form W can be considered, some definitions relating to strong discontinuities and distributions must be discussed.

3.6.1   Strong Discontinuities and Distributions

In order to derive the elastic-decohesive constutive model, a detour into discontinuities and distributions is needed. Cracks are explicitly included in this constitutive model and the framework of strong discontinuities developed by Simo *et al.* [43] and applied to a finite strain regime by Armero and Garikipati [4], [11] among others can be used for the theoretical basis.

Consider a discontinuity in $\mathcal{B}$ along a surface Γ with unit normal $\mathbf{N_\Gamma}$ as shown in Figure 3.4. Assume that in a local region $\Omega_\Gamma \subset \mathcal{B}$, the discontinuity splits the region into two parts, Ω_Γ^+ and Ω_Γ^-. The deformation mapping can then be written as

$$\boldsymbol{\varphi}(\mathbf{X}) = \bar{\boldsymbol{\varphi}}(\mathbf{X}) + [\![\boldsymbol{\varphi}]\!] H_\Gamma(\mathbf{X}) \tag{3.111}$$

where $\bar{\boldsymbol{\varphi}}$ is the continuous part of the deformation, $[\![\boldsymbol{\varphi}]\!]$ is the jump discontinuity and the Heaviside function on Γ is defined as

$$H_\Gamma(\mathbf{X}) = \begin{cases} 1 \ \mathbf{X} \in \Omega_\Gamma^+ \\ 0 \ \mathbf{X} \in \Omega_\Gamma^- \end{cases}. \tag{3.112}$$
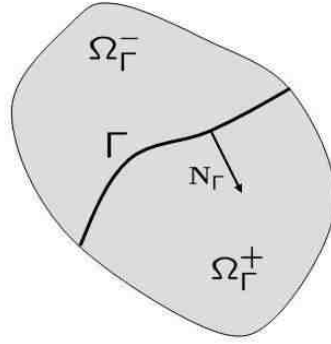
Figure 3.4: Ice region with discontinuity surface

The deformation gradient corresponding to $\boldsymbol{\varphi}(\mathbf{X})$ is then

$$\mathbf{F} = \mathrm{Grad}_\mathbf{X} \bar{\boldsymbol{\varphi}} + \mathrm{Grad}_\mathbf{X}[\![\boldsymbol{\varphi}]\!] H_\Gamma + [\![\boldsymbol{\varphi}]\!] \mathrm{Grad}_\mathbf{X} H_\Gamma. \tag{3.113}$$

The final component of the deformation gradient can be understood in terms of distributions. See for example Stakgold [44] or Hunter and Nachtergaele [20]. Let ϕ be a test function from the Schwartz space, $\mathcal{S}$, where $\mathrm{supp}(\phi) \subset \Omega_\Gamma$. Here $\mathcal{S}$ is defined as

$$\mathcal{S} = \{\phi \in C^\infty(\mathbb{R}^3) \text{ s.t. } \|\mathbf{X}^\alpha D^\beta \phi\|_\infty < \infty \ \forall \alpha, \beta\} \tag{3.114}$$

for

$$\mathbf{X}^\alpha = \prod_{i=1}^{3} X_i^{\alpha_i} \tag{3.115}$$

and

$$D^\beta = \left(\frac{\partial}{\partial X_1}\right)^{\beta_1} \left(\frac{\partial}{\partial X_2}\right)^{\beta_2} \left(\frac{\partial}{\partial X_3}\right)^{\beta_3}. \tag{3.116}$$

Given a function $f(\mathbf{X}) : \Omega_\Gamma \to \mathbb{R}^3$ define the linear functional

$$\langle f, \phi \rangle = \int_{\Omega_\Gamma} f \cdot \phi d\Omega \tag{3.117}$$

In a distributional sense, the derivative of a function f can be defined as

$$\langle \mathrm{Grad}_\mathbf{X} f, \phi \rangle = \int_{\Omega_\Gamma} \mathrm{Grad}_\mathbf{X} f \cdot \phi d\Omega = -\int_{\Omega_\Gamma} f \cdot \mathrm{Grad}_\mathbf{X} \phi d\Omega = -\langle f, \mathrm{Grad}_\mathbf{X} \phi \rangle \tag{3.118}$$

where integration by parts is used along with the fact that ϕ vanishes on the boundary of Ω_Γ. Now consider the Heaviside function on Γ, which can be defined in terms of distributions by the following functional

$$\int_{\Omega_\Gamma} H_\Gamma \cdot \phi d\Omega = \int_{\Omega_\Gamma^+} \phi d\Omega. \tag{3.119}$$

The gradient of H_Γ can then be found as

$$\langle \mathrm{Grad}_\mathbf{X} H_\Gamma, \phi \rangle = -\int_{\Omega_\Gamma} H_\Gamma \cdot (\mathrm{Grad}_\mathbf{X} \phi) d\Omega = -\int_{\Omega_\Gamma^+} \mathrm{Grad}_\mathbf{X} \phi d\Omega. \tag{3.120}$$

Now using the divergence theorem

$$\int_{\Omega_\Gamma^+} \mathrm{Grad}_\mathbf{X} \phi d\Omega = \int_{\partial \Omega_\Gamma^+} (\phi \otimes \mathbf{N}^-) dS \tag{3.121}$$

where $\mathbf{N}^-$ is the normal pointing outward along the boundary and the notation $\otimes$ represents the tensor product operator for two vectors so that in component form $(\mathbf{a} \otimes \mathbf{b})_{ij} = a_i b_j$. Since ϕ vanishes on the boundary, $\partial \Omega_\Gamma$, the integral is only nonzero

along the portion of $\partial\Omega_\Gamma^+$ in the interior of Ω_Γ, which is defined by the surface Γ. If the outward normal is replaced by the normal $\mathbf{N}_\Gamma$, which points into Ω_Γ^+

$$\int_{\Omega_\Gamma^+} \text{Grad}_\mathbf{X}\phi\, d\Omega = -\int_\Gamma (\phi \otimes \mathbf{N}_\Gamma) d\Gamma \tag{3.122}$$

and therefore

$$\langle \text{Grad}_\mathbf{X} H_\Gamma, \phi \rangle = \int_\Gamma (\phi \otimes \mathbf{N}_\Gamma) dS. \tag{3.123}$$

Note that the delta function along Γ is defined in this framework as

$$\langle \delta_\Gamma, \phi \rangle = \int_{\Omega_\Gamma} \delta_\Gamma \phi\, d\Omega = \int_\Gamma \phi\, d\Gamma \tag{3.124}$$

which implies that

$$\langle \text{Grad}_\mathbf{X} H_\Gamma, \phi \rangle = \langle \delta_\Gamma, (\phi \otimes \mathbf{N}_\Gamma) \rangle. \tag{3.125}$$

With these definitions the deformation gradient can be written as

$$\mathbf{F} = \text{Grad}_\mathbf{X}\bar{\boldsymbol{\varphi}} + \text{Grad}_\mathbf{X}[\![\boldsymbol{\varphi}]\!] H_\Gamma + \big([\![\boldsymbol{\varphi}]\!] \otimes \mathbf{N}_\Gamma\big)\delta_\Gamma. \tag{3.126}$$

Note that $[\![\boldsymbol{\varphi}]\!]$ is assumed to be continuously differentiable in general. Now define the regular part of $\mathbf{F}$ as

$$\overline{\mathbf{F}} = \text{Grad}_\mathbf{X}\bar{\boldsymbol{\varphi}} + \text{Grad}_\mathbf{X}[\![\boldsymbol{\varphi}]\!] H_\Gamma \tag{3.127}$$

and then

$$\mathbf{F} = \overline{\mathbf{F}} + \big([\![\boldsymbol{\varphi}]\!] \otimes \mathbf{N}_\Gamma\big)\delta_\Gamma \tag{3.128}$$

In the following section, this form will be used in the dissipation inequality for the derivation of the constitutive model.

3.6.2 Elastic-Decohesive Constitutive Model

Consider again the form of the Helmholtz free energy discussed above, $A = W(\mathbf{F}, \mathcal{I}) + V(T)$. In the case of the elastic-decohesive constitutive model it is assumed that the deformation is purely elastic except on the decohesive surface. Therefore, the portion of W that defines the elastic response must depend on the regular part of the deformation gradient, $\overline{\mathbf{F}}$. It can be further shown that for a frame indifferent or objective response, W must depend on $\overline{\mathbf{F}}$ through the right Cauchy-Green strain tensor, $\overline{\mathbf{C}} = \overline{\mathbf{F}}^T \overline{\mathbf{F}}$. For a proof of this see Simo and Hughes [42]. Following Armero [3], assume that W consists of bulk, $\overline{W}$, and surface, $\widetilde{W}$, terms of the following form

$$W = \overline{W}(\overline{\mathbf{C}}) + \widetilde{W}(\tilde{u})\delta_\Gamma \tag{3.129}$$

where $\tilde{u}$ is an internal variable related to the jump in displacement.

Using this form of W, $\dot{A}$ can be written as

$$\dot{A} = \frac{\partial \overline{W}}{\partial \overline{\mathbf{C}}}\dot{\overline{\mathbf{C}}} + \frac{\partial \widetilde{W}}{\partial \tilde{u}}\dot{\tilde{u}}\delta_\Gamma + \frac{\partial V}{\partial T}\dot{T}. \tag{3.130}$$

Recall that the dissipation inequality is of the following form

$$\int_{\Omega_\Gamma} \left(-\dot{A} - \dot{T}\eta + \mathbf{P} : \dot{\mathbf{F}} - \frac{\mathbf{Q}}{T} \cdot \mathrm{Grad}_{\mathbf{X}}T \right) d\Omega \geq 0. \tag{3.131}$$

Substituting $\dot{A}$ into the dissipation inequality gives

$$\int_{\Omega_\Gamma} \left(-\dot{T}\eta + \mathbf{P} : \dot{\mathbf{F}} - \frac{\partial \overline{W}}{\partial \overline{\mathbf{C}}}\dot{\overline{\mathbf{C}}} - \frac{\partial \widetilde{W}}{\partial \tilde{u}}\dot{\tilde{u}}\delta_\Gamma - \frac{\partial V}{\partial T}\dot{T} - \frac{\mathbf{Q}}{T} \cdot \mathrm{Grad}_{\mathbf{X}}T \right) d\Omega \geq 0. \tag{3.132}$$

Using the definition of $\mathbf{F}$ above, the dissipation inequality becomes

$$\int_{\Omega_\Gamma} \left(-\dot{T}\eta + \mathbf{P} : \left(\dot{\overline{\mathbf{F}}} + (\llbracket \dot{\boldsymbol{\varphi}} \rrbracket \otimes \mathbf{N}_\Gamma)\delta_\Gamma \right) - \frac{\partial \overline{W}}{\partial \overline{\mathbf{C}}}\dot{\overline{\mathbf{C}}} - \frac{\partial \widetilde{W}}{\partial \tilde{u}}\dot{\tilde{u}}\delta_\Gamma - \frac{\partial V}{\partial T}\dot{T} \right) d\Omega$$
$$+ \int_{\Omega_\Gamma} -\frac{\mathbf{Q}}{T} \cdot \mathrm{Grad}_{\mathbf{X}}T d\Omega \geq 0 \tag{3.133}$$

Now define the second Piola-Kirchhoff stress as $\mathbf{S} = \overline{\mathbf{F}}^{-1}\mathbf{P}$. Substituting this relationship into the dissipation inequality and rearranging terms gives

$$\int_{\Omega_\Gamma} \left(\left(-\dot{T}\eta - \frac{\partial V}{\partial T}\dot{T} \right) + \left(\overline{\mathbf{F}}\mathbf{S} : \dot{\overline{\mathbf{F}}} - \frac{\partial \overline{W}}{\partial \overline{\mathbf{C}}}\dot{\overline{\mathbf{C}}} \right) + \mathbf{P} : (\llbracket \dot{\boldsymbol{\varphi}} \rrbracket \otimes \mathbf{N}_\Gamma)\delta_\Gamma - \frac{\partial \widetilde{W}}{\partial \tilde{u}}\dot{\tilde{u}}\delta_\Gamma \right) d\Omega$$
$$+ \int_{\Omega_\Gamma} -\frac{\mathbf{Q}}{T} \cdot \mathrm{Grad}_{\mathbf{X}} T d\Omega \geq 0.$$

$$(3.134)$$

Note that

$$\overline{\mathbf{F}}\mathbf{S} : \dot{\overline{\mathbf{F}}} = \frac{1}{2}\mathbf{S} : \dot{\overline{\mathbf{C}}} \tag{3.135}$$

and therefore

$$\int_{\Omega_\Gamma} \left(-\left(\eta + \frac{\partial V}{\partial T} \right)\dot{T} + \left(\frac{1}{2}\mathbf{S} - \frac{\partial \overline{W}}{\partial \overline{\mathbf{C}}} \right) : \dot{\overline{\mathbf{C}}} + \mathbf{P} : (\llbracket \dot{\boldsymbol{\varphi}} \rrbracket \otimes \mathbf{N}_\Gamma)\delta_\Gamma - \frac{\partial \widetilde{W}}{\partial \tilde{u}}\dot{\tilde{u}}\delta_\Gamma \right) d\Omega$$
$$+ \int_{\Omega_\Gamma} -\frac{\mathbf{Q}}{T} \cdot \mathrm{Grad}_{\mathbf{X}} T d\Omega \geq 0.$$

$$(3.136)$$

If $\dot{\overline{\mathbf{C}}}$ and $\dot{T}$ are arbitrary rates, then the following relationships must hold if the dissipation inequality is to be satisfied

$$\mathbf{S} = 2\frac{\partial \overline{W}}{\partial \overline{\mathbf{C}}} \tag{3.137}$$

$$\eta = -\frac{\partial V}{\partial T}. \tag{3.138}$$

The first equation for the stress is the elastic part of the constitutive model. The equation for the entropy, η, will be discussed later.

Given these relationships the reduced dissipation inequality becomes

$$\int_{\Omega_\Gamma} \left(\mathbf{P} : (\llbracket \dot{\boldsymbol{\varphi}} \rrbracket \otimes \mathbf{N}_\Gamma)\delta_\Gamma - \frac{\partial \widetilde{W}}{\partial \tilde{u}}\dot{\tilde{u}}\delta_\Gamma \right) d\Omega + \int_{\Omega_\Gamma} -\frac{\mathbf{Q}}{T} \cdot \mathrm{Grad}_{\mathbf{X}} T d\Omega \geq 0 \tag{3.139}$$

Now, for an isothermal process, the second integral in Equation 3.139 is zero and the first integral must satisfy the inequality by itself. Conversely, for a purely elastic process with no decohesion the first integral is zero and the second integral must satisfy the inequality separately. If $\mathbf{Q}$ obeys Fourier's Law of conduction, then

$$\mathbf{Q} = -k(\mathbf{X}, T)\mathrm{Grad}_{\mathbf{X}}T \tag{3.140}$$

and

$$-\frac{\mathbf{Q}}{T} \cdot \mathrm{Grad}_{\mathbf{X}}T = +\frac{k(\mathbf{X}, T)}{T}\mathrm{Grad}_{\mathbf{X}}T \cdot \mathrm{Grad}_{\mathbf{X}}T. \tag{3.141}$$

With this form the inequality for the second integral alone is automatically satisfied given that $k(\mathbf{X}, T) > 0$. Therefore, for the remaining discussion, consider only the following piece of the reduced dissipation inequality

$$\int_{\Omega_\Gamma} \left(\mathbf{P} : (\llbracket \dot{\boldsymbol{\varphi}} \rrbracket \otimes \mathbf{N}_\Gamma)\delta_\Gamma - \frac{\partial \widetilde{W}}{\partial \tilde{u}}\dot{\tilde{u}}\delta_\Gamma \right) d\Omega \geq 0 \tag{3.142}$$

In a finite strain context there are several stress tensors and strain tensors that may be used interchangeably if the appropriate conversions are employed. The elastic-decohesive constitutive model will be derived in terms of the Kirchhoff stress, $\boldsymbol{\tau} = \mathbf{P}\overline{\mathbf{F}}^T = \overline{\mathbf{F}}\mathbf{S}\overline{\mathbf{F}}^T$ because using this stress measure results in a formulation that is similar in form to the infinitesimal strain case. Each stress measure must be used with its conjugate strain measure for the equations to remain consistent. The conjugate strain to the Kirchhoff stress is the rate of deformation tensor defined as $\bar{\mathbf{d}} = \mathrm{sym}(\dot{\overline{\mathbf{F}}}\mathbf{F}^{-1})$. Given these definitions the following stress and strain rate relationships hold

$$\mathbf{P} : \dot{\overline{\mathbf{F}}} = \mathbf{S} : \frac{1}{2}\dot{\overline{\mathbf{C}}} = \boldsymbol{\tau} : \bar{\mathbf{d}}. \tag{3.143}$$

The first part of the elastic-decohesive constitutive model is the elastic relation from Equation 3.137, which can be written in rate form as

$$\dot{\mathbf{S}} = 4\frac{\partial^2 \overline{W}}{\partial \mathbf{C}^2} : \frac{1}{2}\dot{\overline{\mathbf{C}}} = \mathbb{C} : \frac{1}{2}\dot{\overline{\mathbf{C}}} \tag{3.144}$$

where $\mathbb{C}$ is the fourth-order elasticity tensor in the reference configuration. The Cauchy-Green strain tensor can be related to the rate of deformation in the following way

$$
\begin{aligned}
\dot{\overline{\mathbf{C}}} &= (\dot{\overline{\mathbf{F}}}\overline{\mathbf{F}}^T + \overline{\mathbf{F}}\dot{\overline{\mathbf{F}}}^T) \\
&= \overline{\mathbf{F}}(\overline{\mathbf{F}}^{-1}\dot{\overline{\mathbf{F}}} + \dot{\overline{\mathbf{F}}}^T\overline{\mathbf{F}}^{-T})\overline{\mathbf{F}}^T \\
&= \overline{\mathbf{F}}\overline{\mathbf{d}}\overline{\mathbf{F}}^T
\end{aligned}
\tag{3.145}
$$

Using this relationship the elastic constitutive relation is

$$
\dot{\mathbf{S}} = \mathbb{C} : \frac{1}{4}(\overline{\mathbf{F}}^T\overline{\mathbf{d}}\overline{\mathbf{F}})
\tag{3.146}
$$

To transform this into a relationship between $\boldsymbol{\tau}$ and $\overline{\mathbf{d}}$, define the Lie derivative of the Kirchhoff stress as $\mathcal{L}_v\boldsymbol{\tau} = \overline{\mathbf{F}}\dot{\mathbf{S}}\overline{\mathbf{F}}^T$. Then

$$
\mathcal{L}_v\boldsymbol{\tau} = \overline{\mathbf{F}}\mathbb{C} : (\overline{\mathbf{F}}^T\overline{\mathbf{d}}\overline{\mathbf{F}})\overline{\mathbf{F}}^T = \mathbf{c} : \overline{\mathbf{d}}
\tag{3.147}
$$

where $\mathbf{c}$ is the elasticity tensor in the current configuration and is related to $\mathbb{C}$ by

$$
c_{ijkl} = F_{iI}F_{jJ}F_{kK}F_{lL}\mathbb{C}_{IJKL}.
\tag{3.148}
$$

For the decohesive portion of the constitutive model, consider the dissipation inequality (Equation 3.142), which is written in terms of $\boldsymbol{\tau}$ as

$$
\int_{\Omega_\Gamma} \left(\boldsymbol{\tau} : (\llbracket\dot{\boldsymbol{\varphi}}\rrbracket \otimes \mathbf{n}_\Gamma)\delta_\Gamma - \frac{\partial\widetilde{W}}{\partial\tilde{u}}\dot{\tilde{u}}\delta_\Gamma \right) d\Omega \geq 0
\tag{3.149}
$$

where $\mathbf{n}_\Gamma = \overline{\mathbf{F}}^{-T}\mathbf{N}_\Gamma$ is the normal in the current configuration. Let $\tilde{t} = -\partial\widetilde{W}/\partial\tilde{u}$ and the remaining portion of the dissipation inequality becomes

$$
\mathcal{D} = \int_{\Omega_\Gamma} \left(\boldsymbol{\tau} : \llbracket\dot{\boldsymbol{\varphi}}\rrbracket \otimes \mathbf{n} + \tilde{t}\dot{\tilde{u}} \right) \delta_\Gamma d\Omega \geq 0
\tag{3.150}
$$

which is equivalent to

$$
\mathcal{D} = \int_\Gamma \left(\mathbf{t} \cdot \llbracket\dot{\boldsymbol{\varphi}}\rrbracket + \tilde{t}\dot{\tilde{u}} \right) d\Gamma \geq 0
\tag{3.151}
$$

for a traction, $\mathbf{t}$, defined as $\mathbf{t} = \boldsymbol{\tau}\mathbf{n}$.

Assume the existence of a damage function, $\Phi(\mathbf{t}, \tilde{t})$, analogous to a yield function in plasticity, that defines an elastic domain $\mathbb{E}$ in stress space

$$\mathbb{E} = \{(\mathbf{t}, \tilde{t}) \in \mathbb{R}^3 \times \mathbb{R} \text{ s.t. } \Phi(\mathbf{t}, \tilde{t}) < 0\}. \tag{3.152}$$

Flow rules for the discontinuity and $\tilde{u}$ can be derived by defining a minimization problem with the constraint $\Phi = 0$. This is based on the principle of maximum plastic dissipation, which states that for given plastic strains, the actual stress tensor is the one which allows the dissipation to reach its maximum over all possible stress tensors that satisfy the yield criterion [42]. In this context the decohesive strains, $(\llbracket \dot{\boldsymbol{\varphi}} \rrbracket \otimes \mathbf{n}\delta_\Gamma)$ must satisfy this property rather than the plastic strains. This principle can be expressed as a minimization problem by considering the following functional

$$\mathcal{L} = -\mathcal{D} + \int_{\Omega_0} \omega\Phi d\Omega \tag{3.153}$$

where the Lagrange multiplier, ω, is called the decohesive evolution parameter. Expanding $\mathcal{L}$ results in

$$\mathcal{L}(\mathbf{t}, \tilde{t}) = -\int_\Gamma \left(\mathbf{t} \cdot \llbracket \dot{\boldsymbol{\varphi}} \rrbracket + \tilde{t}\dot{\tilde{u}}\right) d\Gamma + \int_\Omega \omega\Phi(\mathbf{t}, \tilde{t})d\Omega. \tag{3.154}$$

In order for this equation to make sense $\omega\Phi$ must be restricted to the discontinuity surface, Γ. Now Φ is defined in all stress space, but the evolution of the jump discontinuity only occurs on Γ. Therefore, let $\omega = \tilde{\omega}\delta_\Gamma$ and then $\mathcal{L}$ becomes

$$\mathcal{L}(\mathbf{t}, \tilde{t}) = \int_\Gamma \left(-\mathbf{t} \cdot \llbracket \dot{\boldsymbol{\varphi}} \rrbracket - \tilde{t}\dot{\tilde{u}} + \tilde{\omega}\Phi(\mathbf{t}, \tilde{t})\right) d\Gamma. \tag{3.155}$$

The first variation of $\mathcal{L}$ is

$$\delta\mathcal{L} = -\frac{\partial}{\partial\xi}\mathcal{L}(\mathbf{t} + \xi\boldsymbol{\nu}, \tilde{T} + \xi\mu)\Big|_{\xi=0}. \tag{3.156}$$

An extremum of $\mathcal{L}$ can be found by setting $\delta\mathcal{L}$ equal to zero. Using the functional form above results in

$$\delta\mathcal{L} = -\int_\Gamma \left(\boldsymbol{\nu} \cdot \llbracket \dot{\boldsymbol{\varphi}} \rrbracket + \mu\dot{\tilde{u}} - \tilde{\omega}\left(\frac{\partial\Phi}{\partial\mathbf{t}} \cdot \boldsymbol{\nu} + \frac{\partial\Phi}{\partial\tilde{t}}\mu\right)\right) d\Gamma. \tag{3.157}$$

Rearranging terms

$$\delta\mathcal{L} = \int_{\Gamma} \left(\left([\![\dot{\boldsymbol{\varphi}}]\!] - \tilde{\omega}\frac{\partial\Phi}{\partial\mathbf{t}} \right) \cdot \boldsymbol{\nu} + \left(\dot{\tilde{u}} - \tilde{\omega}\frac{\partial\Phi}{\partial\tilde{t}} \right) \mu \right) d\Gamma. \tag{3.158}$$

Now $\delta\mathcal{L} = 0$ for arbitrary variations $(\boldsymbol{\nu}, \mu)$ implies that the following associative flow rules hold on Γ

$$\begin{aligned} [\![\dot{\boldsymbol{\varphi}}]\!] &= \tilde{\omega}\frac{\partial\Phi}{\partial\mathbf{t}} \\ \dot{\tilde{u}} &= \tilde{\omega}\frac{\partial\Phi}{\partial\tilde{t}}. \end{aligned} \tag{3.159}$$

These flow rules along with the consistency condition $(\dot{\Phi} = 0)$ define the decohesive portion of the constitutive model. In this case the consistency condition is

$$\dot{\Phi} = \frac{\partial\Phi}{\partial\mathbf{t}} \cdot \dot{\mathbf{t}} + \frac{\partial\Phi}{\partial\tilde{t}}\dot{\tilde{t}} = 0. \tag{3.160}$$

Now the traction can be defined as $\mathbf{t} = \boldsymbol{\tau}\mathbf{n} = \mathbf{P}\overline{\mathbf{F}}^{T}\mathbf{F}^{-T}\mathbf{N} = \mathbf{P}\mathbf{N}$ and therefore, the material derivative of the traction can be written as

$$\begin{aligned} \dot{\mathbf{t}} = \dot{\mathbf{P}}\mathbf{N} &= (\dot{\overline{\mathbf{F}}}\mathbf{S} + \overline{\mathbf{F}}\dot{\mathbf{S}})\mathbf{N} \\ &= \dot{\overline{\mathbf{F}}}\overline{\mathbf{F}}^{-1}\overline{\mathbf{F}}\mathbf{S}\overline{\mathbf{F}}^{T}\mathbf{n} + \overline{\mathbf{F}}\dot{\mathbf{S}}\overline{\mathbf{F}}^{T}\mathbf{n} \\ &= \bar{\mathbf{l}}\boldsymbol{\tau}\mathbf{n} + \mathcal{L}_{v}(\boldsymbol{\tau})\mathbf{n} = \bar{\mathbf{l}}\mathbf{t} + (\mathbf{c} : \bar{\mathbf{d}})\mathbf{n} \end{aligned} \tag{3.161}$$

where $\bar{\mathbf{l}} = \dot{\overline{\mathbf{F}}}\overline{\mathbf{F}}^{-1}$ and $\bar{\mathbf{d}} = \text{sym}(\bar{\mathbf{l}})$. Define the hardening law as

$$\dot{\tilde{t}} = \frac{\partial^{2}\widetilde{W}}{\partial\tilde{u}^{2}}\dot{\tilde{u}} = \mathbb{H}\dot{\tilde{u}} \tag{3.162}$$

After substituting the expression for $\dot{\mathbf{t}}$ and the expression for the hardening law, the consistency condition becomes

$$\dot{\Phi} = \frac{\partial\Phi}{\partial\mathbf{t}} \cdot \left((\bar{\mathbf{l}}\mathbf{t} + (\mathbf{c} : \bar{\mathbf{d}})\mathbf{n}\right) + \frac{\partial\Phi}{\partial\tilde{t}}\mathbb{H}\dot{\tilde{u}} \tag{3.163}$$

Now $\bar{\mathbf{l}} = \mathbf{l} - \tilde{\mathbf{l}}$ where $\tilde{\mathbf{l}} = [\![\dot{\boldsymbol{\varphi}}]\!] \otimes \mathbf{n}\delta_{\Gamma}$. Given that $\mathbf{d} = \text{sym}(\mathbf{l})$, $\bar{\mathbf{d}} = \mathbf{d} - \tilde{\mathbf{d}}$ where $\tilde{\mathbf{d}} = ([\![\dot{\boldsymbol{\varphi}}]\!] \otimes \mathbf{n})^{s}\delta_{\Gamma}$ Adding this relationship and the flow rules to the consistency condition results in

$$\dot{\Phi} = \frac{\partial\Phi}{\partial\mathbf{t}} \cdot \left(\left(\mathbf{l} - \tilde{\omega}\frac{\partial\Phi}{\partial\mathbf{t}} \otimes \mathbf{n}\delta_{\Gamma}\right)\mathbf{t} + \mathbf{c} : \left(\mathbf{d} - \tilde{\omega}\left(\frac{\partial\Phi}{\partial\mathbf{t}} \otimes \mathbf{n}\right)^{s}\delta_{\Gamma}\right)\mathbf{n} \right) + \tilde{\omega}\frac{\partial\Phi}{\partial\tilde{t}}\mathbb{H}\frac{\partial\Phi}{\partial\tilde{t}} = 0$$

$$(3.164)$$

Now consider, for the elastic-decohesive constitutive model, the following convenient stored-energy function

$$W = \overline{W}(\overline{\mathbf{C}}) + \widetilde{W}(\tilde{u})\delta_\Gamma$$
$$= \lambda \frac{J^2 - 1}{4} - \left(\frac{\lambda}{2} + G\right)\ln J + \frac{1}{2}G(\mathrm{tr}\overline{\mathbf{C}} - 3) + \frac{1}{2}\langle 1 - \tilde{u}\rangle^2 \delta_\Gamma \qquad (3.165)$$

where G is the shear modulus, λ is the first Lamé parameter, and $J = \det(\overline{\mathbf{F}})$. The elastic portion of the stored-energy is due to Ciarlet [42]. Using this stored-energy function $\mathbf{S}$ is calculated as

$$\mathbf{S} = 2\frac{\partial \overline{W}}{\partial \overline{\mathbf{C}}} = \lambda \frac{(J^2 - 1)}{2}\overline{\mathbf{C}}^{-1} + G(\mathbf{I} - \overline{\mathbf{C}}^{-1}) \qquad (3.166)$$

From this $\boldsymbol{\tau}$ can be determined as

$$\boldsymbol{\tau} = \overline{\mathbf{F}}\mathbf{S}\overline{\mathbf{F}}^T = \lambda \frac{(J^2 - 1)}{2}\mathbf{I} + G(\overline{\mathbf{F}}\overline{\mathbf{F}}^T - \mathbf{I}) \qquad (3.167)$$

The material elasticity tensor can be calculated as

$$\mathbb{C} = 4\frac{\partial \overline{W}}{\partial \overline{\mathbf{C}}} = \lambda J^2 \overline{\mathbf{C}}^{-1} \otimes \overline{\mathbf{C}}^{-1} + \left(2G + \lambda(1 - J^2)\right)\frac{\partial \overline{\mathbf{C}}^{-1}}{\partial \overline{\mathbf{C}}} \qquad (3.168)$$

and the spatial elasticity tensor ($c_{ijkl} = F_{iI}F_{jJ}F_{kK}F_{lL}\mathbb{C}_{IJKL}$) can be calculated from $\mathbb{C}$ as

$$\mathbf{c} = \lambda J^2 \mathbf{I} \otimes \mathbf{I} + 2G\left(1 + \frac{\lambda}{2G}(1 - J^2)\right)\mathbb{I} \qquad (3.169)$$

where $\mathbb{I}$ has components $\mathbb{I}_{ijkl} = \delta_{ik}\delta_{jl} + \delta_{il}\delta_{jk}$. Let $\hat{\lambda} = \lambda J^2$ and

$$\hat{G} = G + \frac{\lambda}{2}(1 - J^2) \qquad (3.170)$$

then the spatial elasticity tensor has the same form as the small strain constant elasticity tensor

$$c_{ijkl} = \hat{\lambda}\delta_{ij}\delta_{kl} + 2\hat{G}(\delta_{ik}\delta_{jl} + \delta_{il}\delta_{jk}) \qquad (3.171)$$

Assume that the jump discontinuity lies in the plane of the ice and that Γ is smooth. Then define the normal and tangential directions to the displacement jump in the plane of the ice in terms of the global coordinates in the current configuration as

$$
\begin{aligned}
\mathbf{n} &= (\cos\theta, \sin\theta) \\
\mathbf{s} &= (-\sin\theta, \cos\theta)
\end{aligned}
\tag{3.172}
$$

where θ is the angle the normal makes to the x_1 coordinate in the plane of the ice.

In terms of the elastic response in the bulk material, plane stress is assumed. Note that this assumption is inconsistent with the general assumption of incompressibility used in deriving the ice thickness distribution. Given that $\mathcal{L}_v(\boldsymbol{\tau}) = \mathbf{c} : \overline{\mathbf{d}}$, the stress components in terms of the coordinates defined by the normal to the displacement jump are

$$
\begin{aligned}
\mathcal{L}_v(\tau)_{nn} &= \mathcal{E}_1 \bar{d}_{nn} + \mathcal{E}_2 \bar{d}_{ss} \\
\mathcal{L}_v(\tau)_{ss} &= \mathcal{E}_2 \bar{d}_{nn} + \mathcal{E}_1 \bar{d}_{ss} \\
\mathcal{L}_v(\tau)_{ns} &= 2\hat{G} \bar{d}_{ns}
\end{aligned}
\tag{3.173}
$$

where

$$
\mathcal{E}_1 = \hat{\lambda} + 2\hat{G} - \frac{\hat{\lambda}}{\hat{\lambda} + 2\hat{G}} \; , \; \mathcal{E}_2 = \hat{\lambda} - \frac{\hat{\lambda}}{\hat{\lambda} + 2\hat{G}}
\tag{3.174}
$$

The elastic-decohesive model used in the sea ice application is due to Schreyer [37], [38]. For this application a damage function of following form is used

$$
\begin{aligned}
\Phi &= \left(\frac{t_s}{t_{sm}}\right)^2 + e^{\kappa B_n} - 1 \\
B_n &= \frac{t_n}{t_{nf}} - \tilde{t}\left(1 - \frac{\langle -\tau_{ss}\rangle^2}{f_c'^2}\right)
\end{aligned}
\tag{3.175}
$$

where t_{nf} is the failure stress in tension, t_{sm}, the failure stress in shear, and f_c' is the uniaxial compressive strength [47]. A plot of this function in shown in Figure 3.5. Note that this damage function depends additionally on the other component

of stress in the plane of the ice $\tau_{ss} = \mathbf{s} \cdot \boldsymbol{\tau} \cdot \mathbf{s}$. This term allows the modeling of axial splitting, which is seen experimentally in ice [40].
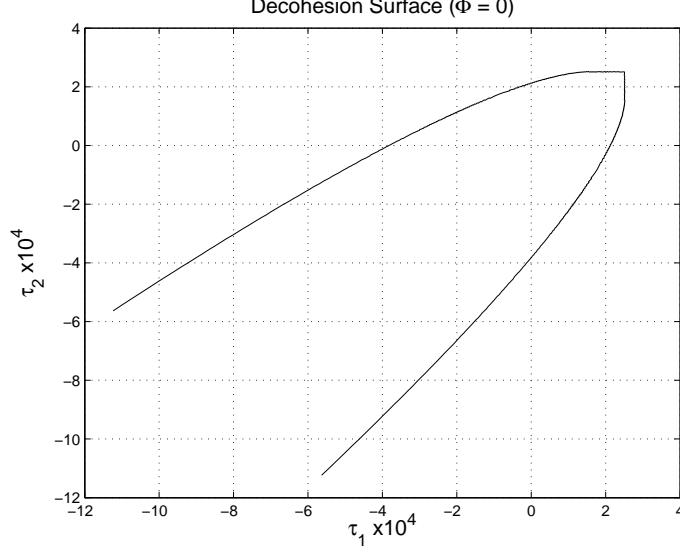
Figure 3.5: Elastic-Decohesive Failure Function, $\Phi = 0$.

Now define $\hat{\omega} = D\tilde{\omega}$ where $D = u_0 t_{nf}$ is a factor which makes $\hat{\omega}$ dimensionless. Then the flow rules for the jump in displacement in the plane of the ice can be written as

$$\llbracket \dot{\varphi_n} \rrbracket = \hat{\omega} u_0 \kappa e^{\kappa B_n}$$
$$\llbracket \dot{\varphi_s} \rrbracket = 2\hat{\omega} u_0 \frac{t_{nf} t_s}{t_{sm}^2}$$

(3.176)

Rather than using an associative rule for $\dot{\tilde{u}}$ define

$$\dot{\tilde{u}} = \frac{\llbracket \dot{\varphi_n} \rrbracket}{u_0} = \hat{\omega} \kappa e^{\kappa B_n}$$

(3.177)

The consistency condition is then

$$\dot{\Phi} = \kappa e^{\kappa B_n} \left(\frac{\dot{t}_n}{t_{nf}} - \dot{\tilde{t}} \left(1 - \frac{\langle -\tau_{ss} \rangle^2}{f_c'^2} \right) - 2\widetilde{\dot{t}} \frac{\langle -\tau_{ss} \rangle}{f_c'^2} \dot{\tau}_{ss} \right) + \frac{2\dot{t}_s t_s}{t_{sm}^2} = 0.$$

(3.178)

3.6.3 Thermodynamic Heat Equation

To derive the heat equation for a column of sea ice, the energy equation, Equation 3.103, can be written in terms of the Helmholtz free energy as

$$\int_{\Omega_\Gamma} \left(\dot{A} + \dot{T}\eta + T\dot{\eta} - \mathbf{P} : \mathbf{F} + \mathrm{Div}_\mathbf{X}\mathbf{Q} - \rho_0\mathcal{R} \right) d\Omega = 0. \tag{3.179}$$

Using the relationships derived from the dissipation inequality above, the energy equation becomes

$$\int_{\Omega_\Gamma} \left(T\dot{\eta} - \mathbf{P} : (\llbracket \dot{\boldsymbol{\varphi}} \rrbracket \otimes \mathbf{N})\delta_\Gamma + \tilde{\mathbf{t}}\dot{\tilde{u}}\delta_\Gamma + \mathrm{Div}_\mathbf{X}\mathbf{Q} - \rho_0\mathcal{R} \right) d\Omega = 0. \tag{3.180}$$

To derive the thermodynamic heat equation used in sea ice modeling from this general equation a number of assumptions must be made. First assume that the mechanical dissipation on the discontinuity surface can be neglected. Then the energy equation simplifies to

$$\int_{\Omega_\Gamma} \left(T\dot{\eta} + \mathrm{Div}_\mathbf{X}\mathbf{Q} - \rho_0\mathcal{R} \right) d\Omega = 0 \tag{3.181}$$

and the corresponding local expression is

$$T\dot{\eta} + \mathrm{Div}_\mathbf{X}\mathbf{Q} - \rho_0 R = 0. \tag{3.182}$$

Next assume, as in the previous section, that $\mathbf{Q}$ satisfies Fourier's Law of Heat Conduction, then

$$\mathbf{Q} = -k(\mathbf{X}, T)\mathrm{Grad}_\mathbf{X} T \tag{3.183}$$

where $k(\mathbf{X}, T)$ is the thermal conductivity. When considering the dissipation inequality the following relationship between entropy and temperature is obtained

$$\eta = -\frac{\partial V}{\partial T}. \tag{3.184}$$

In rate form this can be written as

$$\dot{\eta} = -\frac{\partial^2 V}{\partial T^2}\dot{T}. \tag{3.185}$$

For a heat capacity at constant volume that does not depend on temperature the following form for $V(T)$, may be used

$$V(T) = \rho_0 C(\mathbf{X}) T \left(1 - \log\frac{T}{T_0} \right) \tag{3.186}$$

where T_0 is a reference temperature. This form is based on Equation 2.17 in [55]. In the case of sea ice, the heat capacity is taken to be a function of temperature as well as position. For a heat capacity of the form

$$C(\mathbf{X}, T) = C_0 + \frac{\mathcal{F}(\mathbf{X})}{T^2} \tag{3.187}$$

where C_0 is a constant, $V(T)$ can be of the form

$$V(T) = -\rho_0 \left(C_0 \left(T - T\log\frac{T}{T_0} \right) - \frac{\mathcal{F}(\mathbf{X})}{2T} \right). \tag{3.188}$$

With this assumption Equation 3.185 becomes

$$\dot{\eta} = \rho_0 \left(C_0 + \frac{\mathcal{F}(\mathbf{X})}{T^2} \right) \frac{\dot{T}}{T} = \rho_0 C(\mathbf{X}, T) \frac{\dot{T}}{T}. \tag{3.189}$$

Substituting this into the energy equation results in

$$\rho_0 C(\mathbf{X}, T) \dot{T} = \text{Div}_{\mathbf{X}} (k(\mathbf{X}, T) \text{Grad}_{\mathbf{X}} T) - \rho_0 \mathcal{R} \tag{3.190}$$

In the case of sea ice, it is generally assumed that the temperature and conductivity vary vertically for a column of ice. Therefore, the full three-dimensional equation reduces to

$$\rho_0 C(X_3, T) \frac{dT}{dt} = \frac{\partial}{\partial X_3} \left(k(X_3, T) \frac{\partial T}{\partial X_3} \right) - \rho_0 \mathcal{R}(X_3) \tag{3.191}$$

The only source of internal heating for sea ice is the shortwave solar radiation penetrating the surface of the ice. The change in intensity of radiation with change in depth can be formulated according to Beer's Law as

$$\frac{dI(X_3)}{dX_3} = -\kappa I(X_3) \tag{3.192}$$

where κ is the bulk extinction coefficient, which is the absorption and scattering integrated over all wavelengths and angles. Solving for $I(X_3)$ results in

$$I(X_3) = I_0 e^{-\kappa X_3} \tag{3.193}$$

where I_0 is the intensity at the top surface of the ice. Using this equation and setting $\rho_0 \mathcal{R}(X_3) = dI(X_3)/dX_3$ gives

$$\rho_0 C(X_3, T)\frac{dT}{dt} = \frac{\partial}{\partial X_3}\left(k(X_3, T)\frac{\partial T}{\partial X_3}\right) + \kappa I_0 e^{-\kappa X_3} \tag{3.194}$$

For sea ice, brine pockets, or melted ponds of high salinity water, have an important effect on the thermodynamics. To account for this effect, the heat capacity and thermal conductivity are assumed to depend on depth through a salinity profile, $S(X_3)$. Bitz and Lipscomb [7] use the following expressions based on formulas introduced by Untersteiner [52]

$$C(S, T) = C_0 + \frac{L_0 \mu S(X_3)}{T^2} \tag{3.195}$$

and

$$k(S, T) = k_0 + \frac{\beta S(X_3)}{T} \tag{3.196}$$

where $C_0 = 2110$ J/(kg K) is the heat capacity of freshwater ice, $L_0 = 334$ kJ/kg is the latent heat of fusion of freshwater ice, $\mu = 0.054$ K/ppt, $k_0 = 2.034$ W/(m K) is the thermal conductivity of freshwater ice, and $\beta = 0.117$ W/(m ppt). A derivation of the equation for heat capacity can be found in [26]. After including these functional forms, the heat equation for sea ice becomes

$$\rho_0 \left(C_0 + \frac{L_0 \mu S(X_3)^2}{T}\right)\frac{dT}{dt} = \frac{\partial}{\partial X_3}\left(\left(k_0 + \frac{\beta S(X_3)}{T}\right)\frac{\partial T}{\partial X_3}\right) + \kappa I_0 e^{-\kappa X_3} \tag{3.197}$$

To determine the change in ice thickness due to melting or ice growth, boundary conditions must be applied to balance the incoming and outgoing fluxes. At the ice

atmosphere interface the net flux as a function of the temperature at the top of the ice layer, T_0, is first calculated as

$$F_{net}(T_0) = F_r(1 - \alpha) - I_0 + F_L - \sigma T_0^4 + F_s + F_l + \left(k(S,T) \frac{\partial T}{\partial X_3} \right) \bigg|_{X_3 = Z_t} \quad (3.198)$$

where α is the surface albedo, F_r is the incoming short-wave solar radiation, I_0 is flux of radiative energy through the surface into the ice, F_L is the flux of long-wave radiation from the clouds and atmosphere, F_s is the flux of sensible heat, F_l is the flux of latent heat, ϵ_L is the long-wave emissivity, σ is the Stefan-Boltzmann constant, F_s is the flux of sensible heat, and F_l is the flux of latent heat. If $F_{net}(T_0 = 0°) < 0$, then the surface temperature, T_0 is calculated by setting F_{net} equal to zero and solving the flux equation above for T_0. If $F_{net}(T_0 = 0°) \geq 0$, the surface temperature is set to the melting temperature $(T_0 = 0°C)$ and the change in thickness at the top surface is calculated by solving

$$-q(S(Z_{bot}), T_0) \frac{dh}{dt} = F_r(1-\alpha) - I_0 + F_L - \sigma T_0^4 + F_s + F_l + \left(k(S,T) \frac{\partial T}{\partial z} \right) \bigg|_{X_3 = Z_t} \quad (3.199)$$

where $q(S,T)$ is the latent heat of fusion or the energy required to melt a unit volume of sea ice at temperature, T, and salinity S. This quantity is defined as

$$q(S(Z_{bot}), T_0) = \rho \left(C_0(T_m - T_0) + L_0 \left(1 - \frac{T_m}{T_0} \right) + C_w(-T_m) \right) \quad (3.200)$$

where $T_m = -0.054S(Z_{bot})$ is the melting temperature of ice with salinity $S(Z_{bot})$ and C_w is the heat capacity of ocean water.

Similarly, the change in thickness at the ice-water interface is governed by

$$q(S(Z_b), T_{bot}) \frac{dh}{dt} = \left(k(S,T) \frac{\partial T}{\partial X_3} \right) \bigg|_{X_3 = Z_b} - F_w \quad (3.201)$$

where F_w is the heat flux from the ocean and $T_{bot} = -1.8°C$ is the freezing temperature of sea water.

The numerical implementation of this thermodynamic model as well as the momentum equation, elastic-decohesive constitutive model, and thickness distribution are discussed in the next chapter.

Chapter 4

Numerical Modeling

4.1 Introduction

The ice governing equations derived in the previous section have been discretized and solved numerically using the Material-Point Method (MPM), a particle-in-cell method that combines Lagrangian material points with a background finite element mesh that was developed for solid mechanics applications by Sulsky [47],[48],[45]. For the sea ice problem, the ice is decomposed into a finite set of Lagrangian material points with associated area, mass, and thickness distribution. The material points are unconnected, so large deformations can be modeled without the risk of grid tangling. To solve the momentum equation changes in the material-point velocity are mapped to a background grid where gradients can be more easily calculated. The background grid used for this application is a finite element mesh with the material points acting as integration points. The constitutive model is solved at each material point, which makes modeling history-dependent materials straighforward. Similarly, associating an ice thickness distribution with a material point makes the modeling of the horizontal transport term in the evolution equation simple. The vertical transport is solved for each thickness category at each material point using an incremental remapping scheme developed by Lipscomb [27].

The next section describes the discretization of the momentum equation and the overall MPM algorithm. Section 4.3 contains a discussion of the numerical algorithm used to solve the elastic-decohesive constitutive model. Section 4.4 describes the implementation of the ice thickness distribution evolution equation, which is solved at each material point.

4.2   Momentum Equation in MPM

To discretize the equations of motion for ice, first consider a discretization of the horizontal region of ice $\mathcal{B}_2 \subset \mathbb{R}^2$ defined in Section 3.2, which can be divided into N_p disjoint subregions such that

$$\mathcal{B}_2 = \bigcup_{p=1}^{N_p} \Omega_p. \tag{4.1}$$

Each region Ω_p is then associated with a material point in MPM. For a material point with an initial density, $\rho_p(0)$, average thickness, $h_p(0)$, and area, $\Omega_p(0)$, the mass can be calculated as

$$m_p = \int_{\Omega_p(0)} \rho_0(\mathbf{X}) h_0(\mathbf{X}) d\Omega \tag{4.2}$$

which can be approximated as

$$m_p \approx \rho_p(0) h_p(0) \Omega_p(0). \tag{4.3}$$

The total mass in the region can be obtained as a sum of material-point masses as

$$m(0) = \int_{\mathcal{B}_2} \rho_0 h_0 d\Omega \approx \sum_{p=1}^{N_p} \rho_p(0) h_p(0) \Omega_p(0). \tag{4.4}$$

For most problems in MPM, mass conservation is automatically satisfied by holding the material-point mass constant throughout the calculation. However, in the sea ice application, mass is not conserved. Thermodynamic effects can increase mass due to freezing and reduce mass due to melting. Therefore for the sea ice, the material point mass depends upon time and for a given time, t, the material point mass can be approximated as

$$m_p(t) \approx \rho_p(t) h_p(t) \Omega_p(t). \tag{4.5}$$

In addition to mass, density, and average thickness, each material point has an associated velocity ($\mathbf{v}_p$), stress ($\mathbf{P}_p$, $\boldsymbol{\sigma}_p$), internal variables for the constitutive model

such as jump in displacement ($[\![\boldsymbol{\varphi}]\!]_p$), and thickness distribution (g_p). These values evolve over time based on the change in velocity obtained from the solution of the momentum equation on the background grid. For this problem consider a background grid made up of elements, $\Omega^e, e = 1, ..., N_e$, and corresponding nodes $\mathbf{x}_I, I = 1, ..., N_n$. The boundary of the background grid does not need to coincide with the boundary of the ice region, but the ice region must be contained within the background grid for all time so that

$$\bigcup_{p=1}^{N_p} \Omega_p \subset \bigcup_{e=1}^{N_e} \Omega_e. \tag{4.6}$$

To derive the discrete momentum equation, first convert the two-dimensional momentum equation (Equation 2.87) to the current configuration, which results in

$$\int_{\boldsymbol{\varphi}(\mathcal{B}_2)} \rho h \left(\dot{\mathbf{v}} - 2\omega \sin \phi (\mathbf{e}_3 \times \mathbf{v})\right) d\Omega = \int_{\boldsymbol{\varphi}(\mathcal{B}_2)} \left(\operatorname{div}(h\boldsymbol{\sigma}) + \mathbf{t}_b + \mathbf{t}_t\right) d\Omega \tag{4.7}$$

where $\rho(\mathbf{x}, t)$ is the density in the current configuration, $h(\mathbf{x}, t)$ is the ice thickness in the current configuration, $\boldsymbol{\sigma} = J^{-1}\mathbf{P}\mathbf{F}^T$, $\operatorname{div}(\cdot)$ represents the divergence with respect to the current configuration, and the ocean and atmospheric surface tractions can be written as

$$\begin{aligned} \mathbf{t}_a &= c_a \rho_a \|\mathbf{v}_a\| Q_a \mathbf{v}_a \\ \mathbf{t}_w &= c_w \rho_w \|(\mathbf{v} - \mathbf{v}_w)\| Q_w (\mathbf{v} - \mathbf{v}_w). \end{aligned} \tag{4.8}$$

To write this equation in the variational or weak formulation, first consider a variation, $\mathbf{w}$, from the space of admissible variations

$$\mathbb{W} = \left\{ (\mathbf{w} : \boldsymbol{\varphi}(\mathcal{B}_2) \to \mathbb{R}^2) \text{ s.t } \mathbf{w} = 0 \text{ on } \boldsymbol{\varphi}(\partial \mathcal{B}_u) \right\}. \tag{4.9}$$

Now multiply the momentum equation by the variation to obtain

$$\begin{aligned} \int_{\boldsymbol{\varphi}(\mathcal{B}_2)} \rho h \left(\dot{\mathbf{v}} - 2\omega \sin \phi (\mathbf{e}_3 \times \mathbf{v})\right) \cdot \mathbf{w} d\Omega &= \int_{\boldsymbol{\varphi}(\mathcal{B}_2)} \operatorname{div}(h\boldsymbol{\sigma}) \cdot \mathbf{w} d\Omega \\ &+ \int_{\boldsymbol{\varphi}(\mathcal{B}_2)} (\mathbf{t}_b + \mathbf{t}_t) \cdot \mathbf{w} d\Omega \end{aligned} \tag{4.10}$$

Using the divergence theorem on the first integral on the right-hand side results in

$$\int_{\boldsymbol{\varphi}(\mathcal{B}_2)} \rho h \left(\dot{\mathbf{v}} - 2\omega \sin \phi (\mathbf{e}_3 \times \mathbf{v}) \right) \cdot \mathbf{w} d\Omega = \int_{\boldsymbol{\varphi}(\mathcal{B}_2)} \mathrm{grad}(\mathbf{w}) \cdot h\boldsymbol{\sigma} d\Omega$$
$$+ \int_{\boldsymbol{\varphi}(\mathcal{B}_2)} (\mathbf{t}_b + \mathbf{t}_t) \cdot \mathbf{w} d\Omega + \int_{\boldsymbol{\varphi}(\partial\mathcal{B}_2)} \bar{\mathbf{t}} \cdot \mathbf{w} dS \tag{4.11}$$

where the final surface integral comes in as a boundary term from the divergence theorem and $\bar{\mathbf{t}}$ is the prescribed traction along the boundary.

Approximate solutions of the momentum equation can be obtained for a finite element background grid by using nodal basis functions, N_I, to represent grid quantities. Given a finite dimensional subspace, $\mathbb{W}^h \subset \mathbb{W}$, define a test function in this space as

$$\mathbf{w}^h(\mathbf{x}) = \sum_{I=1}^{N_n} N_I(\mathbf{x})\mathbf{w}_I. \tag{4.12}$$

The superscript h, not to be confused with the ice thickness, is used in this context to denote a grid quantity with mesh size $h > 0$. For this application consider a background grid composed of quadrilateral elements. The nodes corresponding to an individual element can be written as $\mathbf{x}_I^e, I = 1, 2, 3, 4$. The local element shape functions can be obtained by considering a mapping from a square master element with natural coordinates, $\boldsymbol{\xi} = (\xi_1, \xi_2), (0 \leq \xi_1 \leq 1, 0 \leq \xi_2 \leq 1)$, as shown in Figure 4.1. For any individual element, the mapping between it and the master element can be written as

$$\mathbf{x}^h(\boldsymbol{\xi}, t) = \sum_{I=1}^{4} N_I^e(\boldsymbol{\xi})\mathbf{x}_I^e(t) \tag{4.13}$$

where the element shape functions are defined as

$$\begin{aligned} N_1^e(\boldsymbol{\xi}) &= (1 - \xi_1)(1 - \xi_2) \\ N_2^e(\boldsymbol{\xi}) &= \xi_1(1 - \xi_2) \\ N_3^e(\boldsymbol{\xi}) &= \xi_1\xi_2 \\ N_4^e(\boldsymbol{\xi}) &= (1 - \xi_1)\xi_2. \end{aligned} \tag{4.14}$$
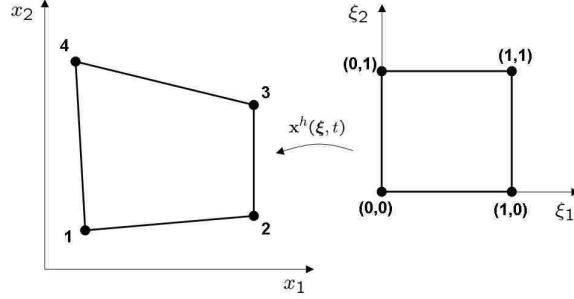
Figure 4.1: Mapping from master element to finite element

For a given node, the element shape functions for surrounding elements contribute to the global shape function, which is defined as

$$N_I(\mathbf{x}) = N_I(\boldsymbol{\xi}(\mathbf{x})) = \sum_{e=1}^{N_e} \sum_{J=1}^{4} N_J^e(\boldsymbol{\xi}) L_{JI}^e \tag{4.15}$$

where L_{JI}^e is the connectivity matrix. The matrix is defined so that $L_{JI}^e = 1$ if the element node J is a node of one of the surrounding elements of node I and $L_{JI}^e = 0$ otherwise. Using these global shape functions, gradients of a quantity can be calculated as

$$\text{Grad}(\mathbf{w}^h) = \text{Grad}\left(\sum_{I=1}^{N_n} N_I(\boldsymbol{\xi}(\mathbf{x}))\mathbf{w}_I\right) = \sum_{I=1}^{N_n} \frac{\partial N_I}{\partial \boldsymbol{\xi}} \frac{\partial \boldsymbol{\xi}}{\partial \mathbf{x}} \mathbf{w}_I. \tag{4.16}$$

With the above definition of the global shape functions, the velocity and acceleration can be written as

$$\begin{aligned}
\mathbf{v}^h(\mathbf{x}) &= \sum_{I=1}^{N_n} N_I(\mathbf{x})\mathbf{v}_I \\
\dot{\mathbf{v}}^h(\mathbf{x}) &= \sum_{I=1}^{N_n} N_I(\mathbf{x})\dot{\mathbf{v}}_I
\end{aligned} \tag{4.17}$$

and the weak form of the momentum balance becomes

$$\int_{\boldsymbol{\varphi}(\mathcal{B}_2)} \rho h \dot{\mathbf{v}}^h \cdot \mathbf{w}^h d\Omega = \int_{\boldsymbol{\varphi}(\mathcal{B}_2)} \mathrm{grad}(\mathbf{w}^h) \cdot h \boldsymbol{\sigma} d\Omega + \int_{\boldsymbol{\varphi}(\mathcal{B}_2)} \mathbf{F}^{ext} \cdot \mathbf{w}^h d\Omega + \int_{\boldsymbol{\varphi}(\partial \mathcal{B}_2)} \bar{\mathbf{t}} \cdot \mathbf{w}^h dS.$$

$$(4.18)$$

Expand to get

$$\sum_{I=1}^{N_n} \mathbf{w}_I \cdot \sum_{J=1}^{N_n} \int_{\boldsymbol{\varphi}(\mathcal{B}_2)} \rho h \dot{\mathbf{v}}_J N_I(\mathbf{x}) N_J(\mathbf{x}) d\Omega = \sum_{I=1}^{N_n} \mathbf{w}_I \cdot \int_{\boldsymbol{\varphi}(\mathcal{B}_2)} \mathrm{grad}(N_I(\mathbf{x})) \boldsymbol{\sigma} h d\Omega$$

$$+ \sum_{I=1}^{N_n} \mathbf{w}_I \cdot \int_{\boldsymbol{\varphi}(\mathcal{B}_2)} N_I(\mathbf{x}) \mathbf{F}^{ext} d\Omega + \sum_{I=1}^{N_n} \mathbf{w}_I \cdot \int_{\partial \boldsymbol{\varphi}(\mathcal{B}_2)} N_I(\mathbf{x}) \bar{\mathbf{t}} dS. \qquad (4.19)$$

To obtain the semi-discrete equation, a quadrature rule for the integration over the domain must be used. In the case of MPM, the material points act as integration points leading to

$$\sum_{I=1}^{N_n} \mathbf{w}_I \cdot \sum_{p=1}^{N_p} \sum_{J=1}^{N_n} \rho_p h_p \Omega_p \dot{\mathbf{v}}_J N_J(\mathbf{x}_p) N_I(\mathbf{x}_p) = \sum_{I=1}^{N_n} \mathbf{w}_I \cdot \sum_{p=1}^{N_p} \mathrm{grad}(N_I(\mathbf{x}_p)) h_p \Omega_p \boldsymbol{\sigma}_p$$

$$+ \sum_{I=1}^{N_n} \mathbf{w}_I \cdot \sum_{p=1}^{N_p} N_I(\mathbf{x}_p) \Omega_p \mathbf{F}^{ext} + \sum_{I=1}^{N_n} \mathbf{w}_I \cdot \int_{\partial \boldsymbol{\varphi}(\mathcal{B}_2)} \bar{\mathbf{t}} N_I(\mathbf{x}_p) dS. \qquad (4.20)$$

This equation must hold for arbitrary $\mathbf{w}^h \in \mathcal{W}^h$, which implies that

$$\sum_{p=1}^{N_p} \sum_{J=1}^{N_n} \rho_p h_p \Omega_p \dot{\mathbf{v}}_J N_J(\mathbf{x}_p) N_I(\mathbf{x}_p) = \sum_{p=1}^{N_p} \mathrm{grad}(N_I(\mathbf{x}_p)) h_p \Omega_p \boldsymbol{\sigma}_p$$

$$+ \sum_{p=1}^{N_p} N_I(\mathbf{x}_p) \Omega_0 \mathbf{F}^{ext} + \int_{\partial \boldsymbol{\varphi}(\mathcal{B}_2)} \bar{\mathbf{t}} N_I(\mathbf{x}_p) dS. \qquad (4.21)$$

Simplifying, this becomes

$$\sum_{J=1}^{N_n} m_{IJ} \dot{\mathbf{v}}_J = \mathbf{F}_I^{int} + \mathbf{F}_I^{ext} \qquad (4.22)$$

where

$$\mathbf{F}_I^{int} = \sum_{p=1}^{N_p} \mathrm{grad} N_I(\mathbf{x}_p) h_p \boldsymbol{\sigma}_p \qquad (4.23)$$

$$\mathbf{F}_I^{ext} = \sum_{p=1}^{N_p} N_I(\mathbf{x}_p)\mathbf{F}^{ext} + \int_{\varphi(\partial \mathcal{B}_2)} \bar{t}N_I(\mathbf{x}_P)dS \tag{4.24}$$

and

$$m_{IJ} = \sum_{p=1}^{N_p} \rho_p h_p \Omega_p N_J(\mathbf{x}_p)N_I(\mathbf{x}_p). \tag{4.25}$$

In practice, the lumped mass matrix is used, which is the row sum of the consistent mass matrix, m_{IJ}, and is defined as $m_I = \rho h N_I(\mathbf{x}_p)$[48]. The advantage of using the lumped mass matrix is that a computationally costly matrix inversion is avoided for each step. Using the lumped mass matrix the momentum equation becomes

$$m_I \mathbf{A}_I = \mathbf{F}_I^{ext} + \mathbf{F}_I^{int}. \tag{4.26}$$

Finally, this equation must be discretized in time. A centered difference formula for the acceleration can be written as

$$\dot{\mathbf{v}}_I^k \equiv \mathbf{a}_I^k = \frac{1}{\Delta t^k}\left(\mathbf{v}_I^{k+1/2} - \mathbf{v}_I^{k-1/2}\right). \tag{4.27}$$

Using this discretization for acceleration results in the velocity being lagged a half a time step behind the acceleration or displacement. Turn this into an equation for the velocity at time $k + 1/2$ to obtain

$$\mathbf{v}_I^{k+1/2} = \mathbf{v}_I^{k-1/2} + \Delta t^k \mathbf{a}_I^k. \tag{4.28}$$

For the time discretization, an updated Lagrangian formulation is used where the timestep k configuration is used as the reference configuration of the $k + 1$ timestep. Given the values $m_p^k, \mathbf{v}_p^{k-1/2}, h_p^k, \Omega_p^k, \boldsymbol{\sigma}_p^k$, the following algorithm is used to obtain the values at timestep $k + 1$.

1. Map the material point mass and momentum to the nodes:

$$m_I^k = \sum_{p=1}^{N_p} m_p^k N_I(\mathbf{x}_p^k) \tag{4.29}$$

$$m_I^k \mathbf{v}_I^{k-1/2} = \sum_{p=1}^{N_p} m_p^k \mathbf{v}_p^{k-1/2} N_I(\mathbf{x}_p^k). \tag{4.30}$$

2. Calculate the external forces at the nodes:

$$\mathbf{F}_I^{ext,k} = \sum_{p=1}^{N_p} \left(\Omega_p^k \mathbf{t}_{a,p}^k + \Omega_p^k \mathbf{t}_{w,p}^k - m_p^k f_c(\mathbf{e}_3 \times \mathbf{v}_p^{k-1/2}) \right) N_I(\mathbf{x}_p^k) \tag{4.31}$$

where

$$\mathbf{t}_{a,p}^k = c_a \rho_a \|\mathbf{v}_a(\mathbf{x}_p^k)\| Q_a \mathbf{v}_a(\mathbf{x}_p^k) \tag{4.32}$$

$$\mathbf{t}_{w,p}^k = c_w \rho_w \|(\mathbf{v}_p^{k-1/2} - \mathbf{v}_w(\mathbf{x}_p^k)\| Q_w(\mathbf{v}_p^{k-1/2} - \mathbf{v}_w(\mathbf{x}_p^k)). \tag{4.33}$$

3. Calculate the internal forces at the nodes:

$$\mathbf{F}_I^{int,k} = \sum_{p=1}^{N_p} \Omega_p^k h_p^k \boldsymbol{\sigma}_p^k \mathrm{grad}(N_I(\mathbf{x}_p^k)). \tag{4.34}$$

4. Solve the momentum equation on the grid:

$$m_I^k \left(\mathbf{v}_I^{k+1/2} - \mathbf{v}_I^{k-1/2} \right) = \left(\mathbf{F}_I^{ext,k} + \mathbf{F}_I^{int,k} \right) \Delta t^k. \tag{4.35}$$

5. Update the velocity and move the material points:

$$\mathbf{v}_p^{k+1/2} = \mathbf{v}_p^{k-1/2} + \Delta t^k \sum_{I=1}^{N_n} \left(\mathbf{v}_I^{k+1/2} - \mathbf{v}_I^{k-1/2} \right) N_I(\mathbf{x}_p^k) \tag{4.36}$$

$$\mathbf{x}_p^{k+1} = \mathbf{x}_p^k + \Delta t^k \sum_{I=1}^{N_n} \mathbf{v}_I^{k+1/2} N_I(\mathbf{x}_p^k). \tag{4.37}$$

6. Calculate the deformation gradient and strain increment:

$$\mathbf{f}_p^{k+1} = \mathbf{I} + \Delta t^k \sum_{I=1}^{N_n} \mathrm{Grad}(N_I(\mathbf{x}_p^k)) \mathbf{v}_I^{k+1/2} \tag{4.38}$$

$$\mathbf{F}_p^{k+1} = \mathbf{f}_p^{k+1}\mathbf{F}_p^k \tag{4.39}$$

$$\Delta\mathbf{e}_p^{k+1} = \frac{1}{2}\left(\mathbf{I} - (\mathbf{f}_p^{k+1})^{-T}(\mathbf{f}_p^{k+1})^{-1}\right). \tag{4.40}$$

7. Update the material-point area:

$$\Omega_p^{k+1} = \det(\mathbf{f}_p^{k+1})\Omega_p^k. \tag{4.41}$$

8. Evaluate the constitutive model:

$$\Delta\mathbf{e}_p^{n+1} \rightarrow \boldsymbol{\tau}_p^{k+1} \tag{4.42}$$

where $\boldsymbol{\tau}_p^{k+1} = J_p\boldsymbol{\sigma}_p$.

9. Update thickness distribution:

$$g_{n,p}^k \rightarrow g_{n,p}^{k+1}. \tag{4.43}$$

10. Regrid, locate particles, and calculate new natural coordinates, $\boldsymbol{\xi}$.

The details for steps 8 and 9 are discussed in the following sections.

4.3 Elastic-Decohesive Constitutive Model

The stress at the current time step is calculated using the elastic-decohesive constitutive model. Recall from the previous chapter that by using the framework of strong discontinuities, the deformation gradient can be broken up into regular and singular parts as

$$\mathbf{F} = \overline{\mathbf{F}} + (\llbracket\boldsymbol{\varphi}\rrbracket \otimes \mathbf{N}_\Gamma)\delta_\Gamma \tag{4.44}$$

where the regular part is defined as $\overline{\mathbf{F}} = \mathrm{Grad}_{\mathbf{X}}\boldsymbol{\varphi}$ and $\mathbf{N}_\Gamma$ is the normal to the discontinuity surface, Γ. The discontinuity is defined over a region Ω_Γ in the derivation of the constitutive model and it is natural when considering the implementation in MPM to associate the discontinuity with the material-point area, Ω_p. For this application, it is assumed that $[\![\boldsymbol{\varphi}]\!]$ is constant over the region Ω_p.

Note that in the following discussion the stress tensors $(\mathbf{P}, \mathbf{S}, \boldsymbol{\tau})$, tractions $(\mathbf{T}, \mathbf{t})$, and displacements $(\boldsymbol{\varphi}, [\![\boldsymbol{\varphi}]\!])$, are assumed to be material-point quantities. However, the p subscript will be left off to simplify the notation.

The singular part of the deformation gradient cannot be handled numerically. Therefore, a regularization of the term must be done for the numerical implementation. Given properties of distributions reviewed in the last chapter

$$
\begin{aligned}
\int_{\Omega_p} \mathbf{P} : ([\![\boldsymbol{\varphi}]\!] \otimes \mathbf{N}_\Gamma \delta_\Gamma) d\Omega &= \int_{\Omega_p} \mathbf{T} \cdot ([\![\dot{\boldsymbol{\varphi}}]\!] \delta_\Gamma d\Omega \\
&= \int_{\Gamma_p} \mathbf{T} \cdot ([\![\dot{\boldsymbol{\varphi}}]\!] d\Gamma.
\end{aligned}
\tag{4.45}
$$

If a length scale is associated with the delta function, $(\delta_\Gamma \rightarrow 1/L)$, these integrals can be approximated as

$$
\int_{\Omega_p} \frac{1}{L}\mathbf{T} \cdot [\![\boldsymbol{\varphi}]\!] d\Omega \approx \frac{1}{L}\mathbf{T} \cdot [\![\dot{\boldsymbol{\varphi}}]\!]\Omega_p
\tag{4.46}
$$

and

$$
\int_{\Gamma_p} \mathbf{T} \cdot [\![\boldsymbol{\varphi}]\!] d\Gamma \approx \mathbf{T} \cdot [\![\dot{\boldsymbol{\varphi}}]\!]\Gamma_p.
\tag{4.47}
$$

Equating these results gives a length scale

$$
\frac{1}{L} = \frac{\Gamma_p}{\Omega_p}.
\tag{4.48}
$$

In the sea ice code where a rectangular grid is used the length scale is approximated by

$$
L = \sqrt{(\Delta x)^2 + (\Delta y)^2}
\tag{4.49}
$$

where Δx and Δy are the cell lengths in the x and y direction of the fixed background grid.

As in the derivation in the previous chapter, the numerical implementation of the elastic-decohesive constitutive model will use the Kirchhoff stress tensor $\boldsymbol{\tau} = \mathbf{P}\overline{\mathbf{F}}^T$ and rate of deformation tensor $\mathbf{d} = \mathrm{sym}(\dot{\mathbf{F}}\overline{\mathbf{F}}^{-1})$. The elastic-decohesive constitutive model consists of several parts. First is an elastic relation giving the Lie derivative of τ as a function of rate of deformation, shown below in coordinates defined by the spatial normal to the discontinuity

$$
\begin{aligned}
\mathcal{L}_v(\tau)_{nn} &= \mathcal{E}_1 \bar{d}_{nn} + \mathcal{E}_2 \bar{d}_{ss} \\
\mathcal{L}_v(\tau)_{ss} &= \mathcal{E}_2 \bar{d}_{nn} + \mathcal{E}_1 \bar{d}_{ss} \\
\mathcal{L}_v(\tau)_{ns} &= 2\hat{G} \bar{d}_{ns}
\end{aligned}
\tag{4.50}
$$

where

$$
\mathcal{E}_1 = \hat{\lambda} + 2\hat{G} - \frac{\hat{\lambda}}{\hat{\lambda} + 2\hat{G}} \ , \ \mathcal{E}_2 = \hat{\lambda} - \frac{\hat{\lambda}}{\hat{\lambda} + 2\hat{G}}
\tag{4.51}
$$

and $\hat{\lambda}$ and $\hat{G}$ are defined as in Equation (3.174). This elastic relationship can be discretized in time to relate increments of stress and deformation at a timestep $k+1$ as

$$
\begin{aligned}
\Delta t \mathcal{L}_v(\tau)_{nn}^{k+1} &= \mathcal{E}_1 \Delta t \bar{d}_{nn}^{k+1} + \mathcal{E}_2 \Delta t \bar{d}_{ss}^{k+1} \\
\Delta t \mathcal{L}_v(\tau)_{ss}^{k+1} &= \mathcal{E}_2 \Delta t \bar{d}_{nn}^{k+1} + \mathcal{E}_1 \Delta t \bar{d}_{ss}^{k+1} \\
\Delta t \mathcal{L}_v(\tau)_{ns}^{k+1} &= 2\hat{G} \Delta t \bar{d}_{ns}^{k+1}.
\end{aligned}
\tag{4.52}
$$

This relationship is between an increment of stress and the elastic or regular part of the deformation. Numerically, the incremental deformation gradient is calculated as

$$
\mathbf{f}_p^{k+1} = \mathbf{I} + \Delta t^k \sum_{I=1}^{N_n} \mathrm{grad}(N_I(\mathbf{x}_p^k))\mathbf{v}_I^{k+1/2}
\tag{4.53}
$$

and the full deformation gradient is calculated from the increment of the displacement gradient as

$$\mathbf{F}_p^{k+1} = \mathbf{f}_p^{k+1}\mathbf{F}_p^k = \mathbf{I} + \Delta t^k \sum_{I=1}^{N_n} \text{grad}(N_I(\mathbf{x}_p^k))\mathbf{v}_I^{k+1/2}\mathbf{F}_p^k \tag{4.54}$$

The increment of deformation in terms of the Eulerian strain tensor $\mathbf{e}$ can be defined as [42]

$$\Delta \mathbf{e}^{k+1} = \Delta t \mathbf{d}^{k+1} = \frac{1}{2}\left(\mathbf{I} - (\mathbf{f}^{k+1})^{-T}(\mathbf{f}^{k+1})^{-1}\right). \tag{4.55}$$

This relationship is obtained by considering the following equation for the time derivative of the Cauchy-Green strain tensor as a function of the rate of deformation

$$\dot{\mathbf{C}} = 2\mathbf{F}^T \mathbf{d}\mathbf{F}. \tag{4.56}$$

For a simple discretization in time this becomes

$$\frac{\mathbf{C}^{k+1} - \mathbf{C}^k}{\Delta t} = 2(\mathbf{F}^{k+1})^T \mathbf{d}^{k+1}\mathbf{F}^{k+1}. \tag{4.57}$$

Using Equation (4.56) the previous equation can be rewritten as

$$(\mathbf{F}^{k+1})^T\mathbf{F}^{k+1} - (\mathbf{F}^k)^T\mathbf{F}^k = 2(\mathbf{F}^{k+1})^T\mathbf{d}^{k+1}\Delta t\mathbf{F}^{k+1}. \tag{4.58}$$

After rearranging terms the following is obtained

$$\mathbf{d}^{k+1}\Delta t = \frac{1}{2}(\mathbf{F}^{k+1})^{-T}\left((\mathbf{F}^{k+1})^T\mathbf{F}^{k+1} - (\mathbf{F}^k)^T\mathbf{F}^k\right)(\mathbf{F}^{k+1})^{-1}, \tag{4.59}$$

which, after simplifying, results in Equation (4.55).

Using the regularization of the δ-function described above, the elastic part of the rate of deformation can be written as

$$\bar{\mathbf{d}} = \mathbf{d} - \frac{1}{L}(\llbracket\dot{\boldsymbol{\varphi}}\rrbracket \otimes \mathbf{n})^s. \tag{4.60}$$

In terms of increments at time $k + 1$ this becomes

$$\Delta t\bar{\mathbf{d}}^{k+1} = \Delta t\mathbf{d}^{k+1} - \frac{1}{L}(\Delta\llbracket\boldsymbol{\varphi}\rrbracket^{k+1} \otimes \mathbf{n}^{k+1})^s. \tag{4.61}$$

Now the incremental jump in displacement evolves based on the flow rules related to the following failure function

$$
\begin{aligned}
\Phi &= \left(\frac{t_s}{t_{sm}}\right)^2 + \mathrm{e}^{\kappa B_n} - 1 \\
B_n &= \frac{t_n}{t_{nf}} - \tilde{t}\left(1 - \frac{\langle -\tau_{ss}\rangle^2}{f_c'^2}\right)
\end{aligned}
\tag{4.62}
$$

where t_s is the traction in the tangential direction to the crack, t_n is the traction in the normal direction to the crack, t_{nf} is the failure stress in tension, t_{sm}, the failure stress in shear, and f_c' is the uniaxial compressive strength. The discretized flow rules for a time $k+1$ in coordinates defined by the crack surface are

$$
\begin{aligned}
\Delta[\![\varphi_n]\!]^{k+1} &= \Delta\hat{\omega}u_0\kappa\mathrm{e}^{\kappa B_n} \\
\Delta[\![\varphi_s]\!]^{k+1} &= 2\Delta\hat{\omega}u_0\frac{t_{nf}t_s}{t_{sm}^2} \\
\Delta\tilde{u}^{k+1} &= \Delta\hat{\omega}\kappa\mathrm{e}^{\kappa B_n}.
\end{aligned}
\tag{4.63}
$$

Using these expressions, the components of the elastic strain increment tensor can be written as

$$
\begin{aligned}
\Delta t\bar{d}_{nn}^{k+1} &= \Delta t d_{nn}^{k+1} - \frac{\Delta\hat{\omega}u_0\kappa\mathrm{e}^{\kappa B_n}}{L} \\
\Delta t\bar{d}_{ns}^{k+1} &= \Delta t d_{ns}^{k+1} - \frac{2\Delta\hat{\omega}u_0}{2L}\frac{t_{nf}t_s}{t_{sm}^2} \\
\Delta t\bar{d}_{sn}^{k+1} &= \Delta t d_{sn}^{k+1} - \frac{2\Delta\hat{\omega}u_0}{2L}\frac{t_{nf}t_s}{t_{sm}^2} \\
\Delta t\bar{d}_{ss}^{k+1} &= \Delta t d_{ss}^{k+1}.
\end{aligned}
\tag{4.64}
$$

81

With these definitions the consistency condition ($\dot{\Phi} = 0$) can be written as

$$
\begin{aligned}
\Delta\Phi = {}& \frac{\kappa e^{\kappa B_n}}{\tau_{nf}} \left(\left(\Delta t l_{nn} - \frac{\Delta\hat{\omega} u_0 \kappa e^{\kappa B_n}}{L} \right) t_n \right) \\
&+ \frac{\kappa e^{\kappa B_n}}{\tau_{nf}} \left(\Delta t l_{ns} t_s + \mathcal{E}_1 \left(\Delta t d_{nn} - \frac{\Delta\hat{\omega} u_0 \kappa e^{\kappa B_n}}{L} \right) + \mathcal{E}_2 \Delta t d_{ss} \right) \\
&- \kappa e^{\kappa B_n} \left(H(1 - \tilde{u})\dot{\tilde{u}} \left(1 - \frac{\langle -\tau_{ss}\rangle^2}{f_c'^2} \right) \right) \\
&- 2 \frac{\kappa e^{\kappa B_n} 2\tilde{t}\langle -\tau_{ss}\rangle}{f_c'^2} \left(t_s \left(\Delta t l_{sn} - \frac{2\Delta\hat{\omega} u_0 t_{nf} t_s}{L t_{sm}^2} + \Delta t l_{ns} \right) + 2\Delta t l_{ss}\tau_{ss} \right) \\
&- 2 \frac{\kappa e^{\kappa B_n} 2\tilde{t}\langle -\tau_{ss}\rangle}{f_c'^2} \left(\mathcal{E}_2 \left(\Delta t d_{nn} - \frac{\Delta\hat{\omega} u_0 \kappa e^{\kappa B_n}}{L} \right) + \mathcal{E}_1 \Delta t d_{ss} \right) \\
&+ \frac{2t_s}{t_{sm}^2} \left(\left(\Delta t l_{sn} - \frac{2\Delta\hat{\omega} u_0 t_{nf} t_s}{L t_{sm}^2} \right) t_n + \Delta t l_{ss} t_s + 2\hat{G} \left(\Delta t d_{ns} - \frac{2\Delta\hat{\omega} u_0 t_{nf} t_s}{2 L t_{sm}^2} \right) \right) \\
={}& 0.
\end{aligned}
$$

(4.65)

An objective approximation to the Lie derivative of the Kirchhoff stress is [42]

$$
\mathcal{L}_v \boldsymbol{\tau}^{k+1} = \frac{\boldsymbol{\tau}^{k+1} - \mathbf{f}^{k+1}\boldsymbol{\tau}^k(\mathbf{f}^{k+1})^T}{\Delta t}.
$$

(4.66)

Using this formula and the elastic constitutive relation ($\mathcal{L}_v(\boldsymbol{\tau}) = \mathbf{c} : \bar{\mathbf{d}}$), an equation for $\boldsymbol{\tau}^{k+1}$ can be found as

$$
\boldsymbol{\tau}^{k+1} = \mathbf{f}^{k+1}\boldsymbol{\tau}^k(\mathbf{f}^{k+1})^T + \mathbf{c} : \Delta t \bar{\mathbf{d}}^{k+1}.
$$

(4.67)

Now the above discussion assumes a direction for the discontinuity surface defined by $\mathbf{n} = (\sin\theta, \cos\theta)$. The elastic-decohesive constitutive model differs from other models assuming strong discontinuities [33] [4] in the way the normal direction to the crack surface is determined. Here it is determined by maximizing Φ with respect to the direction angle θ rather than by using a bifurcation analysis. Given principal values of stress, τ_1 and τ_2. The two-dimensional stress tensor in coordinates defined by the normal and tangent to the decohesive surface is

$$
\boldsymbol{\tau} = \begin{bmatrix} \tau_1 \cos^2\theta + \tau_2 \sin^2\theta & (\tau_1 - \tau_2)\cos\theta\sin\theta \\ (\tau_1 - \tau_2)\cos\theta\sin\theta & \tau_2 \cos^2\theta + \tau_1 \sin^2\theta. \end{bmatrix}
$$

(4.68)

Let $x = \sin^2 \theta$, then the components can be written as

$$\boldsymbol{\tau} = \begin{bmatrix} \tau_1 x + \tau_2(1-x) & (\tau_1 - \tau_2)\sqrt{(x-x^2)} \\ (\tau_1 - \tau_2)\sqrt{(x-x^2)} & \tau_2 x + \tau_1(1-x). \end{bmatrix} \tag{4.69}$$

The failure function can then be found in terms of x as

$$\Phi = \frac{(x-x^2)(\tau_1 - \tau_2)^2}{\tau_{sm}^2} + e^{\kappa B_n} - 1$$

$$B_n = \frac{\tau_1(1-x) + \tau_2 x}{\tau_{nf}} - f_n\left(1 - \frac{\langle -\tau_1 x - \tau_2(1-x)\rangle^2}{f_c'^2}\right). \tag{4.70}$$

The derivative of this function with respect to x is

$$\frac{\partial \Phi}{\partial x} = \frac{(1-2x)(\tau_1 - \tau_2)^2}{\tau_{sm}^2} + \kappa e^{\kappa B_n}\left(\frac{\tau_2 - \tau_1}{\tau_{nf}} - f_n(\tau_2 - \tau_1)\frac{2\langle -\tau_1 x - \tau_2(1-x)\rangle}{f_c'^2}\right). \tag{4.71}$$

The bisection algorithm is then used to find the zero of this equation with respect to x. Two possible normals are determined from this. The normal is chosen for a given time step by requiring that the sign of the vorticity at the material point is the same as the sign for the rate of rotation associated with the crack, $\mathbf{n} \times \Delta[\![\dot{\boldsymbol{\varphi}}]\!]$, which is proportional to $\mathbf{n} \times \mathbf{t}$ [37].

Using the previous results the elastic-decohesive model is implemented in the following steps:

1. Calculate a trial stress based on the total deformation increment, $\Delta t \mathbf{d}^{k+1}$,

$$\boldsymbol{\tau}^{tr} = \mathbf{f}^{k+1}\boldsymbol{\tau}^k(\mathbf{f}^{k+1})^T + \mathbf{c} : \Delta t \mathbf{d}^{k+1}. \tag{4.72}$$

2. If no decohesion direction is set, calculate the direction by maximizing Φ over θ where $\mathbf{n} = (\cos\theta, \sin\theta)$.

3. Evaluate the failure function, Φ, for the trial stress and direction $\mathbf{n}$, if $\Phi < 0$ the step is elastic and $\boldsymbol{\tau}^{k+1} = \boldsymbol{\tau}^{tr}$, if $\Phi > 0$ continue to the next step.

4. Assume the total rate of deformation increment is fixed and use Newtons's method to solve for the increment of $\hat{\omega}$

$$\Delta\hat{\omega} = -\frac{\Phi}{\Phi'} \tag{4.73}$$

where

$$
\begin{aligned}
\Phi' = &-\left(\kappa \mathrm{e}^{\kappa B_n}\right)^2 \left((\mathcal{E}_1 + t_n)\frac{u_0}{t_{nf}L}\right) \\
&+ \left(\kappa \mathrm{e}^{\kappa B_n}\right)^2 H(1-\tilde{u})\left(\left(1 - \frac{\langle -\tau_{ss}\rangle^2\rangle}{f_c'^2}\right)\right) \\
&+ 2\langle 1-\tilde{u}\rangle\frac{\langle -\tau_{ss}\rangle}{f_c'^2}\frac{u_0}{L}\kappa \mathrm{e}^{\kappa B_n}\left(\frac{2t_{nf}t_s^2}{t_{sm}^2} + \mathcal{E}_2\kappa \mathrm{e}^{\kappa B_n}\right) \\
&- 4\frac{t_{nf}t_s^2}{t_{sm}^4}\frac{u_0}{L}(\hat{G} + t_n).
\end{aligned}
\tag{4.74}
$$

5. Calculate $\boldsymbol{\tau}^{k+1}$ based on the final $\Delta\hat{\omega}$ as

$$\boldsymbol{\tau}^{k+1} = \mathbf{f}^{k+1}\boldsymbol{\tau}^k(\mathbf{f}^{k+1})^T + \mathbf{c} : \left(\Delta t\mathbf{d}^{k+1} - \frac{1}{L}\left(\Delta[\![\boldsymbol{\varphi}]\!] \otimes \mathbf{n}\right)^s\right). \tag{4.75}$$

4.4 Ice Thickness Distribution (ITD)

In the sea ice algorithm, the ITD evolution equation is evaluated after the constitutive equation for stress. The numerical implementation of the ITD evolution equation requires discretizations in thickness space, horizontal space, and time. The discretization in horizontal space is straightforward. Let the region over which the distribution is defined, $\Omega_{\mathbf{x}}$, be equal to the region associated with a material point, Ω_p. Then use the notation, $g_p(h, t)$, to define the ITD at a material point where the following relationships hold

$$\int_0^{h_{max}} g_p(h, t)dh = 1 \tag{4.76}$$

and

$$G_p(h, t) = \int_0^h g_p(\tilde{h}, t) d\tilde{h}. \tag{4.77}$$

The discretization in thickness space, where $g_p(h, t)$ is integrated over $N_c + 1$ thickness bands to obtain partial area fractions $g_{p,n}(t)$ for $0 \le n \le N_c$, is described in the next section. This results in an evolution equation for fractional ice area in each thickness band, which is similar in form to the continuum ITD equation (Equation 3.30). These equations can be divided into three pieces: vertical transport, horizontal transport and redistribution, which can be seen in the continuum evolution equation for $g_p(h, t)$ as

$$\dot{g}_p = -\frac{\partial(f g_p)}{\partial h} - g_p \mathrm{div}_{\mathbf{x}} \mathbf{v} + \psi. \tag{4.78}$$

An operator split in time is used to solve each of the pieces in sequence for each thickness band. Sections 4.4.2, 4.4.3, and 4.4.4 describe the numerical implementation of the vertical transport, horizontal transport and redistribution respectively.

4.4.1 Discrete Ice Thickness Categories

Consider a thickness partition where H_n is the maximum thickness of thickness bin, n. Let $H_0 = 0$ be the thickness of open water. To discretize the equation for g_p consider a partial area fraction defined by

$$g_{p,n} = \int_{H_{n-1}}^{H_n} g_p(h, t) dh \quad \text{for } n = 1, ..., N_c. \tag{4.79}$$

In practice the ice thickness distribution is treated as having a singularity at zero so that $g_p(0, t) = g_{p,0}(t)\delta(0)$ and for $n = 0$

$$g_{p,0}(t) = \int_{H_0^-}^{H_0^+} g_p(h, t) dh. \tag{4.80}$$

For the continuous ice thickness distribution, area conservation can be written as

$$\int_0^\infty g_p(h,t)dh = 1. \tag{4.81}$$

Although mathematically h can range from 0 to ∞, physically there is a maximum thickness for the ice, h_{max} such that $g_p(h,t) = 0$ for $h > h_{max}$. Given that $H(N_c) \geq h_{max}$, area conservation can be written as

$$\int_0^{h_{max}} g_p(h,t)dh = g_{p,0}(t) + \sum_{n=1}^{N_c} \int_{H_{n-1}}^{H_n} g_{p,n}(t) = \sum_{n=0}^{N_c} g_{p,n}(t) = 1. \tag{4.82}$$

Similarly, the discrete partial volumes of ice can be defined as

$$v_{p,n}(t) = \int_{H_{n-1}}^{H_n} hg_p(h,t)dh \quad \text{for } 1 \leq n \leq N_c \tag{4.83}$$

and $v_{p,0} = 0$. In each bin, n, the average ice thickness can be calculated as $h_{p,n} = v_{p,n}/g_{p,n}$. Note that in the MPM implementation, each material point is associated with a thickness distribution. The average thickness associated with a material point and used in the momentum equation can be calculated as

$$h_p(t) = \frac{\sum_{n=0}^{N_c} h_{p,n} g_{p,n}}{\sum_{n=0}^{N_c} g_{p,n}} = \sum_{n=1}^{N_c} v_{p,n}. \tag{4.84}$$

The discretized ice thickness evolution equation can be obtained by explicitly integrating the continuum equation over the thickness bins. First, consider the case where $1 \leq n \leq N_c$, which can be written as

$$\int_{H_{n-1}}^{H_n} \frac{dg_p}{dt}dh = \int_{H_{n-1}}^{H_n} \left(-(\text{div}_{\mathbf{x}}\mathbf{v})g_p - \frac{\partial(fg_p)}{\partial h} + \psi \right) dh. \tag{4.85}$$

For fixed thickness bins, this becomes

$$\frac{dg_{p,n}}{dt} = -(\text{div}_{\mathbf{x}}\mathbf{v})g_{p,n} - f(H_n,t)g_p(H_n,t) + f(H_{n-1},t)g_p(H_{n-1},t) + \psi_n. \tag{4.86}$$

Note that $g_p(H_n,t)$ and $g_p(H_{n-1},t)$ are point values for g_p and not equivalent to $g_{p,n}$ or $g_{p,n-1}$. The next section, which covers the numerical implementation of vertical transport, will consider these terms in more detail, but for now just define

$$\mathcal{G}_{p,n} = -\int_{H_{n-1}}^{H_n} \frac{\partial(fg_p)}{\partial h}dh \tag{4.87}$$

so that

$$\frac{dg_{p,n}}{dt} = -(\text{div}_{\mathbf{x}}\mathbf{v})g_{p,n} + \psi_n + \mathcal{G}_n. \tag{4.88}$$

Recall that the ridging term is of the following form

$$\psi = \delta(h)r_{op} + \frac{n_p(h,t) - a_p(h,t)}{N}r_{cl}. \tag{4.89}$$

where r_{op} is the opening rate, $n_p(h,t)$ is the distribution of newly ridged ice, $a_p(h,t)$ is the distribution of ice participating in ridging, r_{cl} is the closing rate, and N is a normalization factor. The delta function term will only contribute to the open water fraction, and therefore for $1 \leq n \leq N_c$, ψ_n is defined as

$$\psi_n = \int_{H_{n-1}}^{H_n} \psi dh = \int_{H_{n-1}}^{H_n} \left(\frac{n_p(h,t) - a_p(h,t)}{N}r_{cl}\right) dh. \tag{4.90}$$

To derive an explicit expression for the redistribution in a category consider each piece of the redistribution separately. The discrete distribution of ice participating in ridging is defined as

$$a_{p,n} = \int_{H_{n-1}}^{H_n} b(h)g_p(h,t)dh \tag{4.91}$$

where $b_p(h,t)$ multiplying the ice thickness distribution $g_p(h,t)$ results in a distribution $a_p(h,t)$ that skews toward the thinner ice. Lipscomb *et al.* [28] recommend an exponential function for $b_p(h,t)$ of the following form

$$b_p(h,t) = \frac{\exp(-G(h)/a^*)}{a^*[1 - \exp(-1/a^*)]} \tag{4.92}$$

where the cummulative distribution function, $G(h)$, is defined so that $\partial G/\partial h = g_p(h,t)$ and a^* is a constant. This form of $b(h,t)$ results in improved stability for the discrete equations over the original Thorndike [51] function. Using this form of $b(h,t)$, $a_{p,n}(t)$ can be written as

$$\begin{aligned} a_{p,n} &= \int_{H_{n-1}}^{H_n} \frac{\exp(-G_p(h)/a^*)}{a^*[1 - \exp(-1/a^*)]}g(h)dh \\ &= \frac{1}{a^*[1 - \exp(-1/a^*)]} \int_{H_{n-1}}^{H_n} \exp(-G(h)/a^*)\frac{\partial G}{\partial h}dh. \end{aligned} \tag{4.93}$$

This equation can be integrated explicitly to obtain

$$a_{p,n} = \frac{\exp(-G_{p,n-1}/a^*) - \exp(-G_{p,n}/a^*)}{[1 - \exp(-1/a^*)]} \tag{4.94}$$

for $G_{p,n} = G_p(H_n)$ and $G_{p,n-1} = G_p(H_{n-1})$.

Now consider the discrete distribution of new ice $n_{n,p}$, which can be written as

$$n_{p,n}(t) = \int_{H_{n-1}}^{H_n} n_p(h,t)dh = \int_{H_{n-1}}^{H_n} \left(\int_0^\infty a_p(\tilde{h},t)\gamma(\tilde{h},h)d\tilde{h} \right) dh \tag{4.95}$$

where $\gamma(\tilde{h},h)$ is assumed to be the following exponential function due to Lipscomb *et al.* [28]

$$\gamma(\tilde{h},h) = \frac{\lambda(\tilde{h})}{k(\tilde{h})}\exp\left(-\frac{(h - H_{min}(\tilde{h}))}{\lambda(\tilde{h})} \right) \quad \text{for } H_{min}(\tilde{h}) \leq h < \infty \tag{4.96}$$

where $\lambda(\tilde{h}) = \mu\sqrt{\tilde{h}}$, $H_{min}(\tilde{h}) = \min(2\tilde{h}, \tilde{h}+1)$, and $k(\tilde{h}) = \tilde{h}/(H_{min}(\tilde{h})+\lambda(\tilde{h}))$. With this function n_n becomes

$$n_{p,n}(t) = \int_{H_{n-1}}^{H_n} \left(\int_0^\infty a_p(\tilde{h},t)\frac{\lambda(\tilde{h})}{k(\tilde{h})}\exp\left(-\frac{(h - H_{min}(\tilde{h}))}{\lambda(\tilde{h})} \right) d\tilde{h} \right) dh. \tag{4.97}$$

Then changing the order of integration results in

$$n_{p,n}(t) = \int_0^\infty a_p(\tilde{h},t) \left(\int_{H_L}^{H_n} \frac{\lambda(\tilde{h})}{k(\tilde{h})}\exp\left(-\frac{(h - H_{min}(\tilde{h}))}{\lambda(\tilde{h})} \right) dh \right) d\tilde{h} \tag{4.98}$$

where $H_L = \max(H_{n-1}, H_{min}(\tilde{h}))$ is used since $\gamma(\tilde{h},h) = 0$ for $h < H_{min}(\tilde{h})$. Then after integrating over h

$$n_{p,n}(t) = \int_0^\infty \frac{a_p(\tilde{h},t)}{k(\tilde{h})} \left(\exp\left(-\frac{(H_L - H_{min}(\tilde{h}))}{\lambda(\tilde{h})} \right) - \exp\left(\frac{(H_n - H_{min}(\tilde{h}))}{\lambda(\tilde{h})} \right) \right) d\tilde{h}. \tag{4.99}$$

Although the integral over $\tilde{h}$ formally has a limit of ∞, in practice there is a limiting value of thickness that may change as the ice undergoes ridging and thermodynamic growth. This limiting value is the upper bound of the last ice thickness

category, N_c. Therefore the integral can be broken up based on the ice thickness discretization as

$$n_{p,n}(t) =$$
$$\sum_{m=0}^{N_c} \int_{H_{m-1}}^{H_m} \frac{a_p(\tilde{h}, t)}{k(\tilde{h})} \left(\exp \left(-\frac{(H_L - H_{min}(\tilde{h}))}{\lambda \tilde{h}} \right) - \exp \left(\frac{(H_n - H_{min}(\tilde{h}))}{\lambda \tilde{h}} \right) \right) d\tilde{h}.$$
(4.100)

Define

$$\mathcal{H}(\tilde{h}) = \frac{1}{k(\tilde{h})} \left(\exp \left(-\frac{(H_L - H_{min}(\tilde{h}))}{\lambda(\tilde{h})} \right) - \exp \left(\frac{(H_n - H_{min}(\tilde{h}))}{\lambda(\tilde{h})} \right) \right). \quad (4.101)$$

Then, $\mathcal{H} : [H_{m-1}, H_m] \to \mathbb{R}$ is a continuous function and $a : [H_{m-1}, H_m] \to \mathbb{R}$ is a positive function. Therefore by the mean value theorem there exists a $\xi_m \in (H_{m-1}, H_m)$ such that

$$\int_{H_{m-1}}^{H_m} \mathcal{H}(\tilde{h}) a_p(\tilde{h}, t) d\tilde{h} = \mathcal{F}(\xi_m) \int_{H_{m-1}}^{H_m} a(\tilde{h}) d\tilde{h}. \quad (4.102)$$

Using the fact that

$$a_{p,m}(t) = \int_{H_{m-1}}^{H_m} a(\tilde{h}) d\tilde{h} \quad (4.103)$$

the discrete distribution of ridged ice becomes

$$n_n = \sum_{m=0}^{N_c} \frac{a_{p,m}}{k(\xi_m)} \left(\exp \left(-\frac{(H_L - H_{min}(\xi_m))}{\lambda(\xi_m)} \right) - \exp \left(\frac{(H_n - H_{min}(\xi_m))}{\lambda(\xi_m)} \right) \right). \quad (4.104)$$

Now making the approximation that $\xi_m = h_m$, the mean value of thickness for category m, $n_{p,n}$ can be approximated by

$$n_{p,n} \approx \sum_{m=1}^{N_c} \frac{a_{p,m}}{k(h_m)} \left(\exp \left(-\frac{(H_L - H_{min}(h_m))}{\lambda(h_m)} \right) - \exp \left(\frac{(H_n - H_{min}(h_m))}{\lambda(h_m)} \right) \right). \quad (4.105)$$

This assumption introduces an error in $g_{p,n}$ of order $(H_m - H_{m-1})$.

The final part of the ridging scheme is the normalization term N. The continuous N is defined as

$$N = \int_0^\infty \left(a_p(h,t) - n_p(h,t) \right) dh. \tag{4.106}$$

The analogous requirement for the discrete N is

$$N = \sum_{n=0}^{N_c} (a_{p,n} - n_{p,n}) \tag{4.107}$$

which for this case is

$$N = \sum_{n=0}^{N_c} a_{p,n}$$
$$- \sum_{n=0}^{N_c} \sum_{m=1}^{N_c} \frac{a_{p,m}}{k(h_m)} \left(\exp\left(-\frac{(H_L - H_{min}(h_m))}{\lambda(h_m)} \right) - \exp\left(-\frac{(H_n - H_{min}(h_m))}{\lambda_p(h_m)} \right) \right). \tag{4.108}$$

In a similar manner to the treatment of the continuous N in Section 3.4, separate the terms and change the summation order to obtain

$$N = \sum_{n=0}^{N_c} a_{p,n}(t)$$
$$- \sum_{m=1}^{N_c} \frac{a_{p,m}}{k(h_m)} \sum_{n=0}^{N_c} \left(\exp\left(-\frac{(H_L - H_{min}(h_m))}{\lambda(h_m)} \right) - \exp\left(-\frac{(H_n - H_{min}(h_m))}{\lambda(h_m)} \right) \right). \tag{4.109}$$

Now consider the terms in the sum over n, shown below

$$\sum_{n=0}^{N_c} \left(\exp\left(-\frac{(H_L - H_{min}(h_m))}{\lambda(h_m)} \right) - \exp\left(\frac{(H_n - H_{min}(h_m))}{\lambda(h_m)} \right) \right). \tag{4.110}$$

Recall that $H_L = \max(H_{n-1}, H_{min}(h_m))$ and that there are no contributions to the sum unless $H_{min}(h_m) < H_n$. Therefore the first term in the sum will always be

$$\exp\left(-\frac{(H_{min}(h_m) - H_{min}(h_m))}{\lambda(h_m)} \right) - \exp\left(-\frac{(H_j - H_{min}(h_m))}{\lambda(h_m)} \right)$$
$$= 1 - \exp\left(-\frac{(H_j - H_{min}(h_m))}{\lambda(h_m)} \right) \tag{4.111}$$

where j is the first thickness bin such that $H_{min}(h_m) < H_j$. Notice that the intermediate exponential terms cancel in the sum for categories j through $N_c - 1$ resulting in

$$\sum_{n=0}^{N_c} \exp\left(-\frac{(H_L - H_{min}(h_m))}{\lambda(h_m)}\right) - \exp\left(-\frac{(H_n - H_{min}(h_m))}{\lambda(h_m)}\right)$$

$$= 1 - \exp\left(-\frac{(H_{N_c} - H_{min}(h_m))}{\lambda(h_m)}\right). \tag{4.112}$$

In the limit as $H_{N_c} \to \infty$, the exponential term goes to zero resulting in the final form for N

$$N = \sum_{n=0}^{N_c} a_{p,n} - \sum_{m=1}^{N_c} \left(\frac{a_{p,m}}{k_m}\right) = a_{p,0} + \sum_{m=1}^{N_c} a_{p,m}\left(1 - \frac{1}{k_m}\right). \tag{4.113}$$

Putting the pieces together, the discrete redistribution term for $1 \leq n \leq N_c$ becomes

$$\psi_n = -a_{p,n}\frac{r_{cl}}{N}$$

$$+ \sum_{m=1}^{N_c} \frac{a_{p,m}}{k(h_m)}\left(\exp\left(-\frac{(H_L - H_{min}(h_m))}{\lambda(h_m)}\right) - \exp\left(\frac{(H_n - H_{min}(h_m))}{\lambda(h_m)}\right)\right)\frac{r_{cl}}{N}. \tag{4.114}$$

A similar procedure can be used to obtain the equation for the open water fraction $g_{p,0}$. First integrate the evolution equation for $g_p(h,t)$ between H_0^- and H_0^+ to obtain

$$\int_{H_0^-}^{H_0^+} \frac{dg}{dt} dh = \int_{H_0^-}^{H_0^+} \left(-g_p(h,t)\text{div}_{\mathbf{x}}\mathbf{v} - \frac{\partial(fg)}{\partial h} + \psi\right) dh$$

$$\frac{dg_{p,0}}{dt} = -g_{p,0}\text{div}_{\mathbf{x}}\mathbf{v} - g_p(H_0^+)f(H_0^+) + g_p(H_0^-)f(H_0^-) + \psi_0. \tag{4.115}$$

The redistribution term for open water fraction can be obtained from the following integral

$$\psi_0 = \int_{H_0^-}^{H_0^+} \left(\delta(h)r_{op} + \frac{-a_p(h,t)}{N}\right) dh \tag{4.116}$$

which becomes

$$\psi_0 = r_{op} - \frac{a_{p,0}}{N} \tag{4.117}$$

where

$$a_{p,0}(t) = \frac{1 - \exp(-G_p(0,t)/a^*)}{1 - \exp(-1/a^*)}. \tag{4.118}$$

Note that $n_p(h,t)$, the distribution of new ice, does not contribute in the integral over $[H_0^-, H_0^+]$.

The evolution equation for the open water fraction then becomes

$$\frac{dg_{p,0}}{dt} = -(\text{div}_{\mathbf{x}}\mathbf{v})g_{p,0} + r_{op} - \frac{a_{p,0}}{N}r_{cl} + \mathcal{G}_0 \tag{4.119}$$

and the evolution equation for each thickness category $1 \leq n \leq N_c$ is

$$\frac{dg_n}{dt} = -(\text{div}_{\mathbf{x}}\mathbf{v})g_{p,n} + \mathcal{G}_n - \frac{a_{p,n}}{N}r_{cl}$$
$$+ \sum_{m=1}^{N_c} \frac{a_{p,m}}{k(h_m)} \left(\exp\left(-\frac{(H_L - H_{min}(h_m))}{\lambda(h_m)} \right) - \exp\left(\frac{(H_n - H_{min}(h_m))}{\lambda(h_m)} \right) \right) \frac{r_{cl}}{N}. \tag{4.120}$$

In the derivation of the continuum evolution equation for g, the rate of opening and closing are chosen so that area is conserved and have the following forms

$$r_{cl} = \langle -\text{div}_{\mathbf{x}}\mathbf{v} \rangle$$
$$r_{op} = \langle \text{div}_{\mathbf{x}}\mathbf{v} \rangle \tag{4.121}$$

where $\langle \cdot \rangle$ is defined so that $\langle x \rangle = x$ if $x > 0$ and $\langle x \rangle = 0$ if $x < 0$. Note that for these choices of r_{cl} and r_{op}, the horizontal transport and redistribution terms in the evolution equation for discrete thickness categories together also conserve area. To see this, sum the evolution equation over all categories

$$\sum_{n=0}^{N_c} \frac{dg_{p,n}}{dt} = \sum_{n=0}^{N_c} -(\text{div}_{\mathbf{x}}\mathbf{v})g_{p,n} + \sum_{n=0}^{N_c} \mathcal{G}_n + r_{op} - \frac{a_{p,0}}{N}r_{cl} + \sum_{n=1}^{N_c} \frac{n_{p,n} - a_{p,n}}{N}r_{cl}. \tag{4.122}$$

The left hand side of this equation is

$$\sum_{n=0}^{N_c} \frac{dg_{p,n}}{dt} = \frac{d}{dt} \sum_{n=0}^{N_c} g_{p,n} = 0 \tag{4.123}$$

since

$$\sum_{n=0}^{N_c} g_{p,n} = 1. \tag{4.124}$$

Therefore, the right hand side terms must sum to zero for area conservation. Consider the horizontal transport and redistribution terms together

$$\sum_{n=0}^{N_c} -(\text{div}_{\mathbf{x}}\mathbf{v})g_{p,n} + r_{op} - \left(a_{p,0} + \sum_{n=1}^{N_c}(n_{p,n} - a_{p,n})\right)\frac{r_{cl}}{N}. \tag{4.125}$$

Given that

$$N = a_{p,0} + \sum_{n=1}^{N_c}(n_{p,n} - a_{p,n}) \tag{4.126}$$

and that $g_{p,n}$ sums to 1, this becomes

$$-(\text{div}_{\mathbf{x}}\mathbf{v}) + r_{op} - r_{cl}. \tag{4.127}$$

For $\text{div}_{\mathbf{x}}\mathbf{v} > 0$, r_{op} is $\text{div}_{\mathbf{x}}\mathbf{v}$ and $r_{cl} = 0$, which sums to zero. If $\text{div}_{\mathbf{x}}\mathbf{v} < 0$, r_{op} is equal to zero and $r_{cl} = -(-\text{div}_{\mathbf{x}}\mathbf{v})$, which also sums to zero. Finally, the thermodynamic term must sum to zero separately,

$$\sum_{n=0}^{N_c} \mathcal{G}_n = 0 \tag{4.128}$$

which will be shown in the next section.

4.4.2 Transport in h Due to Thermodynamics

For the thermodynamic growth or melt of ice the following equation must be solved numerically

$$\dot{g}_p + \frac{\partial(fg_p)}{\partial h} = 0. \tag{4.129}$$

This equation is analogous to a continuity equation where f is the analogue of the velocity in thickness space. The previous section assumed that $g_p(h)$ is separated

into fixed discrete thickness bins by integrating over the upper and lower thickness limits of each bin. However, solving this equation assuming fixed thickness bins is the equivalent of solving a continuity equation with an Eulerian method, which can introduce significant dispersion in the results. To avoid this problem, a linear remapping algorithm is used following Lipscomb [27]. This method solves the equation with moving thickness bin boundaries and then maps back to the fixed boundaries using changes in area and volume. The method is described in more detail below. Note that a discretization in horizontal space is assumed such that there exists a thickness distribution for each material point, which can be denoted $g_{n,p}$. For the following discussion, the p subscript will be neglected to simplify the notation.

First assume that the values g_n^k and v_n^k are known for a timestep k. The mean thickness for each category is then given as $h_n^k = v_n^k/g_n^k$ for categories where $g_n^k \neq 0$. Next assume that the thermodynamic algorithm provides a new mean ice thickness for each category n equal to $\hat{h}_n$. Define $\Delta h_n = \hat{h}_n - h_n^k$. Then the updated positions of the category boundaries (H_n) can be calculated using linear interpolation as

$$\hat{H}_n = H_n + \Delta h_n + \frac{\Delta h_{n+1} - \Delta h_n}{h_{n+1}^k - h_n^k}(H_n - h_n^k). \tag{4.130}$$

Now define fractional area and volume in each of the new categories as

$$\hat{g}_n(t) = \int_{\hat{H}_{n-1}}^{\hat{H}_n} \hat{g}(h,t)dh$$

$$\hat{v}_n(t) = \int_{\hat{H}_{n-1}}^{\hat{H}_n} h\hat{g}(h,t)dh. \tag{4.131}$$

Ice area is conserved under thermodynamic growth assuming Lagrangian thickness bins so $\hat{g}_n = g_n^k$. However, the volume in each category changes according to $\hat{v}_n = \hat{h}_n g_n^k$. If the function $\hat{g}(h,t)$ is known, the changes in area and volume in each of the

original categories due to thermodynamic growth or melt can be calculated as

$$\Delta g_n = \int_{H_n^k}^{\hat{H}_n} \hat{g}(h,t)dh$$

$$\Delta v_n = \int_{H_n^k}^{\hat{H}_n} h\hat{g}(h,t)dh.$$

(4.132)

The linear remapping algorithm assumes that $\hat{g}(h,t)$ can be approximated by a linear function such that $\hat{g}(h,t) = a_1(t)h + a_0(t)$. This linear function can then be used to calculate the above changes in area.

To make the equations more tractable, let $\eta_n = h - \hat{H}_{n-1}$ and assume that $g(\eta_n) = \alpha_{1,n}\eta_n + \alpha_{0,n}$. Then the integrals for fractional area and volume become

$$g_n^k = \int_0^{\hat{H}_n - \hat{H}_{n-1}} (\alpha_{1,n}\eta_n + \alpha_{0,n})d\eta_n$$

$$\hat{h}_n g_n^k = \int_0^{\hat{H}_n - \hat{H}_{n-1}} (\eta_n + \hat{H}_{n-1})(\alpha_{1,n}\eta_n + \alpha_{0,n})d\eta_n.$$

(4.133)

Integrating produces equations that can be solved to obtain the coefficients, α_0 and α_1

$$g_n^k = \frac{1}{2}\alpha_{1,n}(\hat{H}_n - \hat{H}_{n-1})^2 + \alpha_{0,n}(\hat{H}_n - \hat{H}_{n-1})$$

$$\hat{h}_n g_n^k = \frac{1}{3}\alpha_{1,n}(\hat{H}_n - \hat{H}_{n-1})^3 + \frac{1}{2}(\alpha_{0,n} + \alpha_{1,n}\hat{H}_{n-1})(\hat{H}_n - \hat{H}_{n-1})^2$$

$$+ \alpha_{0,n}\hat{H}_{n-1}(\hat{H}_n - \hat{H}_{n-1}).$$

(4.134)

Let $\bar{\eta}_n = \hat{H}_n - \hat{H}_{n-1}$, then the coefficients can be written as

$$\alpha_{0,n} = \frac{6g_n^k}{\bar{\eta}_n^2}\left(\frac{2}{3}\bar{\eta}_n - \hat{h}_n + \hat{H}_{n-1}\right)$$

$$\alpha_{1,n} = \frac{12g_n^k}{\bar{\eta}_n^3}\left(-\frac{1}{2}\bar{\eta}_n + \hat{h}_n - \hat{H}_{n-1}\right).$$

(4.135)

It can be shown that the linear version of $\hat{g}(\eta)$ with the above coefficients, may be less than zero if $\hat{h}_n$ is outside of the central third of the thickness range $[H_{n-1}^k, H_n^k]$ [27]. A negative $\hat{g}(\eta)$ is unphysical. Therefore, to handle this possibility, the limits

of integration must be changed so that $\hat{g}(\eta)$ is integrated only over the region where it remains positive. If $\hat{h}_n < 1/3(2\hat{H}_{n-1} + \hat{H}_n)$ then set

$$
\begin{aligned}
hL_n &= \hat{H}_{n-1} \\
hR_n &= 3\hat{h}_n - 2\hat{H}_{n-1}.
\end{aligned}
$$
(4.136)

Then if $\hat{h}_n > 2/3(\hat{H}_{n-1} + 2\hat{H}_n)$ then set

$$
\begin{aligned}
H_{L,n} &= 3\hat{h}_n - 2\hat{H}_n \\
H_{R,n} &= \hat{H}_n.
\end{aligned}
$$
(4.137)

Using these limits and defining $\tilde{\eta} = hR_n - hL_n$ the coefficients can be written as

$$
\begin{aligned}
\alpha_{0,n} &= \frac{6g_n^k}{\tilde{\eta}_n^2}\left(\frac{2}{3}\tilde{\eta}_n - \hat{h}_n + H_{L,n}\right) \\
\alpha_{1,n} &= \frac{12g_n^k}{\tilde{\eta}_n^3}\left(-\frac{1}{2}\tilde{\eta}_n + \hat{h}_n - H_{L,n}\right).
\end{aligned}
$$
(4.138)

The changes in area and volume can then be calculated as

$$
\begin{aligned}
\Delta g_n &= \int_{\eta_{L,n}}^{\eta_{R,n}} \hat{g}(\eta)d\eta \\
\Delta v_n &= \int_{\eta_{L,n}}^{\eta_{R,n}} (\eta + H_{L,n})\hat{g}(\eta)d\eta
\end{aligned}
$$
(4.139)

where $\eta_{R,n} = \min(\hat{H}_n, H_{R,n}) - H_{L,n}$ and $\eta_{R,n} = \max(H_n^k, H_{L,n}) - H_{L,n}$. After integrating this becomes

$$
\begin{aligned}
\Delta g_n &= \frac{1}{2}\alpha_{1,n}\left(\eta_{R,n}^2 - \eta_{L,n}^2\right) + \alpha_{0,n}(\eta_{R,n} - \eta_{L,n}) \\
\Delta v_n &= \frac{1}{3}\alpha_{1,n}\left(\eta_{R,n}^3 - \eta_{L,n}^3\right) + \frac{1}{2}\alpha_{0,n}(\eta_{R,n}^2 - \eta_{L,n}^2) + \Delta g_n H_{L,n}.
\end{aligned}
$$
(4.140)

The updated fractional areas and fractional volumes in the original categories can then be calculated. For the case where $\hat{H}_n > H_n^k$ the updated areas and volumes are

$$
\begin{aligned}
g_n^* &= g_n^k - \Delta g_n \\
v_n^* &= v_n^k - \Delta v_n \\
g_{n+1}^* &= g_{n+1}^k + \Delta g_n \\
v_{n+1}^* &= v_{n+1}^k + \Delta v_n.
\end{aligned}
$$
(4.141)

Alternatively, for the case where $\hat{H}_n < H_n^k$ the updated areas and volumes are

$$
\begin{aligned}
g_n^* &= g_n^k + \Delta g_n \\
v_n^* &= v_n^k + \Delta v_n \\
g_{n-1}^* &= g_{n-1}^k - \Delta g_n \\
v_{n-1}^* &= v_{n-1}^k - \Delta v_n.
\end{aligned}
\tag{4.142}
$$

Note that after summing over all categories, the changes in fractional area (Δg_n) and fractional volume (Δv_n) cancel and therefore, this discretization of the vertical transport is area and volume preserving as desired.

Once the vertical transport equation is solved for the ice. The average thickness in each category is calculated as

$$
h_p^* = \sum_{n=1}^{N_c} v_n^*.
\tag{4.143}
$$

This average thickness is used to update the material point mass as

$$
m_p^{k+1} = h_p^* \Omega_p^{k+1} \rho_p^k.
\tag{4.144}
$$

4.4.3 Horizontal Transport

The horizontal transport portion of the ITD evolution equation after discretizing in thickness space is

$$
\dot{g}_{p,n} = g_{p,n} \text{div}_{\mathbf{x}} \mathbf{v}.
\tag{4.145}
$$

Given $g_{p,n}^*$, which was obtained from the vertical transport algorithm, g_n^{**} is calculated as

$$
g_n^{**} = g_n^* e^{-\text{div}_{\mathbf{x}} \mathbf{v} \Delta t}
\tag{4.146}
$$

where the velocity divergence term is calculated from the incremental deformation gradient, f_p^{k+1}, as

$$\text{div}_{\mathbf{x}}\mathbf{v}\Delta t = \text{tr}(\Delta t \mathbf{d}^{k+1}) = \text{tr}\left(\frac{1}{2}\left(\mathbf{I} - (\mathbf{f}^{k+1})^{-T}(\mathbf{f}^{k+1})^{-1}\right)\right). \tag{4.147}$$

Here $\mathbf{I}$ is the two-dimensional identity and $\text{tr}(\cdot)$ indicates the trace. Similarly, the ice partial volume is updated as

$$v_{p,n}^{**} = v_{p,n}^{*}e^{-\text{div}_{\mathbf{x}}\mathbf{v}\Delta t}. \tag{4.148}$$

The horizontal transport portion of the evolution equation does not conserve area by itself, the mechanical redistribution step must be included for area conservation to be satisfied.

4.4.4 Mechanical Redistribution or Ridging

The equation for the mechanical redistribution portion of the ITD evolution equation discretized in thickness space for each thickness category $1 \leq n \leq N_c$ is

$$\frac{dg_{p,n}}{dt} = \frac{n_{p,n} - a_{p,n}}{N}r_{cl} \tag{4.149}$$

and for the open water fraction is

$$\frac{dg_{p,0}}{dt} = r_{op} - \frac{a_{p,0}}{N}r_{cl}. \tag{4.150}$$

Here r_{cl} is the closing rate and r_{op} is the opening rate. For a simple forward discretization in time, this becomes

$$g_{p,n}^{k+1} = \frac{n_{p,n} - a_{p,n}}{N}r_{cl}\Delta t^{k+1} \tag{4.151}$$

and

$$g_{p,0}^{k+1} = r_{op}\Delta t^{k+1} - \frac{a_{p,0}}{N}r_{cl}\Delta t^{k+1} \tag{4.152}$$

where $a_{p,0}$, $a_{p,n}$ and $n_{p,n}$ depend on $g_{p,0}^{**}$ and $g_{p,n}^{**}$. In order to ensure area conservation in this step r_{cl} and r_{op} are defined so that

$$
\begin{aligned}
r_{cl}\Delta t^{k+1} &= \max(-1 + \mathrm{e}^{-\mathrm{div}_{\mathbf{x}}\mathbf{v}\Delta t^{k+1}}, 0) \\
r_{op}\Delta t^{k+1} &= \max(1 - \mathrm{e}^{-\mathrm{div}_{\mathbf{x}}\mathbf{v}\Delta t^{k+1}}, 0).
\end{aligned}
\tag{4.153}
$$

The mechanical redistribution equation is solved in several steps. First, the current average thickness in each category must be calculated as

$$
h_n^{**} = \frac{v_{p,n}^{**}}{g_{p,n}^{**}}.
\tag{4.154}
$$

The parameter, k_n, is then calculated as

$$
k_n = \frac{H_{min,n} + \lambda_n}{h_n^{**}}
\tag{4.155}
$$

where $H_{min,n} = \min(2h_n^{**}, h_n^{**} + H_{raft})$, $\lambda_n = 4\sqrt{h_n^{**}}$, and $H_{raft} = 1\,\mathrm{m}$ is the maximum thickness of ice to raft [28]. Next the fraction of ice participating in ridging for each category is calculated as

$$
a_{p,n} = \frac{\mathrm{e}^{-G_{p,n-1}/a^*} - \mathrm{e}^{-G_{p,n}/a*}}{1 - \mathrm{e}^{1/a^*}}
\tag{4.156}
$$

where

$$
G_{p,n} = \frac{\sum_{m=0}^{n} g_{p,m}^{**}}{\sum_{n=0}^{N} g_{p,n}^{**}}
\tag{4.157}
$$

and $G_{p,-1} = 0$. Note that the sum of $g_{p,n}^{**}$ in the denominator does not equal one since the horizontal transport step is not area preserving. Given k_n and $a_{p,n}$, the normalization factor can be calculated as

$$
N = a_{p,0} + \sum_{n=1}^{N_c} a_{p,n}\left(1 - \frac{1}{k_n}\right).
\tag{4.158}
$$

Once these preliminary calculations have been done, $g_{p,n}^{k+1}$ can be calculated. If the area is increasing in a material point such that $r_{op}\Delta t^{k+1} > 0$, open water is added to the distribution as

$$
g_{p,0}^{k+1} = g_{p,0}^{**} + r_{op}\Delta t^{k+1}
\tag{4.159}
$$

and the rest of the thickness distribution remains unchanged. However, if the area change is negative, which is true under converging conditions, area is taken away from each category based on the participation fraction.

$$
\begin{aligned}
g_{p,0}^{k+1} &= g_{p,0}^{**} - \frac{a_{p,0}}{N} r_{cl} \Delta t^{k+1} \\
g_{p,n}^{k+1} &= g_{p,n}^{**} - \frac{a_{p,n}}{N} r_{cl} \Delta t^{k+1} + \sum_{m=1}^{N_c} \frac{a_{p,m}}{k_m N} g_{frac,m} r_{cl} \Delta t^{k+1}
\end{aligned}
\tag{4.160}
$$

where

$$
g_{frac,m} = \exp\left(\frac{-h_{L,m} - H_{min,m}}{H_{exp,m}}\right) - \exp\left(\frac{-H_n - H_{min,m}}{H_{exp,m}}\right)
\tag{4.161}
$$

and $h_{L,m} = \max(H_{min,m}, H_{n-1})$.

The volume is updated similarly as

$$
v_{p,n}^{k+1} = v_{p,n}^{**} - \frac{v_{p,n}^{**}}{g_{p,n}^{**}} \frac{a_{p,n}}{N} r_{cl} + \sum_{m=1}^{N_c} \frac{v_{p,m}^{**}}{g_{p,m}^{**}} \frac{a_{p,m}}{N} v_{frac,m} r_{cl} \Delta t^{k+1}
\tag{4.162}
$$

where

$$
v_{frac,m} = \frac{(h_{L,m} + H_{exp,m})\exp\left(\frac{-h_{L,m}-H_{min,m}}{H_{exp,m}}\right) - (H_n + H_{exp,m})\exp\left(\frac{-H_n-H_{min,m}}{H_{exp,m}}\right)}{H_{min,m} + H_{exp,m}}
\tag{4.163}
$$

Note that for the case where $H_{min,m} \geq H_n$, $g_{frac,m}$ and $v_{frac,m}$ are equal to zero.

The updated volume is then used to calculate the updated average thickness for the material point

$$
h_p^{k+1} = \sum_{n=1}^{N_c} v_{p,n}^{k+1}.
\tag{4.164}
$$

Additionally, after this step the updated material point density is calculated as

$$
\rho_p^{k+1} = \frac{m_p^{k+1}}{\Omega_p^{k+1} h_p^{k+1}}.
\tag{4.165}
$$

4.5   Thermodynamics

The change in thickness for each thickness category used in the thermodynamic portion of the ITD equation is obtained from the following thermodynamic model. The first step in calculating the change in thickness is to solve the one-dimensional heat equation for a column of ice of thickness $h_{p,n} = v_{p,n}/a_{p,n}$. The continuum equation in terms of the vertical coordinate, X_3 is

$$\rho_0 \left(C_0 + \frac{L_0 \mu S(X_3)}{T^2} \right) \dot{T} = \frac{\partial}{\partial X_3} \left(\left(k_0 + \frac{\beta S(X_3)}{T} \right) \frac{\partial T}{\partial X_3} \right) + \kappa I_0 e^{-\kappa X_3} \quad (4.166)$$

for a given salinity profile $S(X_3)$. The constants used in these equations are shown in Table 4.1. A fixed temperature is used at the ice-ocean interface, T_{bot}, which is assumed to be equal to the freezing temperature of sea water, $-1.8°C$. The temperature of the ice-atmosphere interface, T_0, depends on the flux conditions at the boundary. The net flux at the top surface is

$$F_{net}(T_0) = F_r(1-\alpha) - I_0 + F_L - \sigma T_0^4 + F_s + F_l + \left(k \frac{\partial T}{\partial z} \right) \bigg|_{X_3 = Z_{top}}. \quad (4.167)$$

If $F_{net}(T_0 = 0°C) < 0$, the new surface temperature, T_0, is calculated by solving $F_{net}(T_0) = 0$ and if $F_{net}(T_0 = 0°C) > 0$ the surface temperature is set to $0°C$.

The change in thickness at the bottom surface is governed by

$$\left(k(S,T)(\frac{\partial T}{\partial X_3}) \right) \bigg|_{X_3 = Z_{bot}} - F_w = (q(S,T)) \big|_{X_3 = Z_{bot}} \frac{dh}{dt} \quad (4.168)$$

where

$$q(S(Z_{bot}), T_{bot}) =$$
$$\rho \left(C_0(-\mu S(Z_{bot}) - T_{bot}) + L_0 \left(1 - \frac{-\mu S(Z_{bot})}{T_{bot}} + C_w \mu S(Z_{bot}) \right) \right). \quad (4.169)$$

Constants in this equation are defined in Table 4.1. If $F_{net}(T_0 = 0°C) > 0$ the surface melt is calculated as

$$-q(S(Z_{top}), T_0) \frac{dh}{dt} = F_r(1-\alpha) - I_0 + F_L - \sigma T_0^4 + F_s + F_e + \left(k(S,T) \frac{\partial T}{\partial z} \right) \bigg|_{X_3 = Z_{top}}.$$

$$\tag{4.170}$$

In this case the enthalpy is

$$q(S(Z_{top}), T_0) = \rho \left(C_0(-\mu S(Z_{top}) - T_0) + L_0 \left(1 - \frac{-\mu S(Z_{top})}{T_0} + C_w(\mu S(Z_{top})) \right) \right).$$

$$\tag{4.171}$$

Table 4.1: Thermodynamic Constants

heat capacity of fresh ice	C_0	2100 J/(kg K)
conductivity of fresh ice	k_0	2.034 W/(m C)
latent heat of fresh ice	L_0	334 kJ/kg
extinction coefficient	κ	1.5 1/m
ice albedo	α	0.63
emissivity	ϵ	$0.95~^{-3}$
melting temp parameter	μ	0.054 K/ppt
conductivity constant	β	0.13 W/(m ppt)

To solve this set of equations a discretization must be done in vertical space. Assume that the ice column is divided into N_l equally spaced layers with thickness $\Delta h = h_{p,n}/N_l$. The salinity is then calculated for each layer as

$$S_l = \frac{S_{max}}{2} \left(1 - \cos\left(\pi x^{\frac{a}{x+b}} \right) \right) \tag{4.172}$$

where $x = (l - 0.5)/N_l$, $S_{max} = 3.2$ ppt, $a = 0.407$ and $b = 0.573$. This formula is derived from fit to data by Schwarzacher [26]. The salinity values are assumed to be center values for the layer. Similarly, the temperatures for each layer, T_l, and heat capacity, C_l, are taken to be center of layer values. However, the conductivity values, k_l, which are used to calculate the fluxes between layers are assumed to be given at the layer boundaries. An illustration of this discretization is given in Figure 4.2.

The heat capacity at a layer, l, is discretized in time by considering an integral over the temperature interval $[T_l^k, T_l^{k+1}]$. This interval corresponds to a time interval
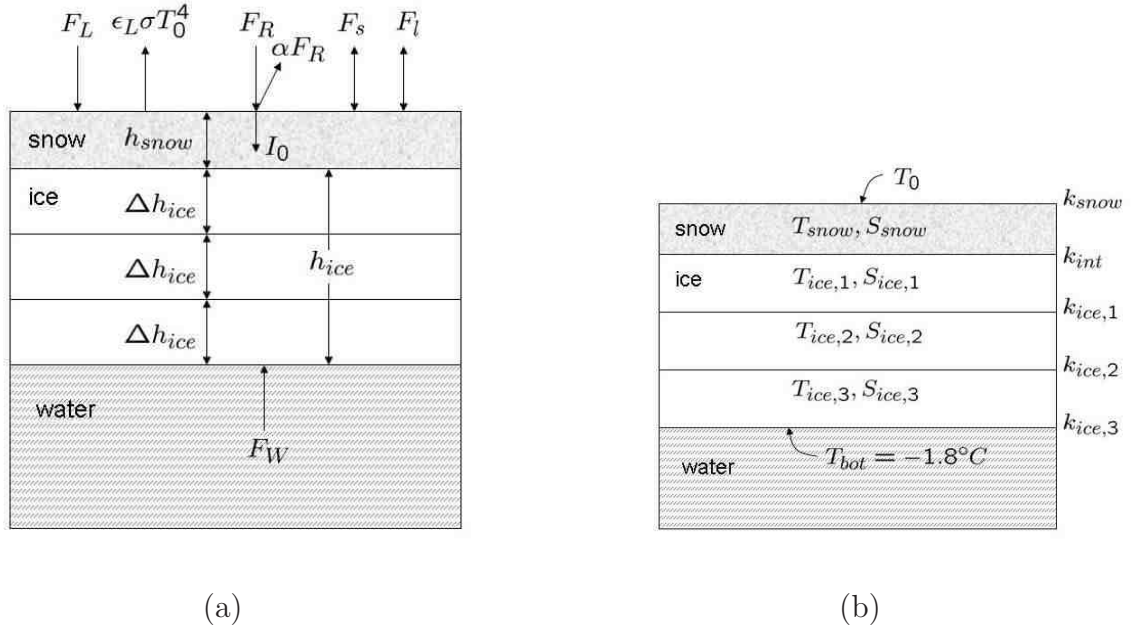
Figure 4.2: Ice column discretization with (a) boundary conditions and (b) locations of discrete variables.

$[t^k, t^{k+1}]$ and so the integral can be written as

$$\int_{T_l^k}^{T_l^{k+1}} \rho C_l dT = \int_{T_l^k}^{T_l^{k+1}} \rho \left(C_0 + \frac{L_0 \mu S_l}{T^2} \right) dT. \tag{4.173}$$

After integrating this becomes

$$\rho C_0 (T_l^{k+1} - T_l^k) - \rho L_0 \mu S_l \left(\frac{1}{T_l^{k+1}} - \frac{1}{T_l^k} \right)$$
$$= \rho (T_l^{k+1} - T_l^k) \left(C_0 + \frac{L_0 \mu S_l}{T_l^{k+1} T_l^k} \right). \tag{4.174}$$

Following Bitz and Lipscomb [7] the right-hand side of the heat equation is discretized as

$$\frac{\partial}{\partial z} k(S, T) \frac{\partial T}{\partial z} \approx \frac{1}{\Delta h} \left(\frac{k_{l+1}(T_{l+1}^{k+1} - T_l^{k+1})}{\Delta h} - \frac{k_l(T_l^{k+1} - T_{l-1}^{k+1})}{\Delta h} \right) \tag{4.175}$$

where

$$k_l = k_0 + \frac{1}{2} \frac{\beta(S_{l-1} + S_l)}{T_{l-1}^k + T_l^k} \tag{4.176}$$

Similarly, the short wave radiation term is discretized as

$$\frac{dI}{dz} \approx I_0 \frac{(\exp(-\kappa(l-1)\Delta h) - \exp(-\kappa l \Delta h)}{\Delta h} \tag{4.177}$$

Putting the pieces together results in the discretized heat equation for a column of ice, which can be written as

$$
\begin{aligned}
\rho \frac{(T_l^{k+1} - T_l^k)}{\Delta t} &\left(C_0 + \frac{L_0 \mu S_l}{T^{k+1} T^k} \right) = \\
&\frac{1}{\Delta h} \left(\frac{k_{l+1}(T_{l+1}^{k+1} - T_l^{k+1})}{\Delta h} - \frac{k_l(T_l^{k+1} - T_{l-1}^{k+1})}{\Delta h} \right) \\
&-I_0 \frac{(\exp(-\kappa(l-1)\Delta h) - \exp(-\kappa l \Delta h)}{\Delta h}.
\end{aligned}
\tag{4.178}
$$

This discretization is second-order in T and first-order in t [7].

In order to apply the boundary conditions a discretization for the conductive flux at the top surface must be chosen. In the case of ice with a snow layer on top the conductive flux is calculated as

$$k(S,T) \frac{\partial T}{\partial z} \bigg|_{z=0} \approx \frac{k_{snow}}{h_{snow}} \left((T_0^{k+1} - T_{snow}^{k+1}) \right) \tag{4.179}$$

where $k_{snow} = 0.3$ W/(m deg). In the case of no snow layer the conductive flux is calculated as

$$k(S,T) \frac{\partial T}{\partial z} \bigg|_{z=0} \approx \frac{k_1}{\Delta h} \left(3(T_0^{k+1} - T_1^{k+1}) - \frac{1}{3}(T_0^{k+1} - T_2^{k+1}) \right) \tag{4.180}$$

If no snow is present then the conductivity of the first layer is calculated as

$$k_1 = k_0 + \frac{\beta S_1}{T_0^k}. \tag{4.181}$$

Otherwise the k_1 is the ice-snow interface conductivity and is defined as

$$k_1 = \frac{2 k_{ice} k_{snow}}{k_{ice} h_{snow} + k_{snow} \Delta h} \tag{4.182}$$

for

$$k_{ice} = k_0 + \frac{\beta S_1}{T_0^k}. \tag{4.183}$$

Similarly, for the bottom layer

$$k(S,T)\frac{\partial T}{\partial z}\bigg|_{X_3=Z_{bot}} \approx \frac{k_{N_l+1}}{\Delta h}\left(3(T_{N_l}^{k+1}-T_{bot})-\frac{1}{3}(T_{N_{l-1}}^{k+1}-T_{bot})\right) \tag{4.184}$$

and

$$k_{N_l+1} = k_0 + \frac{\beta S_{max}}{T_{bot}}. \tag{4.185}$$

The first step in solving for the thermodynamic growth or melt of an ice column is to solve for the temperature profile. Note that Equation 4.173 can be written as

$$-\frac{k_l}{\Delta h^2}T_{l-1}^{k+1} + \left(\frac{\rho C_l}{\Delta t}+\frac{k_{l+1}}{\Delta h^2}+\frac{k_l}{\Delta h^2}\right)T_l^{k+1} - \frac{k_{l+1}}{\Delta h^2}T_{l+1}^{k+1} =$$
$$\frac{\rho C_l}{\Delta t}T_l^k - I_0\frac{(\exp(-\kappa(l-1)\Delta h) - \exp(-\kappa l\Delta h))}{\Delta h}. \tag{4.186}$$

where

$$C_l = C_0 + \frac{L_0\mu S_l}{T_l^{k+1}T_l^k}. \tag{4.187}$$

If the nonlinear dependence of C_l on T_l^{k+1} is ignored for now, this system can be written as a tridiagonal matrix for the updated values of T_l^{k+1}. This equation holds for all interior temperatures such that $2 \leq l \leq N_{l-1}$. For the bottom layer ($l = N_l$) the equation is

$$\left(-\frac{k_{N_l}}{\Delta h^2}+\frac{1}{3}\frac{\rho C_{N_l}}{\Delta t}\frac{k_{N_l+1}}{\Delta h^2}\right)T_{N_{l-1}}^{k+1} + \left(\frac{\rho C_l}{\Delta t}+\frac{k_{N_l}}{\Delta h^2}+3\frac{\rho C_l}{\Delta t}\frac{k_{N_l+1}}{\Delta h^2}\right)T_{N_l}^{k+1} =$$
$$\frac{\rho C_{N_l}}{\Delta t}T_{N_l}^k + \frac{8}{3}\frac{k_{N_l+1}}{\Delta h^2}T_{bot} - I_0\frac{(\exp(-\kappa(N_{l-1})\Delta h)-\exp(-\kappa N_l\Delta h))}{\Delta h}. \tag{4.188}$$

The equation for the top layer varies for the following four cases: $F_{net} < 0$, snow present; $F_{net} < 0$, snow absent; $F_{net} > 0$, snow present; $F_{net} > 0$, snow absent. A discrete version of the net surface flux is

$$F_{net}(T_0) = F_r(1-\alpha) - I_0 + F_L - \sigma(T_0^{k+1}+273.15)^4 + F_s + F_l$$
$$+ \frac{k_1}{\Delta h}\left(3(T_1^{k+1}-T_0^{k+1})-\frac{1}{3}(T_2^{k+1}-T_0^{k+1})\right). \tag{4.189}$$

The surface flux is a nonlinear function of the surface temperature, T_0^{k+1}. However, the flux can be linearized by approximating the outward longwave flux as

$$\sigma(T_0^{k+1} + 273.15)^4 \approx \sigma(T_0^k + 273.15)^4 + 4\sigma(T_0^k + 273.5)^3(T_0^{k+1} - T_0^k) \quad (4.190)$$

For the implementation used here the flux of sensible heat (F_s) and flux of latent heat (F_l) are treated as constants. However, if parametrizations are used for these fluxes so that they are a function of the surface temperature, these terms must be linearized as well.

To account for the fact the C_l is a nonlinear function of temperature, this linear system is solved iteratively using

$$C_l = C_0 + \frac{L_0 \mu S_l}{T_l^* T_l^k} \quad (4.191)$$

where T_l^* is the value of T_l at the current iteration. Similarly, the outward longwave flux is calculated as

$$\sigma(T_0^{k+1} + 273.15)^4 \approx \sigma(T_0^* + 273.15)^4 + 4\sigma(T_0^* + 273.15)^3(T_0^{k+1} - T_0^*). \quad (4.192)$$

After solving for the updated temperature profile, the next step in the thermo-dynamic model is to calculate the change in thickness. At the bottom surface the energy available for melting or growing ice is calculated as

$$E_{melt,grow} = \left(\frac{k_{N_l+1}}{\Delta h}\left(3(T_{N_l}^{k+1} - T_{bot}^{k+1}) - \frac{1}{3}(T_{N_l-1}^{k+1} - T_{bot}^{k+1})\right) - F_{bot}\right)\Delta t. \quad (4.193)$$

In the case of melting this energy is positive and in the case of growing ice it is negative. For melting ice the change in thickness of the bottom layer is calculated as

$$\Delta h_{N_l} = E_{melt,grow}/q_{N_l} \quad (4.194)$$

where

$$q_{N_l} = \rho\left(C_0(-\mu S_{N_l} T_{N_l}^{k+1}) + L_0\left(1 + \frac{\mu S_{N_l}}{T_{N_l}^{k+1}} + C_w \mu S_{N_l}\right)\right). \quad (4.195)$$

Note that q_{N_l} is less than zero and therefore the change in thickness is negative. If more energy remains after the bottom layer melts completely the change in thickness of the N_{l-1} layer is calculated as

$$\Delta h_{N_{l-1}} = \frac{(E_{melt,grow} - \Delta h_{N_l} q_{N_l})}{q_{N_{l-1}}} \tag{4.196}$$

where

$$q_{N_{l-1}} = \rho \left(C_0(-\mu S_{N_{l-1}} T^{k+1}_{N_{l-1}}) + L_0 \left(1 + \frac{\mu S_{N_{l-1}}}{T^{k+1}_{N_{l-1}}} + C_w \mu S_{N_{l-1}} \right) \right). \tag{4.197}$$

This process continues moving up layer by layer until all the melting energy has been used. In the case of growth at the bottom surface the change in thickness is also calculated as in Equation 4.189. However, the change in thickness is now positive and ice is added to the bottom layer.

At the top surface ice or snow can only melt since it is assumed that ice only grows at the bottom surface. If T_0 is equal to zero and $F_{net} > 0$ then the energy available for melting ice or snow at the top surface is calculated as

$$E_{melt} = F_{net} \Delta t \tag{4.198}$$

Then the thickness change of the top layer is calculated as

$$\Delta h_1 = E_{melt,grow} / q_{top} \tag{4.199}$$

where

$$q_{top} = \rho \left(C_0(-\mu S_1 T^{k+1}_1) + L_0 \left(1 + \frac{\mu S_1}{T^{k+1}_1} + C_w \mu S_1 \right) \right) \tag{4.200}$$

If there is energy remaining after the top layer melts the remaining energy is used to calculate the change in thickness of the next layer down in a similar manner.

Once the thickness changes are made the layers are converted back to equal thickness layers while conserving energy and enthalpy. The thickness change for the snow and the total thickness change for the ice is then passed to the vertical transport portion of the ice thickness distribution.

Chapter 5

Satellite Data and Sea Ice Kinematics

5.1 RADARSAT Geophysical Processor System

The modeling of sea ice is connected to the availability of data. The increasing amount of satellite and other data for sea ice makes it possible to compare model results to actual deformations and thickness measures. The data used in this effort come from the RADARSAT Geophysical Processor System (RGPS), which was developed by the Polar Remote Sensing Group at the Jet Propulsion Laboratory (JPL) to extract sea ice motion data from synthetic aperature radar (SAR) imagery [24]. At an initial time, a set of points forming a regular grid is located in the SAR data sets. Then in the images resulting from subsequent satellite passes, the original points are found again using area-based and feature-based tracking. This procedure provides displacements at each point. If the set of points in the original configuration is viewed as the vertices of square cells then the motion of the points determines the deformation of the cells. With this interpretation, grid quantities can be approximated that help provide a picture of the type of deformation the ice is undergoing. Measures such as the divergence, shear, and vorticity can be calculated using the nodal displacements.

Given a two-dimensional horizontal ice velocity with components (u, v) the divergence, shear, and vorticity can be calculated as

$$
\begin{aligned}
\text{divergence} &= \frac{\partial u}{\partial x} + \frac{\partial v}{\partial y} \\
\text{shear} &= \left(\left(\frac{\partial u}{\partial x} - \frac{\partial v}{\partial y} \right)^2 + \left(\frac{\partial u}{\partial y} + \frac{\partial v}{\partial x} \right)^2 \right)^{1/2} \\
\text{vorticity} &= \frac{\partial v}{\partial x} - \frac{\partial u}{\partial y}
\end{aligned}
\tag{5.1}
$$

For a given cell with area A the derivatives above can be approximated as [23]

$$
\begin{aligned}
\frac{\partial u}{\partial x} &= \frac{1}{A} \sum_{i=1}^{N_{vert}} \frac{1}{2}(u_{i+1} + u_i)(y_{i+1} - y_i) \\
\frac{\partial u}{\partial y} &= \frac{1}{A} \sum_{i=1}^{N_{vert}} \frac{1}{2}(u_{i+1} + u_i)(x_{i+1} - x_i) \\
\frac{\partial v}{\partial x} &= \frac{1}{A} \sum_{i=1}^{N_{vert}} \frac{1}{2}(v_{i+1} + v_i)(y_{i+1} - y_i) \\
\frac{\partial v}{\partial y} &= \frac{1}{A} \sum_{i=1}^{N_{vert}} \frac{1}{2}(v_{i+1} + v_i)(x_{i+1} - x_i)
\end{aligned}
\tag{5.2}
$$

where N_{vert} is the number of vertices for the cell, u_i and v_i are the components of the velocity at vertex i, x_i and y_i are the components of the position vector for vertex i, and the vertex index is cyclical (*i.e.* $1+N_{vert} = 1$). Note that points are added to avoid large distortions, so N_{vert} can increase with time.

As an example, satellite views of a 50 kilometer by 50 kilometer region of Arctic ice are shown in Figure 5.1 with the the RGPS grid superimposed. These data were provided by Ron Kwok of JPL. The time span between the first and second observation is 18.5 hours and the satellite images were recorded in mid May 2002. This region undergoes a fairly simple deformation over this time, which can be seen in the grid displacements where a large shear band is visible. Using the discrete definitions of divergence, shear, and vorticity shown above, plots of these parameters for this small region are shown in Figure 5.2. Notice the primary band of deformation visible in all three plots.

RGPS data have also been provided for a larger region in the Beaufort Sea, which lies between Banks Island in the East and Point Barrow in the West, and is indicated by the black rectangle in the Arctic map in Figure 5.3. This region is bounded by the coast of Alaska on one side and, in the winter, by sea ice on the other three sides. The RGPS data for this region cover a period of seventeen days in February and March of 2004.
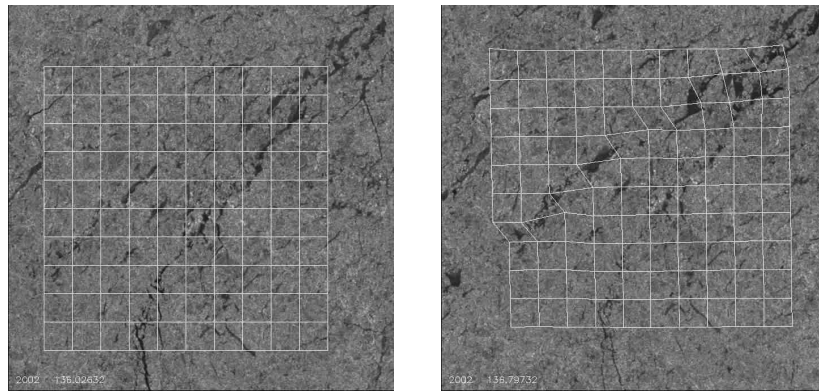
Figure 5.1: Satellite View of Small Region with Grid at Initial and Final Times
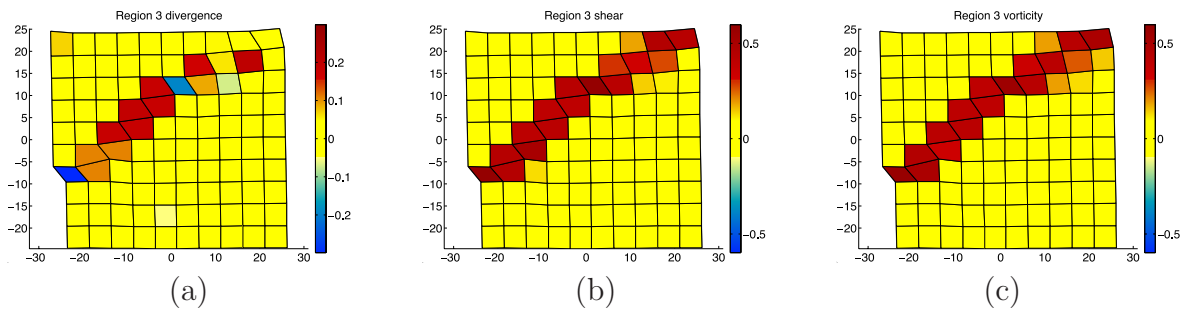

Figure 5.2: Small ice region (a) divergence (b) shear (c) vorticity.

Using the displacements at each of the grid nodes from the RGPS data and Equation 5.2, divergence, shear and vorticity have been calculated for this region. Plots of these quantities for the first day, 23 February 2004 or day 54 of 2004, are shown in Figure 5.4. The same plots for day 70 are shown in Figure 5.5.

Note that linear features in the data are apparent when plotting these quantities. The linear features may correspond to leads or ridges in the ice. The divergence, shear, and vorticity can also be calculated from cell deformations based on calculations in MPM. This is one method for comparing the satellite data with the calculation results. Given that the constitutive model used for this task includes cracks explicitly, a method for evaluating the deformation of the cells from the RGPS data

111

Figure 5.3: Arctic map with Beaufort region indicated.

in terms of discontinuities is desired. The approach taken for this is discussed in the next section.

5.2   Finite Strain Kinematics

The idea behind the finite strain kinematics is to assume that all the deformation in a RGPS cell is due to a discontinuity. With this assumption, the best fit discontinuity for each cell based on the given RGPS deformation can be found. As in the derivation of the elastic-decohesive model in Chapter 3, consider a deformation that consists of a smooth part ($\overline{\varphi}$) and a jump ($[\![\varphi]\!]$) such that

$$\varphi = \overline{\varphi} + [\![\varphi]\!] H_\Gamma \tag{5.3}$$

where H_Γ is the Heaviside function over the discontinuity surface, Γ defined on a region surrounding the discontinuity, Ω_Γ, as

$$H_\Gamma(\mathbf{X}) = \begin{cases} 1 \ \mathbf{X} \in \Omega_\Gamma^+ \\ 0 \ \mathbf{X} \in \Omega_\Gamma^- \end{cases} \tag{5.4}$$

In the context of sea ice kinematics assume that Ω_Γ is a cell area. Using this form of the deformation, the associated deformation gradient can be written as

$$\mathbf{F} = \text{Grad}\overline{\varphi} + \text{Grad}[\![\varphi]\!]H_\Gamma + [\![\varphi]\!] \otimes \mathbf{N}_\Gamma \delta_\Gamma \tag{5.5}$$

Assume that $[\![\varphi]\!]$ is constant over a cell, and therefore

$$\mathbf{F} = \text{Grad}\overline{\varphi} + [\![\varphi]\!] \otimes \mathbf{N}_\Gamma \delta_\Gamma \tag{5.6}$$

The RGPS data provide displacements at the nodes for a region made up of quadrilateral elements. To find the best fit discontinuity for the displacement field, the deformation gradient on each cell must be approximated from the RGPS data and fit to a deformation gradient of the form above. In order to calculate $\mathbf{F}$ for each element, bilinear shape functions are used as in MPM. Consider a parent element as shown in Figure 5.6 with coordinates (ξ_1, ξ_2) defined from 0 to 1. At any point in the original element, a position $\mathbf{X}$ can be described in terms of shape functions and the coordinates of the element nodes $(\mathbf{X_1}, \mathbf{X_2}, \mathbf{X_3}, \mathbf{X_4})$ as

$$\begin{aligned} \mathbf{X}(\xi_\mathbf{1}, \xi_\mathbf{2}) &= \sum_I \mathbf{X_I} N_I \\ &= \mathbf{X_1}(1 - \xi_1)(1 - \xi_2) + \mathbf{X_2}\xi(1 - \xi_2) + \mathbf{X_3}\xi_1\xi_2 + \mathbf{X_4}(1 - \xi_1)\xi_2 \end{aligned} \tag{5.7}$$

Similarly a displacement can be written as

$$\mathbf{u} = \mathbf{u_1}(1 - \xi_1)(1 - \xi_2) + \mathbf{u_2}\xi_1(1 - \xi_2) + \mathbf{u_3}\xi_1\xi_2 + \mathbf{u_4}(1 - \xi_1)\xi_2 \tag{5.8}$$

where $\mathbf{u_j}, j = 1, 2, 3, 4$ are the displacements at element nodes. The displacement, $\mathbf{u}$ can be written in terms of φ as $\mathbf{u} = \varphi - \mathbf{X}$. Therefore the deformation gradient can be related to the displacements as

$$\mathbf{F} = \text{Grad}\varphi = \frac{\partial \varphi}{\partial \mathbf{X}} = \mathbf{I} + \frac{\partial \mathbf{u}}{\partial \mathbf{X}} \tag{5.9}$$

The partial derivatives of $\mathbf{u}$ with respect to $\mathbf{X}$ can be defined using the chain rule as

$$\frac{\partial \mathbf{u}}{\partial \mathbf{X}} = \frac{\partial \mathbf{u}}{\partial \boldsymbol{\xi}} \frac{\partial \boldsymbol{\xi}}{\partial \mathbf{X}} \tag{5.10}$$

Let $\mathbf{u}$ have components (u, v) and $\mathbf{X}$ have components (X, Y). Then for the simple case where the initial configuration of the grid is regular, and the deformation gradient is calculated at the center of each cell (*i.e.* $\xi_1 = \xi_2 = 0.5$), the components of $\mathbf{F}$ are calculated as

$$
\begin{aligned}
F_{11} &= 1 + \frac{1}{J}\left(\frac{1}{4}\big((Y_4 - Y_1) + (Y_3 - Y_2)\big)\big((u_2 - u_1) + (u_3 - u_4)\big)\right) \\
F_{12} &= \frac{1}{J}\left(\frac{1}{4}\big((X_2 - X_1) + (X_3 - X_4)\big)\big((u_2 - u_1) + (u_3 - u_4)]\big)\right) \\
F_{21} &= \frac{1}{J}\left(\frac{1}{4}\big((Y_4 - Y_1) + (Y_3 - Y_2)\big)\big((v_2 - v_1) + (v_3 - v_4)]\big)\right) \\
F_{22} &= 1 + \frac{1}{J}\left(\frac{1}{4}\big((X_2 - X_1) + (X_3 - X_4)\big)\big((u_2 - u_1) + (u_3 - u_4)\big)\right)
\end{aligned}
\tag{5.11}
$$

Here J is the Jacobian of the transformation defined as

$$J = \frac{\partial X}{\partial \xi_1}\frac{\partial Y}{\partial \xi_2} - \frac{\partial Y}{\partial \xi_1}\frac{\partial X}{\partial \xi_2} \tag{5.12}$$

Given this calculated deformation gradient it remains to show the procedure for determining the best fit $[\![\varphi]\!]$ and $\mathbf{N}$. In order to do this, consider a multiplicative decomposition of $\mathbf{F}$ where $\overline{\mathbf{F}} = \mathrm{Grad}\overline{\varphi}$ as

$$
\begin{aligned}
\mathbf{F} &= \overline{\mathbf{F}} + [\![\varphi]\!] \otimes \mathbf{N}\delta_\Gamma \\
&= \overline{\mathbf{F}}(\mathbf{I} + \overline{\mathbf{F}}^{-1}[\![\varphi]\!] \otimes \mathbf{N}\delta_\Gamma) \\
&= \overline{\mathbf{F}}\widetilde{\mathbf{F}}
\end{aligned}
\tag{5.13}
$$

Now assume that the δ-function can be regularized over a grid cell so that

$$\overline{\mathbf{F}}^{-1}[\![\varphi]\!] \otimes \mathbf{N}\delta_\Gamma \rightarrow \frac{1}{L}\overline{\mathbf{F}}^{-1}[\![\varphi]\!] \otimes \mathbf{N} \tag{5.14}$$

Define $\mathbf{J} = \overline{\mathbf{F}}^{-1}[\![\varphi]\!]/L$ and then

$$\mathbf{F} = \overline{\mathbf{F}}(\mathbf{I} + \mathbf{J} \otimes \mathbf{N}) \tag{5.15}$$

When calculating the jump in displacement with this technique, the length scale is taken to be an element length from the initial regular grid.

In the case of these kinematic crack calculations the deformation will be assumed to be entirely due to decohesion, which is equivalent to assuming that is there is no elastic deformation in the cell. Then the regular portion of the deformation gradient must be purely a rotation, which is area preserving. In the first simple case, assume the $\overline{\mathbf{F}}$ is equal to the identity and therefore $\mathbf{F}$ is of the form $\mathbf{F} = (\mathbf{I} + \mathbf{J} \otimes \mathbf{N})$. For each element also assume that the discontinuity passes through the center and that $\mathbf{J}$ is constant over a linear Γ. With these assumptions, the expected $\mathbf{F} - \mathbf{I}$ is a rank one matrix formed from the two vectors $\mathbf{J}$ and $\mathbf{N}$. Starting with the calculated $\mathbf{F}$ from each element of the RGPS data first calculate the singular value decomposition (SVD) of $(\mathbf{F} - \mathbf{I})$ defined as

$$\mathbf{F} - \mathbf{I} = \mathbf{U}\boldsymbol{\Sigma}\mathbf{V}^T \tag{5.16}$$

where $\mathbf{U}$ and $\mathbf{V}$ are unitary matrices and $\boldsymbol{\Sigma}$ is a diagonal matrix with entries (σ_1, σ_2) called the singular values. The singular values are the eigenvalues of the matrix $(\mathbf{F} - \mathbf{I})^T(\mathbf{F} - \mathbf{I})$. For information on the SVD see Golub and Van Loan [13]. For a rank one matrix, $\sigma_2 = 0$, and therefore, the error associated with how far $\mathbf{F} - \mathbf{I}$ is from rank one is just the magnitude of σ_2. Writing the components of the assumed form of $\mathbf{F} - \mathbf{I}$ using the components of $\mathbf{J} = (J_1, J_2)$ and $\mathbf{N} = (N_1, N_2)$ gives

$$\mathbf{F} - \mathbf{I} = \begin{pmatrix} F_{11} - 1 & F_{12} \\ F_{21} & F_{22} - 1 \end{pmatrix} = \begin{pmatrix} J_1 N_1 & J_1 N_2 \\ J_2 N_1 & J_2 N_2 \end{pmatrix} \tag{5.17}$$

The SVD in component form is

$$\mathbf{F} - \mathbf{I} = \begin{pmatrix} U_{11} & U_{12} \\ U_{21} & U_{22} \end{pmatrix} \begin{pmatrix} \sigma_1 & 0 \\ 0 & \sigma_2 \end{pmatrix} \begin{pmatrix} V_{11} & V_{21} \\ V_{12} & V_{22} \end{pmatrix} \tag{5.18}$$

The closest rank one matrix to $\mathbf{F} - \mathbf{I}$ is the matrix produced from the SVD with

$\sigma_2 = 0$, which can be written as

$$\begin{pmatrix} U_{11}\sigma_1 V_{11} & U_{11}\sigma_1 V_{21} \\ U_{21}\sigma_1 V_{11} & U_{21}\sigma_1 V_{21} \end{pmatrix} \qquad (5.19)$$

for a proof see [13]. Assuming that $\mathbf{N}$ is normalized, the components of $\mathbf{J}$ and $\mathbf{N}$ can be equated to the SVD components in the following way

$$\begin{aligned} J_1 &= \sigma_1 U_{11} \\ J_2 &= \sigma_1 U_{21} \\ N_1 &= V_{11} \\ N_2 &= V_{21} \end{aligned} \qquad (5.20)$$

Then the spatial jump is calculated as

$$[\![\boldsymbol{\varphi}]\!] = L\overline{\mathbf{F}}\mathbf{J} = L\mathbf{J} \qquad (5.21)$$

where $\overline{\mathbf{F}}$ is assumed to be the identity in this case.

Plots of the cracks predicted for the small Arctic region discussed above are shown in Figure 5.7. Note that this calculation assumes that there is a crack in every cell as shown in Figure 5.7a. However, a cutoff for cracks with less than a minimum opening magnitude can be chosen to limit the display to substantial cracks as shown in Figure 5.7b where the cutoff is set to be 0.8 kilometers.

In the next more difficult case, $\overline{\mathbf{F}}$ is assumed to be a general rotation, $\mathbf{R}$, which must be determined in addition to $\mathbf{J}$ and $\mathbf{N}$. In order to determine $\mathbf{J}$ and $\mathbf{N}$ for this case, first calculate the singular value decomposition of $\mathbf{F}$ as

$$\mathbf{F} = \mathbf{R}(\mathbf{I} + \mathbf{J} \otimes \mathbf{N}) = \mathbf{U}_1 \Sigma_1 \mathbf{V}_1^T \qquad (5.22)$$

Solving for Σ_1 we get

$$\begin{aligned} \Sigma_1 &= \mathbf{U}_1^T \mathbf{R}(\mathbf{I} + \mathbf{J} \otimes \mathbf{N})\mathbf{V}_1 \\ &= \mathbf{U}_1^T \mathbf{R}\mathbf{V}_1 + \mathbf{U}_1^T \mathbf{R}\mathbf{J} \otimes \mathbf{N}\mathbf{V}_1 \end{aligned} \qquad (5.23)$$

Since $\mathbf{U}_1$ and $\mathbf{V}_1$ are unitary matrices, $\mathbf{U}_1^T \mathbf{R} \mathbf{V}_1$ is just another rotation, so let $\widetilde{\mathbf{R}} = \mathbf{U}_1^T \mathbf{R} \mathbf{V}_1$. Additionally, since $\mathbf{J}$ and $\mathbf{N}$ are vectors, $\mathbf{U}_1^T \mathbf{R} \mathbf{J}$ and $\mathbf{N} \mathbf{V}_1$ are also vectors. Let them be defined as $\widetilde{\mathbf{J}}$ and $\widetilde{\mathbf{N}}$ respectively. Then

$$\Sigma_1 \equiv \widetilde{\mathbf{R}} + \widetilde{\mathbf{J}} \otimes \widetilde{\mathbf{N}} \tag{5.24}$$

In this form it is apparent that $\Sigma_1 - \widetilde{\mathbf{R}}$ is a rank one matrix. Therefore, the next step in the algorithm is to find an intermediate rotation matrix, $\widetilde{\mathbf{R}}$ such that $\Sigma_1 - \widetilde{\mathbf{R}}$ is as close to rank one as possible. $\widetilde{\mathbf{R}}$ can be written as

$$\widetilde{\mathbf{R}} = \begin{pmatrix} \cos\theta & \sin\theta \\ -\sin\theta & \cos\theta \end{pmatrix} \tag{5.25}$$

for some unknown θ. Then $\Sigma_1 - \widetilde{\mathbf{R}}$ can be written as

$$\begin{pmatrix} \sigma_1 - \cos\theta & \sin\theta \\ -\sin\theta & \sigma_2 - \cos\theta \end{pmatrix} \tag{5.26}$$

where σ_1 and σ_2 are the components of Σ_1. For $\Sigma_1 - \widetilde{\mathbf{R}}$ to be rank one, the second singular value of the SVD for the matrix must be zero. $\widetilde{\mathbf{R}}$ then can be found by minimizing the second singular value of $\Sigma_1 - \widetilde{\mathbf{R}}$, which is equivalent to minimizing the smallest eigenvalue of $(\Sigma_1 - \widetilde{\mathbf{R}})^T (\Sigma_1 - \widetilde{\mathbf{R}})$. This matrix can be written as

$$(\Sigma_1 - \widetilde{\mathbf{R}})^T (\Sigma_1 - \widetilde{\mathbf{R}}) = \begin{pmatrix} \sigma_1^2 - 2\sigma_1 \cos\theta + 1 & \sin\theta(\sigma_2 - \sigma_1) \\ \sin\theta(\sigma_2 - \sigma_1) & \sigma_2^2 - 2\sigma_2 \cos\theta + 1 \end{pmatrix} \tag{5.27}$$

and has eigenvalues $(\lambda_{1,2})$,

$$2\lambda_{1,2} = \sigma_2^2 - 2(\sigma_2 + \sigma_1)\cos\theta + \sigma_1^2 + 2\pm$$
$$\sqrt{(\sigma_2^2 - 2(\sigma_2 + \sigma_1)\cos\theta - \sigma_1^2 + 2)^2 + 4(\sin^2\theta(\sigma_1 - \sigma_2)^2)}$$
$$-(\sigma_1^2 - 2\sigma_1\cos\theta + 1)(\sigma_2^2 - 2\sigma_2\cos\theta + 1)) \tag{5.28}$$

The value of θ producing the minimum eigenvalue is calculated numerically using a Matlab minimization subroutine *fminbnd*. Given this minimizing θ, $\widetilde{\mathbf{R}}$ is defined

as shown above. Next, the SVD of $\Sigma_1 - \widetilde{\mathbf{R}}$ is calculated as

$$\Sigma_1 - \widetilde{\mathbf{R}} = \widetilde{\mathbf{U}}\widetilde{\Sigma}\widetilde{\mathbf{V}}^T \tag{5.29}$$

As in the previous case with no rotation, the closest rank one matrix to $\Sigma_1 - \widetilde{\mathbf{R}}$ is the matrix produced from the above SVD with the second singular value equal to zero. Assuming this matrix is equal to

$$\begin{pmatrix} \widetilde{U}_{11}\tilde{\sigma}_1\widetilde{V}_{11} & \widetilde{U}_{11}\tilde{\sigma}_1\widetilde{V}_{21} \\ \widetilde{U}_{21}\tilde{\sigma}_1\widetilde{V}_{11} & \widetilde{U}_{21}\tilde{\sigma}_1\widetilde{V}_{21} \end{pmatrix} \tag{5.30}$$

then

$$\begin{aligned} \tilde{J}_1 &= \tilde{\sigma}_1\widetilde{U}_{11} \\ \tilde{J}_2 &= \tilde{\sigma}_1\widetilde{U}_{21} \\ \tilde{N}_1 &= \widetilde{V}_{11} \\ \tilde{N}_2 &= \widetilde{V}_{21} \end{aligned} \tag{5.31}$$

The next step is to calculate $\mathbf{R}$, $\mathbf{J}$, and $\mathbf{N}$ from the intermediate values

$$\begin{aligned} \mathbf{R} &= \mathbf{U}_1\widetilde{\mathbf{R}}\mathbf{V}^T \\ \mathbf{J} &= \mathbf{R}^T\mathbf{U}_1\widetilde{\mathbf{J}} \\ \mathbf{N} &= \mathbf{V}_1\widetilde{\mathbf{N}} \end{aligned} \tag{5.32}$$

Finally, to plot the jump in spatial coordinates, calculate $[\![\boldsymbol{\varphi}]\!]$ as

$$[\![\boldsymbol{\varphi}]\!] = L\overline{\mathbf{F}}\mathbf{J} = L\mathbf{R}\mathbf{J} \tag{5.33}$$

Plots of the cracks predicted for the small Arctic region using the algorithm allowing a general rotation for $\overline{\mathbf{F}}$ are shown in Figure 5.8. Cracks that are colored red indicate an opening mode and cracks that are colored blue indicate a closing mode. The first figure plots cracks in all cells and the second uses a cutoff of 0.8 km as in the previous case. Note that the majority of cracks along the large deformation band are similar using the two techniques.

This method can also be applied to the Beaufort RGPS data. However, in this case there is not a single deformation over some time interval, but a series of data for multiple days between 23 February and 12 March. In this case the algorithm in the previous section will determine an incremental deformation gradient, f^{n+1}, for the current day $n+1$ assuming that the coordinates, $\mathbf{X}$, are now interpreted as the coordinates defined by the configuration in the previous time step. The cumulative deformation gradient is then calculated with the following multiplicative update

$$\mathbf{F}^{n+1} = \mathbf{f}^{n+1}\mathbf{F}^n. \tag{5.34}$$

With this procedure the best fit discontinuties have been calculated for the Beaufort region and are shown for the first day in Figure 5.9. As before cracks that are colored red indicate opening and cracks that are colored blue indicate a closing mode. In a finite deformation setting the determinant of the total deformation gradient, $J = \det\mathbf{F}$, is a measure of cumulative area change. In Figure 5.9 b J is plotted for the first day. Figure 5.10 displays the predicted cracks with a cutoff of 0.8 km and J for day 70 of the data.

Note that the cracks are aligned with the linear features in Figures 5.4 and 5.5. In the next chapter the RGPS data will be used for comparison with the MPM calculations.
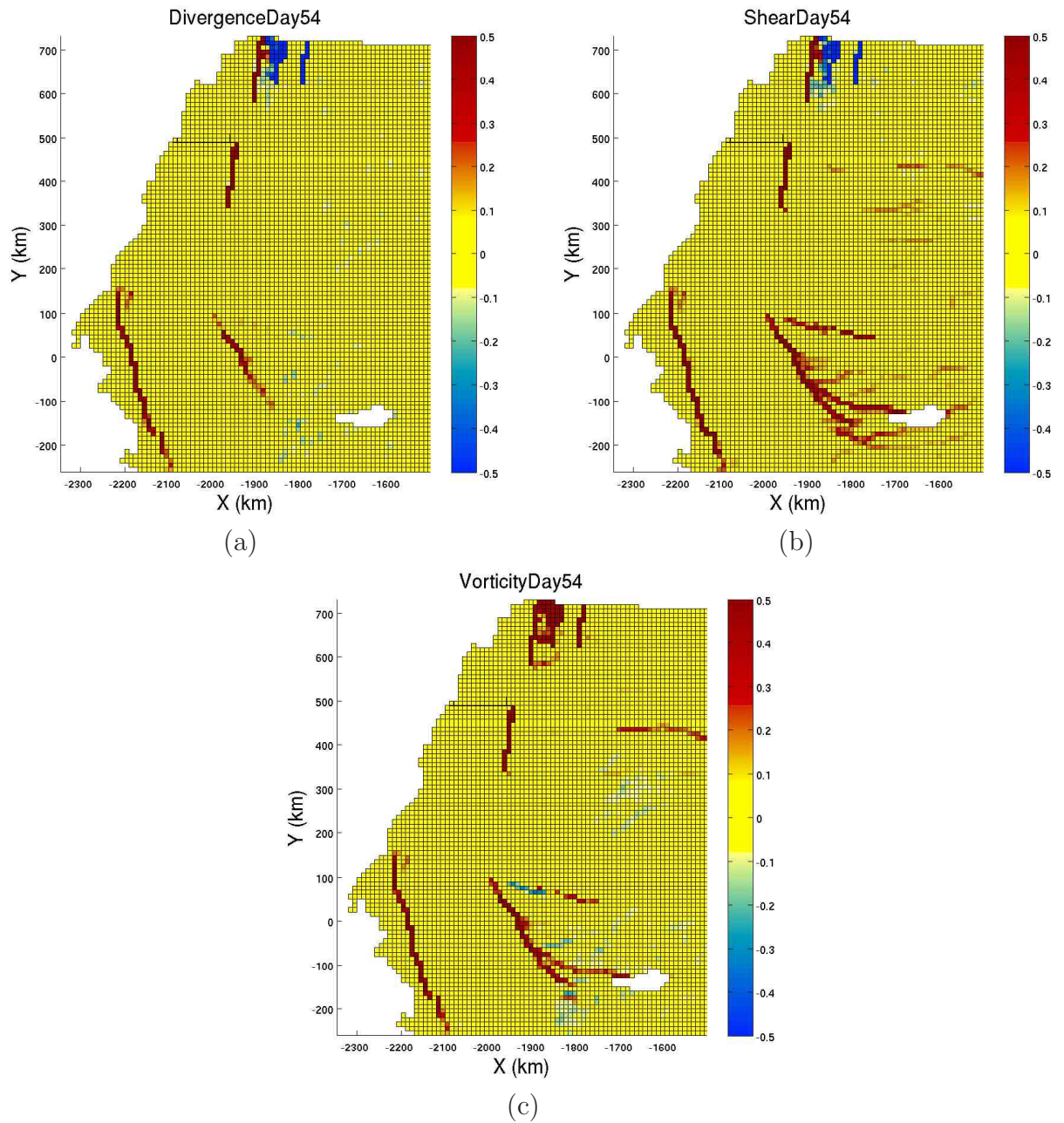
Figure 5.4: Beaufort Sea region day 54 (a) divergence, (b) shear, (c) vorticity.

(a)

(b)

(c)
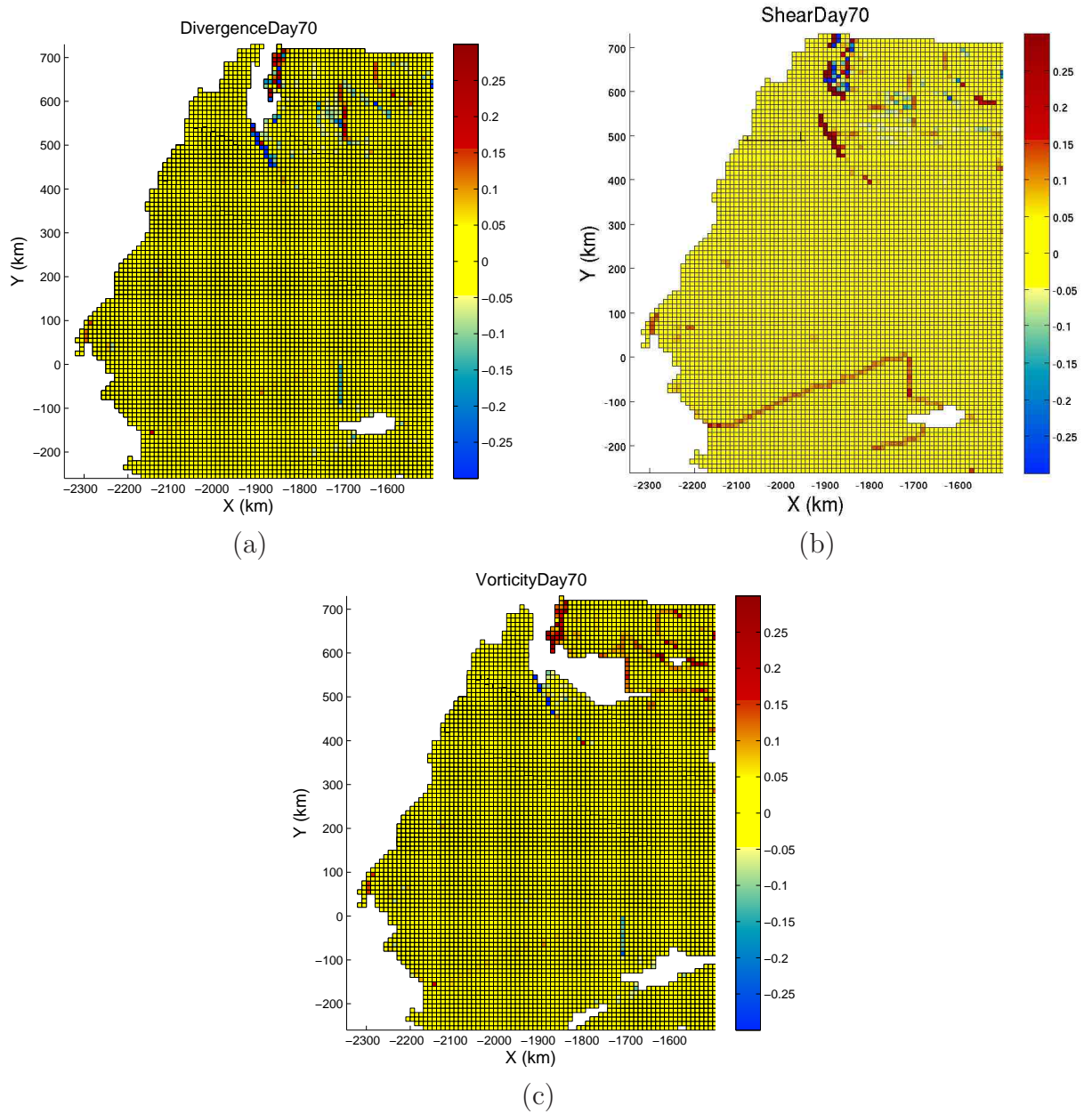
Figure 5.5: Beaufort Sea region day 70 (a) divergence, (b) shear, (c) vorticity.
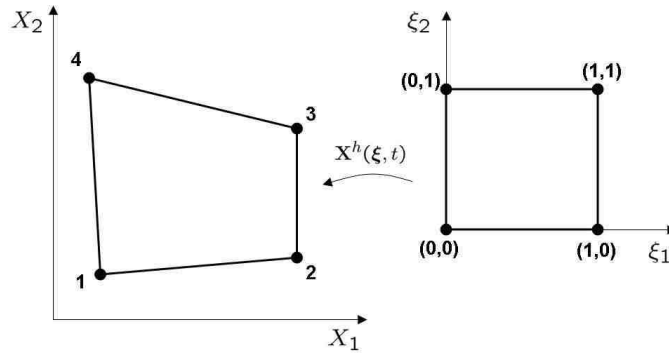
Figure 5.6: Element with numbered nodes and parent element in (ξ_1, ξ_2) space

(a)

(b)
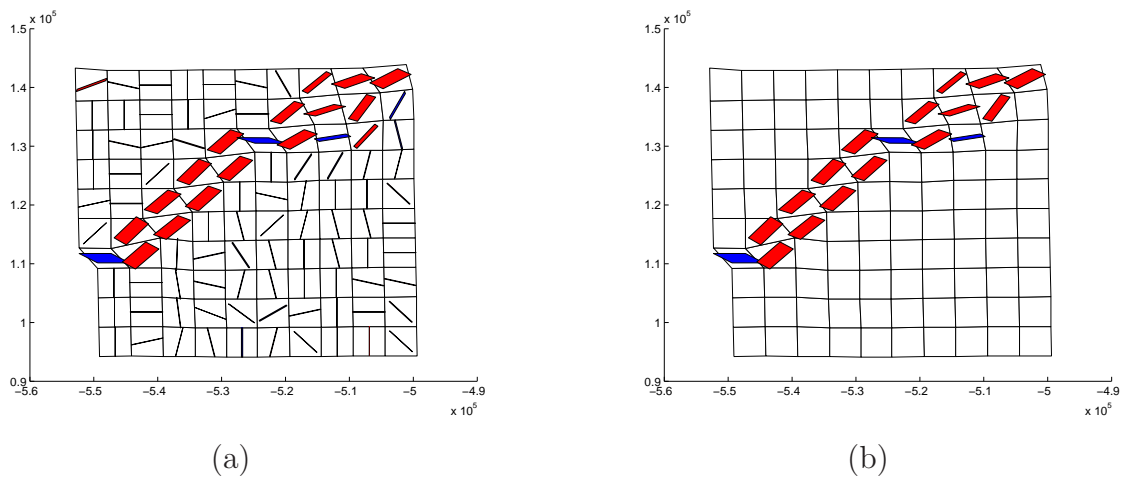
Figure 5.7: Calculated Discontinuities for Small Region with $\overline{\mathbf{F}} = \mathbf{I}$ (a) Cutoff=0, (b) Cutoff=0.8 km

(a) (b)
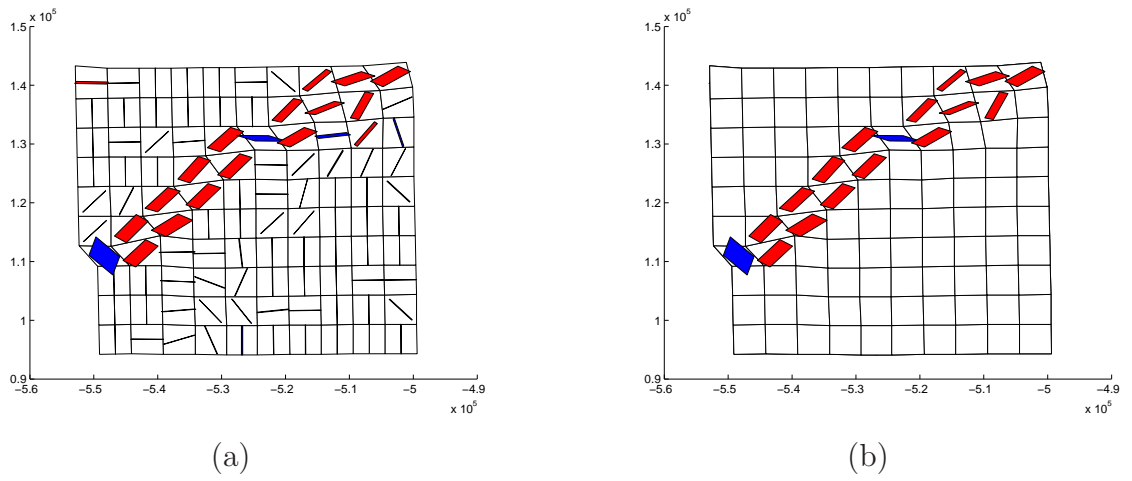
Figure 5.8: Calculated discontinuities for small region with no restrictions on $\overline{\mathbf{F}}$ (a) cutoff=0, (b) cutoff=0.8 km

(a) (b)
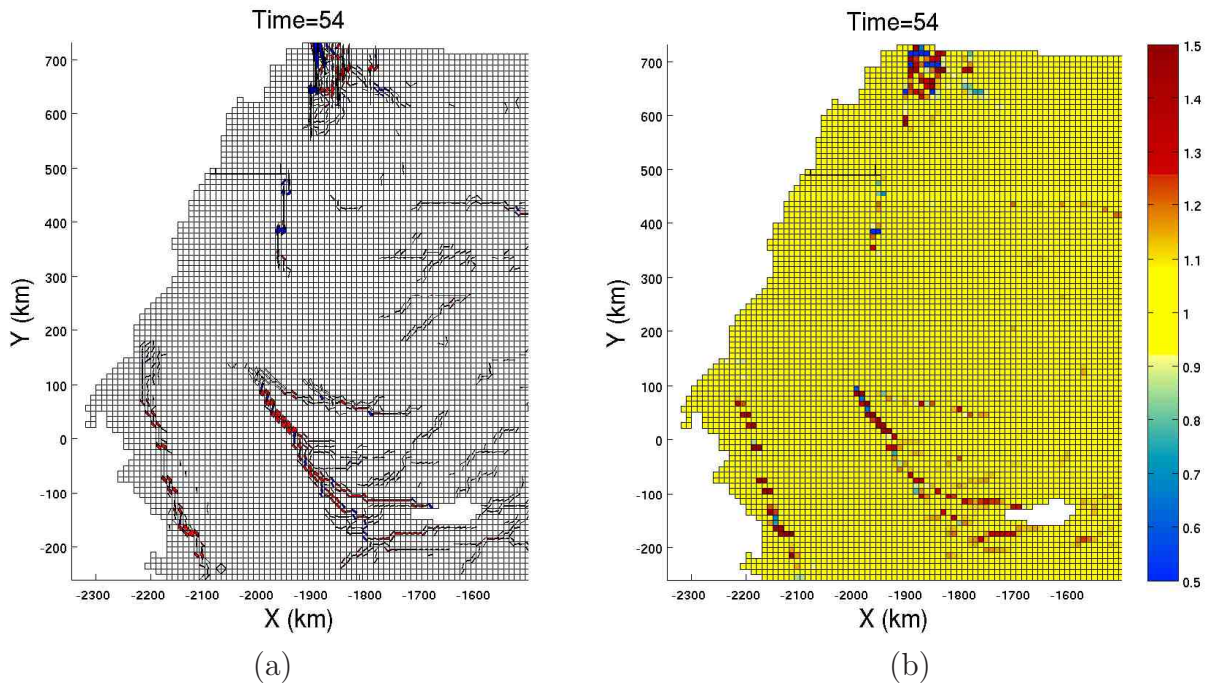
Figure 5.9: Beaufort Sea region day 54 (a) cracks, (b) det(F).
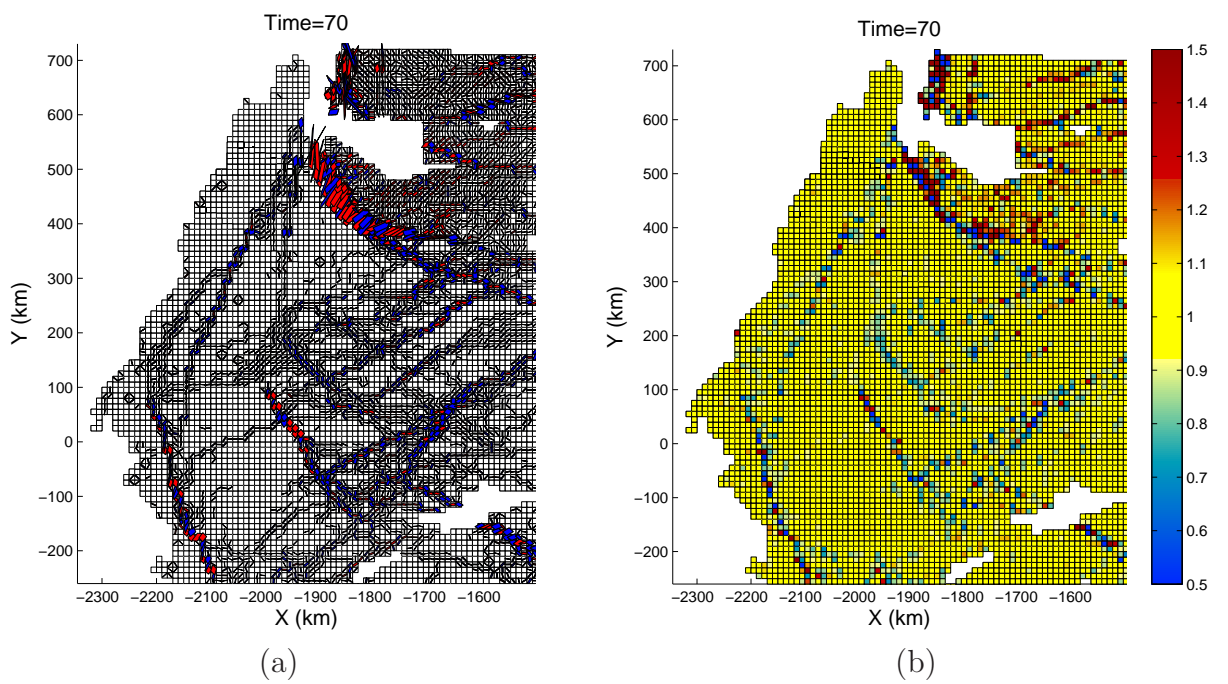
Figure 5.10: Beaufort Sea region day 70 (a) cracks, (b) det(F).

Chapter 6

Calculations

6.1 Introduction

The sea ice model described in the previous two sections has been implemented and used to perform several calculations. The first set of calculations, which are described in Section 6.2, were run in MPM with the elastic-decohesive constitutive model and viscous-plastic model for three small Arctic regions. This calculation compares the constitutive models, but does not include the full ice thickness distribution and thermodynamic models or the wind and ocean drag terms.

The final set of calculations, described in Section 6.4, models the larger region in the Beaufort Sea discussed in Chapter 5 with the full MPM elastic-decohesive sea ice model that includes wind and ocean drag terms, Coriolis forcing, the full ice thickness distribution and thermodynamics. However, before running the ice thickness distribution and thermodynamic models in the larger calculation, a set of simple calculations were performed to test these models directly. A description of these tests can be found in Section 6.3.

6.2 Small Region Comparison Study

To test the initial implementation of the elastic-decohesive model and to compare to the current standard model, a study was performed on three small Arctic regions where satellite data are available [46]. The satellite images were processed by the RADARSAT Geophysical Processor System (RGPS) [25] and were provided by Ron Kwok. Satellite views of the three 50 km by 50 km regions are shown below with the RGPS grids superimposed. The time span of the observations for region one was 20 hours, 1.7 hours for region two, and 18.5 hours for region three. The three regions were chosen to demonstrate different aspects of the model. The first region, has a fairly complex pattern with two main leads interacting. The second region is quiet

over the time span of observation and was chosen to test whether the model would overpredict leads. The third region contains a large shear band. In all cases the data were taken in mid May of 2002.
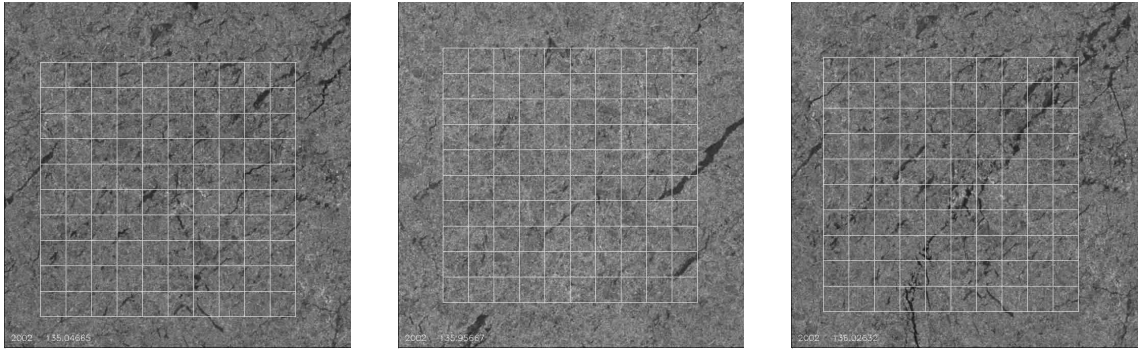

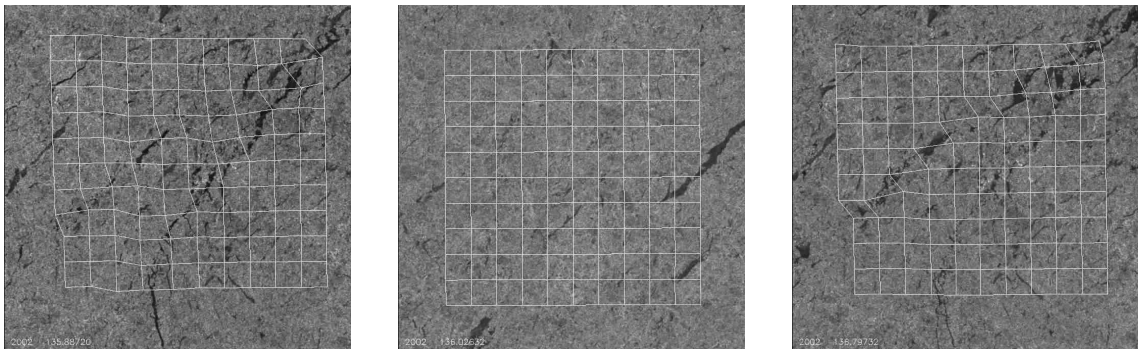Figure 6.1: Satellite View of Region 1, Region 2, and Region 3 with Grid at Initial Times

Figure 6.2: Satellite View of Region 1, Region 2, and Region 3 with Grid at Final Times

MPM calculations were performed using the elastic-decohesive and viscous-plastic constitutive models described in Chapters 3 and 2 respectively [46] [47]. The RGPS displacement data were used to calculate average velocities over the time period at the boundaries of each region. After mean translations were subtracted, these boundary velocities were used as input to the MPM calculations. A Lagrangian grid was used in MPM with one material point per element. The grid was initially

divided into 5 kilometer by 5 kilometer square elements, which corresponds to the RGPS grid. The Coriolis term, water drag, and ocean drag terms were neglected in these calculations. The ice was assumed to be homogeneous and at rest initially.

For the viscous-plastic model, the grid was initialized to have a uniform thickness of 3 meters and compactness of 1. The ice strength parameters used were $P^* = 2.85 \times 10^4 N/m^2$ and $C = 20$. Because these calculations were on a short time scale the ice growth rate in the thermodynamic source terms for A and h was taken to be a piecwise constant with a value of 6 cm/day for open water and 0.1 cm/day for ice of other thickness. In the case of the elastic-decohesive model, a Young's modulus of $E = 1MPa$, and Poisson's ratio of $\nu = 0.36$ were used. Additional parameters for the run included $\tau_{nf} = 15KPa$, $\tau_{tf} = 9KPa$, and $f'_c = 75KPa$.

In both cases the final deformation and grid velocities are similar as shown below in Figures 6.3 and 6.4. These figures contain the velocity vectors at the final time from the RGPS data, viscous-plastic model, and elastic-decohesive model, for regions 1 and 3 respectively. Results from region 2 are not plotted since almost no deformation occurs during the time of observation for the RGPS data or the calculations.
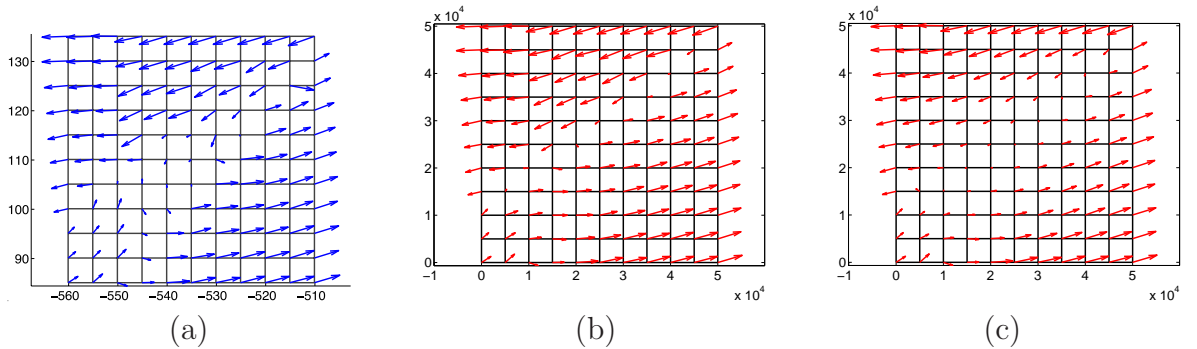
Figure 6.3: Region 1 Velocity from (a) RGPS Data (b) Viscous-Plastic model (c) Elastic-Decohesive model

Additional measures used to quantify the deformation of the ice are divergence, shear, and vorticity, which are calculated from RGPS displacements as shown in
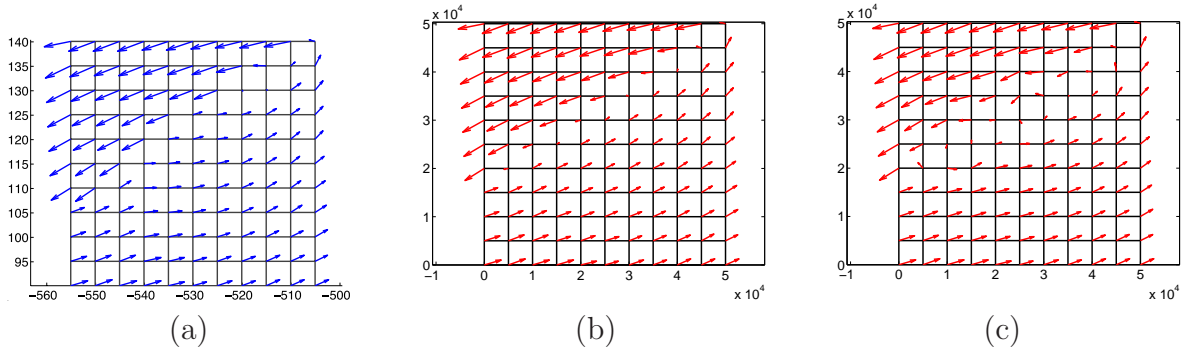
Figure 6.4: Region 3 Velocity from (a) RGPS Data (b) Viscous-Plastic model (c) Elastic-Decohesive model

Equation 5.2. Therefore, for comparison the same data were calculated for the viscous-plastic and elastic-decohesive runs and the results are shown in Figures 6.5 through 6.10.
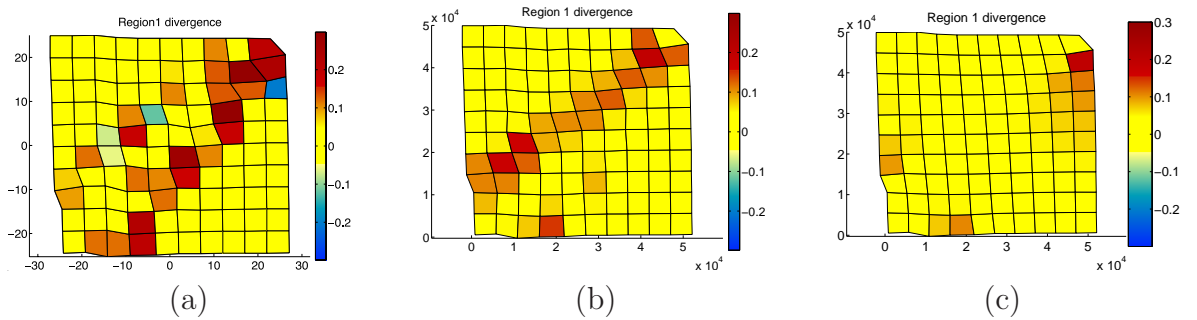

Figure 6.5: Region 1 Divergence from (a) RGPS Data (b) Viscous-Plastic model (c) Elastic-Decohesive model

Overall the calculations showed good correlations to the RGPS velocity. Additionally, the total deformation over the time intervals matched the data, which is to be expected because of the driving boundary velocities. There is moderate correlation between the models and RGPS data for shear and vorticity, but both models had worse correlations to the RGPS divergence, where the models seemed to underpredict the divergence [46].
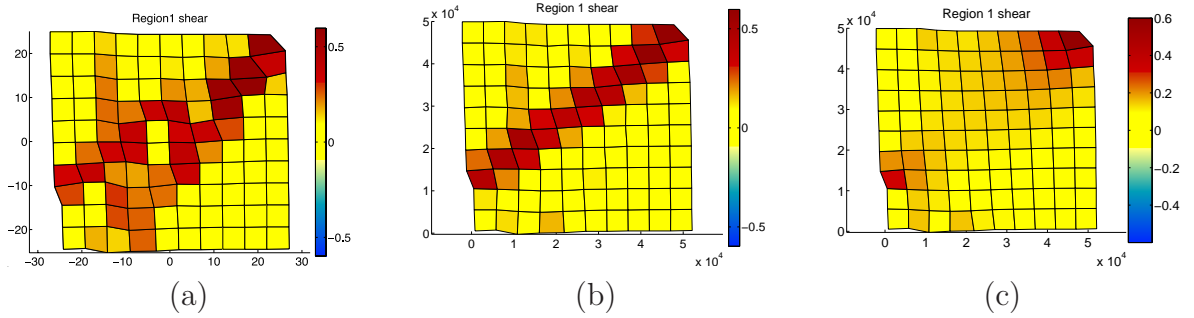
Figure 6.6: Region 1 Shear from (a) RGPS Data (b) Viscous-Plastic model (c) Elastic-Decohesive model
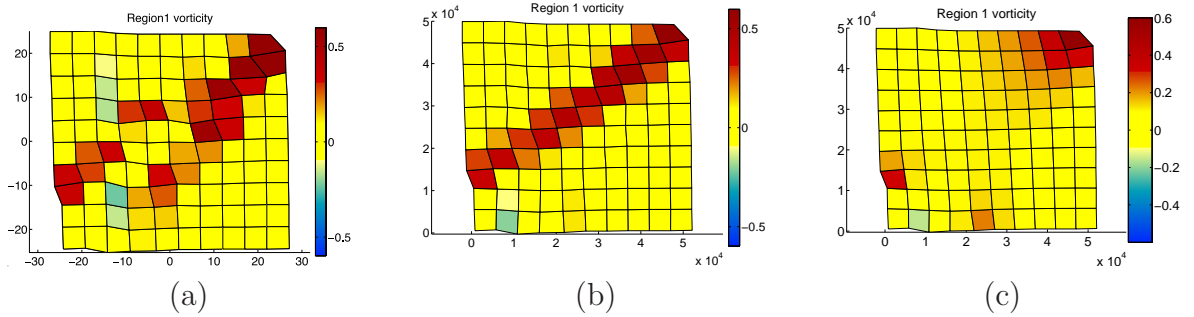
Figure 6.7: Region 1 Vorticity from (a) RGPS Data (b) Viscous-Plastic model (c) Elastic-Decohesive model
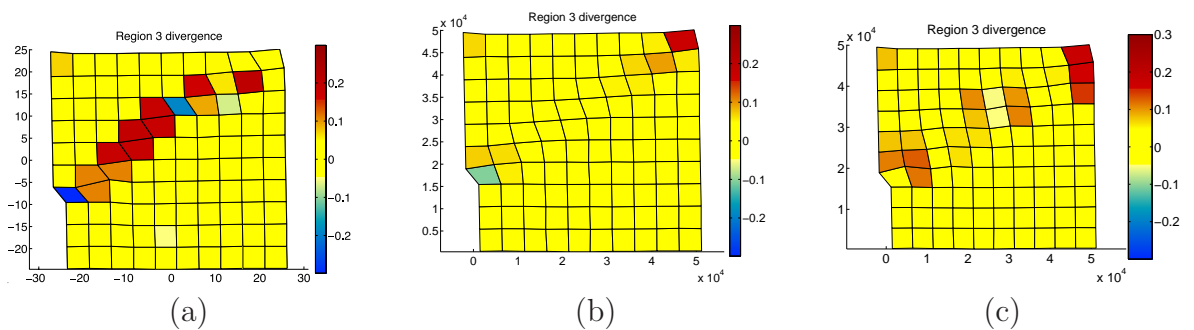

Figure 6.8: Region 3 Divergence from (a) RGPS Data (b) Viscous-Plastic model (c) Elastic-Decohesive model
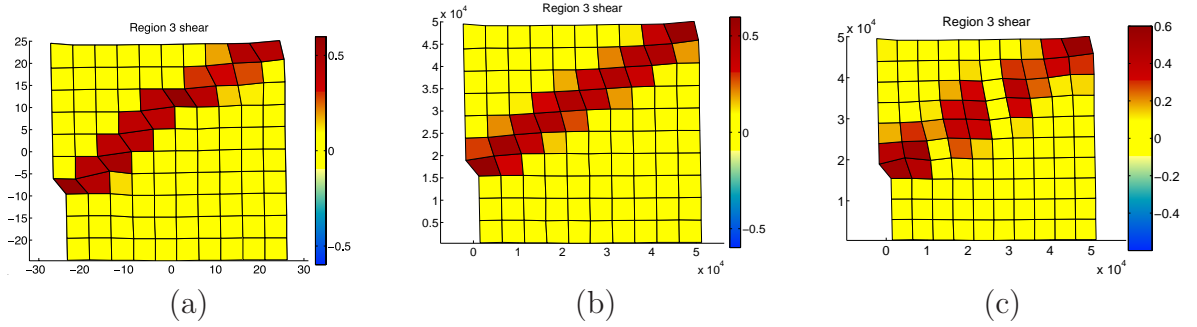
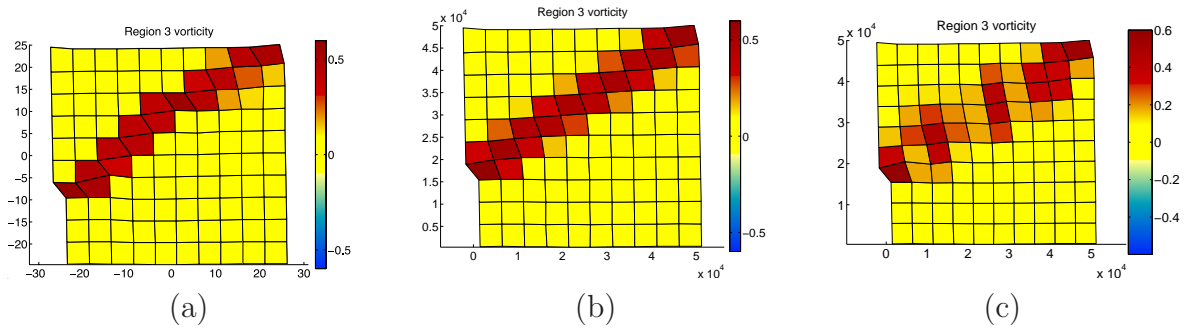Figure 6.9: Region 3 Shear from (a) RGPS Data (b) Viscous-Plastic model (c) Elastic-Decohesive model

Figure 6.10: Region 3 Vorticity from (a) RGPS Data (b) Viscous-Plastic model (c) Elastic-Decohesive model

6.3 ITD and Thermodynamic Test Calculations

To improve the model used in the calculations in Section 6.2, the ice thickness distribution due to Thorndike *et al.* [51] and the thermodynamic model of Bitz and Lipscomb [7] have been implemented. Before using this implementation with the full sea ice model, several test calculations were performed.

In the case of the ice thickness distribution, a test calculation modeled after a calculation in Kubat *et al.* [22] was performed. This calculation models the flow of ice through a channel and demonstrates the effects of ridging along the channel. Since the time interval for the calculation is only 4 days the thermodynamics can

be neglected. For this case, a wind velocity of 10 m/s is used to push ice through a wedge-shaped channel with open end 260 km wide and narrow end 30 km wide. An initial view of the domain of the MPM calculation is shown in Figure 6.11 where the blue points make up the ice region and the red points are the fixed channel boundaries. For the Kubat *et al.* [22] calculation the viscous-plastic constitutive model is used with a three category ice thickness distribution with open water, coherent ice, and ridged ice categories. The region is initialized with an ice thickness of 1 meter and compactness of 0.7. An air drag coefficient of 0.002, water drag coefficient of 0.005 with a quadratic drag rule are used in the calculation. A particle-in-cell method is used for the calculation and the thickness and compactness are particle properties as in the MPM implementation.

In the case of the MPM calculation, a six category ice thickness distribution is used and implemented as shown in Section 4.4. The elastic-decohesive model is also used with the following strength parameters: $t_{nf} = 200$, $t_{sf} = 200$, $f'_c = 1500$. Since different constitutive models were used for the Kubat *et al.* [22] and MPM calculations the comparison cannot be direct. However, in both cases the average thickness after four days has increased along the sides of the channel to approximately 1.5 meters. This comparison is shown in Figure 6.12.

Additionally, a simple translation calculation was done to test that no change in thickness will occur for a rigid body translation. For this calculation a block of ice was given a constant velocity of (0.75,0.25). The results of this calculation are shown in Figure 6.13, where as expected, the thickness did not change over the calculation. Note also, that since the thickness is associated with material points the translating block can be solved for exactly, illustrating the benefits of MPM over the typical Eulerian methods used in sea ice modeling.

For the thermodynamic model, a test calculation was done to predict the equilibrium ice thickness, which is a parameter often used to evaluate sea ice thermodynamic
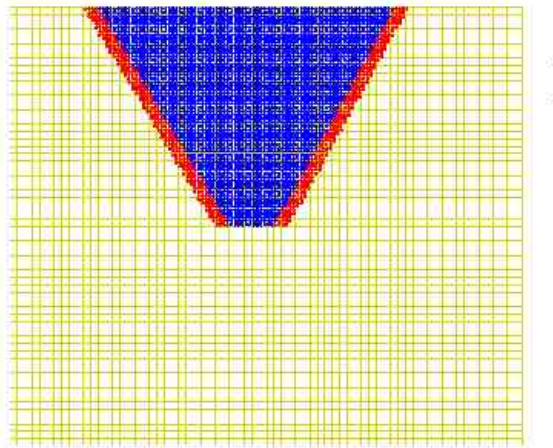
Figure 6.11: Flow through channel calculation initial geometry.

models. For this calculation a 3.0 meter thick layer of ice is subject to the annual flux cycle for fifty years. Figure 6.14 shows the annual cycle of fluxes used to drive the
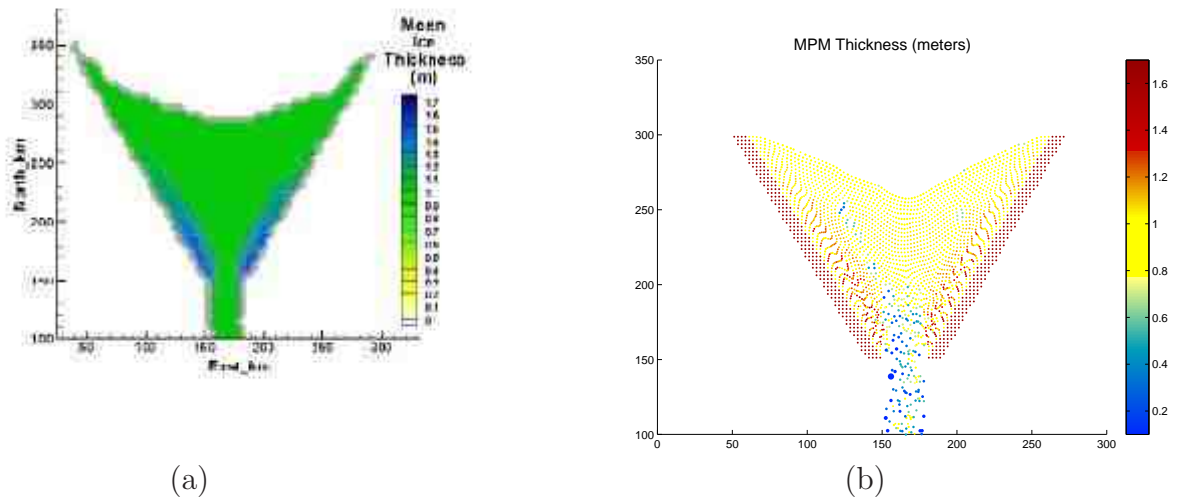

(a)

(b)

Figure 6.12: Flow through channel calculation (a) Kubat *et al.* [22] results (b) elastic-decohesive results.
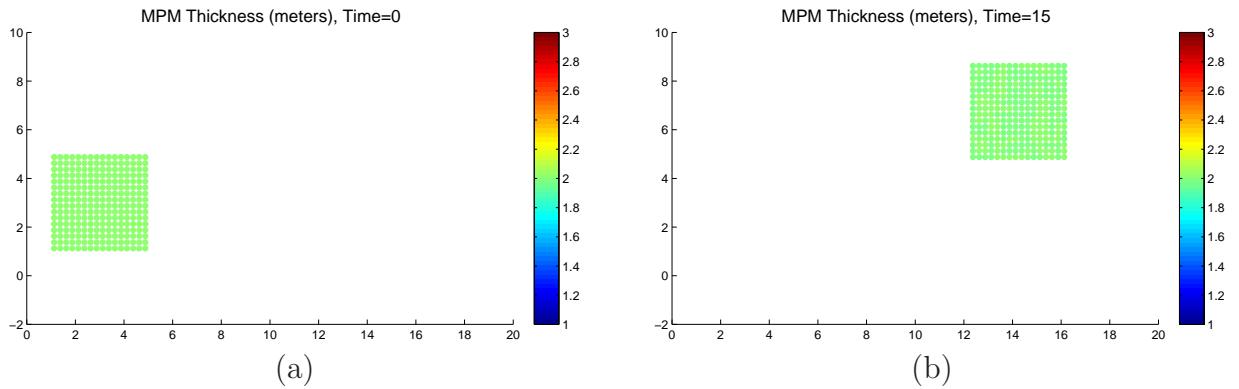
Figure 6.13: Initial (a) and final (b) time plot of ice thickness for simple translation.

thermodynamics. These curves were interpolated from monthly values in Lipscomb's thesis [26], which were based on flux data from Maykut and Untersteiner [30]. The ocean flux, F_w, is taken to be constant and set to 2 W/m^2. The parameters used in the thermodynamic model also, taken from [26] Lipscomb, are shown in Table 6.1.
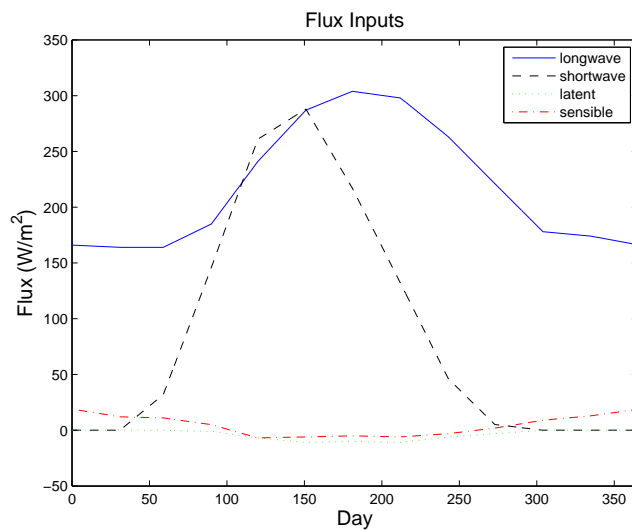

Figure 6.14: Flux inputs for thermodynamic model test.

With these inputs, calculations were run with a time step of 6 hours over 50 years for varying number of layers. Taking the calculation with 81 layers as the

Table 6.1: Thermodynamic Parameters Used for Beaufort Sea Calculations

heat capacity of fresh ice	C_0	2100 J/(kg deg)
conductivity of fresh ice	k_0	2.034 W/(m deg)
latent heat of fresh ice	L_0	334 kJ/kg
extinction coefficient	κ	1.5 m^{-1}
ice albedo	α	0.65
emissivity	ϵ	0.95
melting temp parameter	μ	0.054 K/ppt
conductivity constant	β	0.13 W/(m ppt)

standard, an error based on the Euclidean norm was calculated for the calculations with fewer layers. Plots of the error as a function of the step size (Δh) for a 3 meter thick column of ice with the given number of layers is shown in Figure 6.15. The algorithm exhibits linear convergence as seen in this plot. Annual plots of the middle layer temperature and surface temperature for various discretization are shown in Figure 6.16.
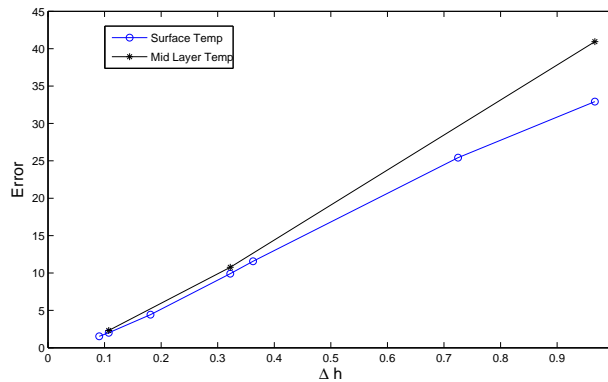

Figure 6.15: Error in layer temperature versus Δh.

For the case of ten ice layers calculations with and without a snow layer were run. For this calculation, a snow layer was included and a simple constant snow flux of 1.0×10^{-6} m/s. The parameters used result in an average thickness for the final

(a)   (b)
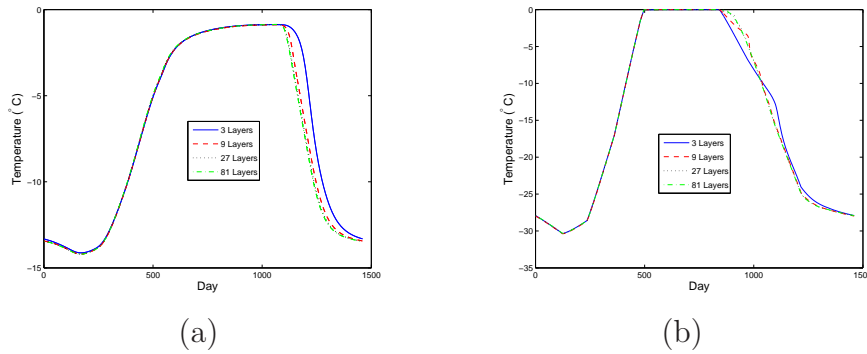
Figure 6.16: Middle layer (a) and surface (b) temperature over a year for increasing number of layers.

year of just over 2.9 meters. Plots of the first year cycle of thickness and average thickness over the fifty years are shown in Figure 6.17.

(a)   (b)
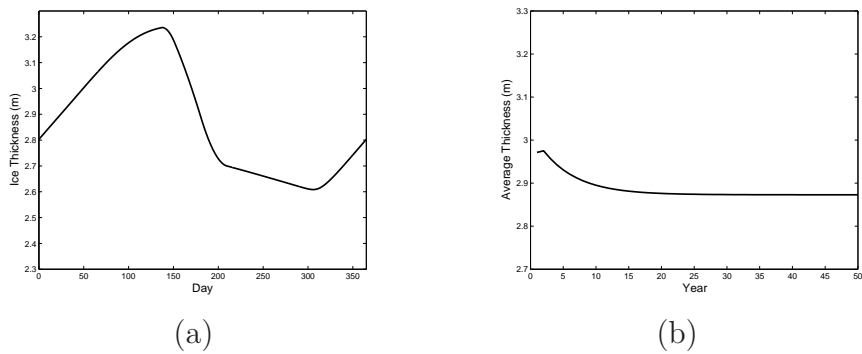
Figure 6.17: Results for thermodynamic routine with snow layer: (a) ice thickness annual cycle (b) annual average over fifty years.

The annual cycle of thickness and average thickness over 50 years are shown in Figure 6.18 for the case where no snow layer is present. Notice that the average thickness in the final year has now decreased to just under 2.8 meters. Without the snow layer more short wave radiation is absorbed within the internal ice layers causing the thickness to drop.

For comparison plots of the ice thickness cycle over a year and the average ice
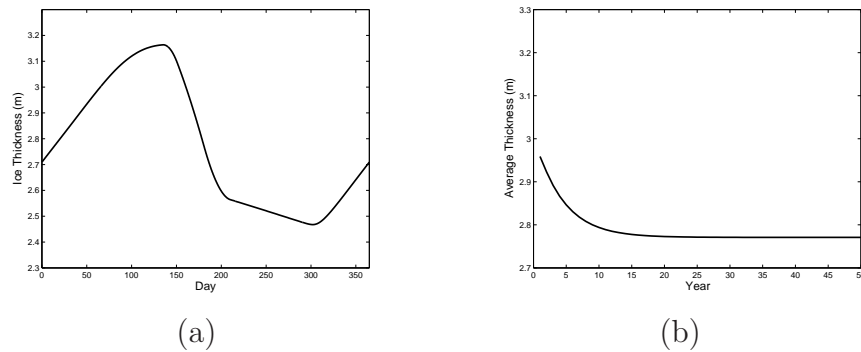
136

Figure 6.18: Results for thermodynamic routine without snow layer: (a) ice thickness annual cycle (b) annual average over fifty years.

thickness over fifty years from Bitz and Lipscomb [7] are shown in Figure 6.19. The solid lines labeled as conserving in these plots are comparable to the model implemented here, although the models differ in some details.
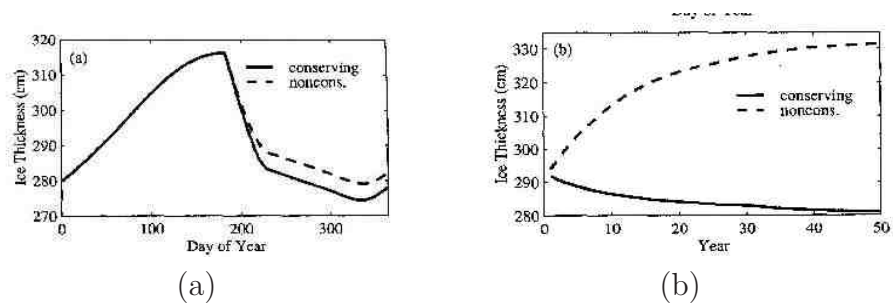

Figure 6.19: Results for thermodynamic routine from Bitz and Lipscomb [7]: (a) ice thickness annual cycle (b) annual average over fifty years.

6.4 Beaufort Sea Calculations

As discussed in Section 5.2, RGPS data have been provided by Ron Kwok of JPL for a region in the Beaufort Sea for 23 February to 12 March 2004. In addition, ocean surface current data, wind velocities, and air temperatures for the same time interval

over the same region have been provided. These data have been used as input for a run of the sea ice code implementation in MPM. The ice thickness distribution and thermodynamic models described in Sections 4.4 and 4.5 are used in these calculations, as well as a small strain version of the elastic-decohesive model described in Section 4.3.

The background grid for the calculation consists of square elements of length 10 km and the ice region is initialized with four material points per cell. The land boundary is defined by rigid material points with a no slip condition as the default contact algorithm between the sea ice material points and the rigid points representing land. RGPS displacements interpolated in time are used for the boundary conditions on the bottom, right and top boundaries of the domain. The parameters used for the calculation are shown in Tables 6.2 and 6.3. Note that the Coriolis force is approximated as a constant in this calculation, although the force more accurately should depend on the latitude.

Table 6.2: General Parameters Used for Beaufort Sea Calculations

initial ice density	ρ	917 kg m^{-3}
initial ice thickness	h_0	2 m
air density	ρ_a	1.20 kg m^{-3}
air drag coefficient	c_a	0.0012
air turning angle	α	0
sea water density	ρ_w	1026 kg m^{-3}
sea turning angle	β	0
sea water drag coeff	c_w	0.00536
Coriolis force	f_c	1.460×10^{-4}

The flux inputs are monthly averages for February and March for the long-wave, short-wave solar, latent heat and sensible heat and are shown in Table 6.4.

The RGPS displacements and ocean surface currents are provided for one day

Table 6.3: Decohesion Parameters Used for Beaufort Sea Calculations

shear modulus	G	3.6765×10^5
bulk modulus	K	11.905×10^5
tensile strength	t_{nf}	15 kPa
shear strength	t_{sf}	9 kPa
compressive strength	f'_c	75 kPa
opening parameter	u_0	200 m

Table 6.4: Flux Inputs Used for Beaufort Sea Calculations

short wave flux	F_S	16 W/m^2
long wave flux	F_L	164 W/m^2
flux of latent heat	F_l	0 W/m^2
flux of sensible heat	F_s	11.5 W/m^2
ocean flux	F_w	2 W/m^2

intervals and the wind velocities at six hour intervals. A plot of the surface currents and wind velocities on the first day of the calculation are shown in Figure 6.20. The dominant force in this calculation and in many sea ice calculations is the atmospheric wind.

In the first calculation, the ice is completely homogeneous to start with intact ice of thickness of 3 meters. Plots of decohesion opening, determinant of the deformation gradient (**F**), ice thickness, and surface temperature are shown for this calculation at day 70 in Figure 6.21. A plot of the kinematic cracks and determinant of **F** for this same day is shown in Figure 6.22 for comparison. Note that there are some fairly significant differences between the kinematic predictions for this time and the calculations. In particular, the kinematic crack plot shows many more features than the MPM calculation plot, which is dominated by a few linear features radiating from the top central portion of the domain. Note that this active region corresponds physically to the area around Point Barrow, which is generally known as an active
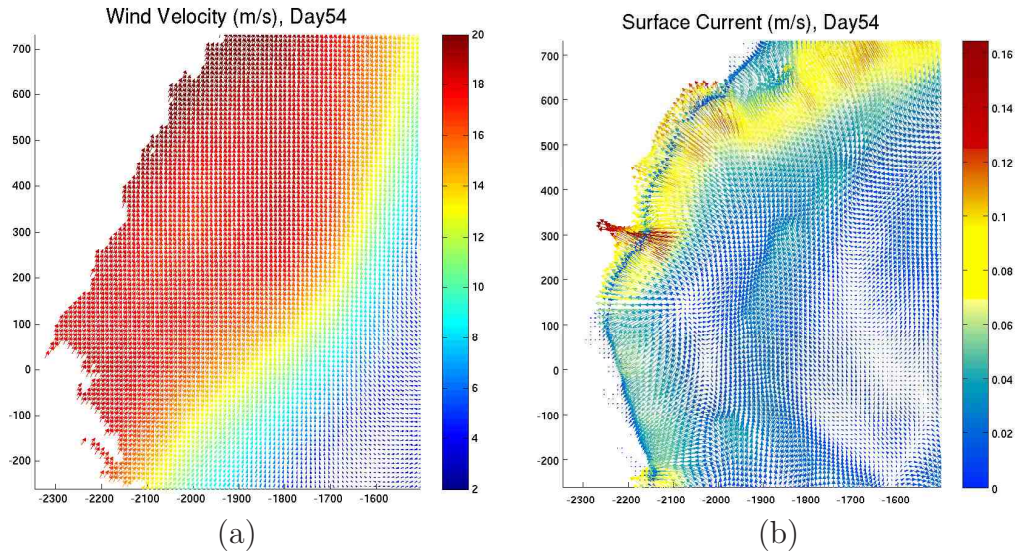
Figure 6.20: (a) Wind velocity day 54 (b) Surface currents day 54

region for sea ice.

The next calculation uses the kinematic cracks calculated using the algorithm from Section 5.3 to initialize the ice with some decohesion. The initial conditions are shown in Figure 6.23 and results from this run are shown in Figure 6.24. In this case, the results match the kinematic predictions better than in the previous case. This indicates that for this short run time the initial conditions are quite important. However, for a much longer run time it is anticipated that the initial conditions would have less of an effect.

Note that in both the no initialization and initialization run, the average material-point thickness plot follows the determinant of $\mathbf{F}$ plot closely. This is not surprising since the ice thickness is driven by the changes in area, which is what the determinant of $\mathbf{F}$ measures.

For comparison a run was completed without the ice thickness distribution or thermodynamics and plots of cracks and decohesion opening are shown in Figure

6.25. The results of this calculation appear very similar to that in Figure 6.24. For this short time period the thermodynamics and ice thickness do not play a significant role in the deformation. However, for longer-scale calculations it is expected that the thermodynamic effects will be important.
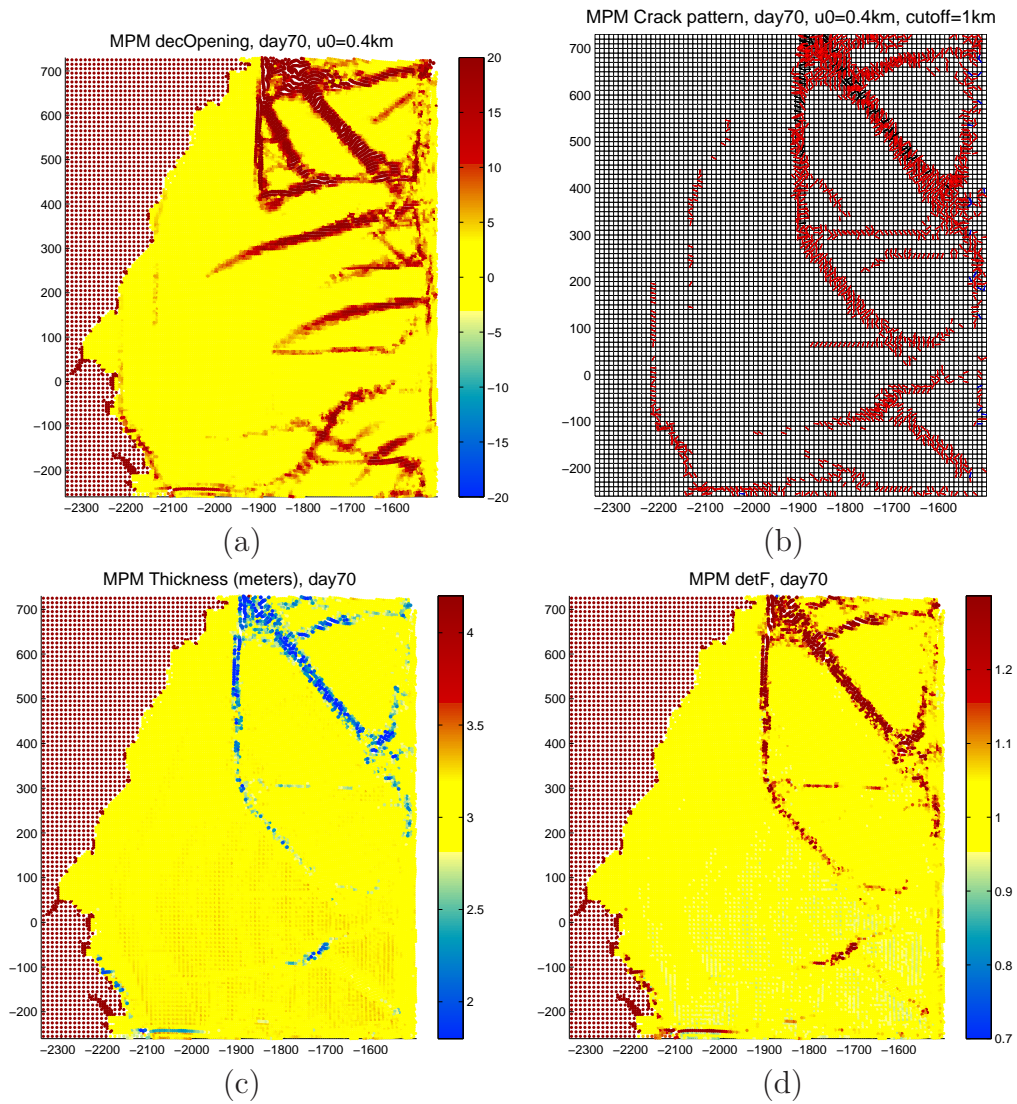
Figure 6.21: Beaufort calculation with no initialization day 70 (a) decohesion opening (b) cracks (c) ice thickness (d) determinant of **F**.
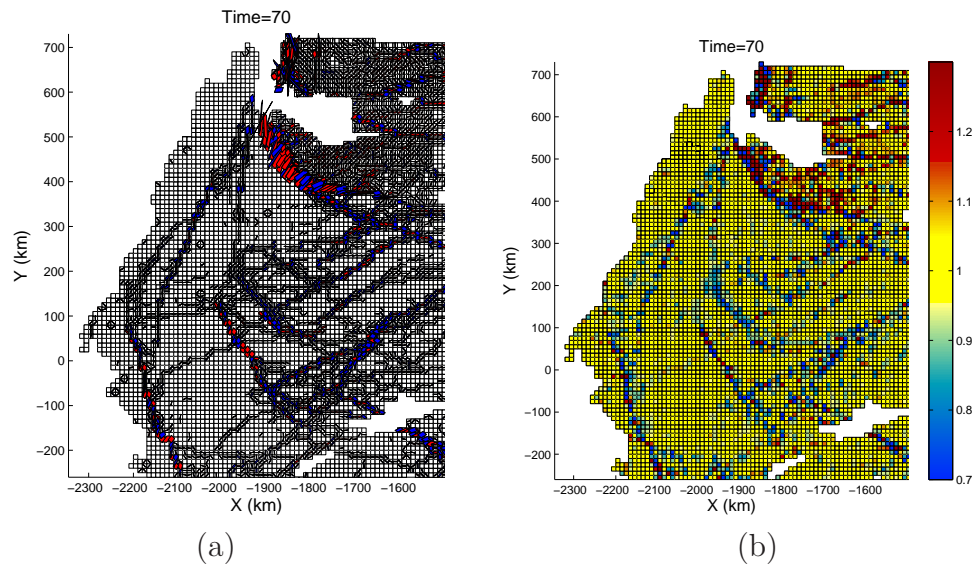
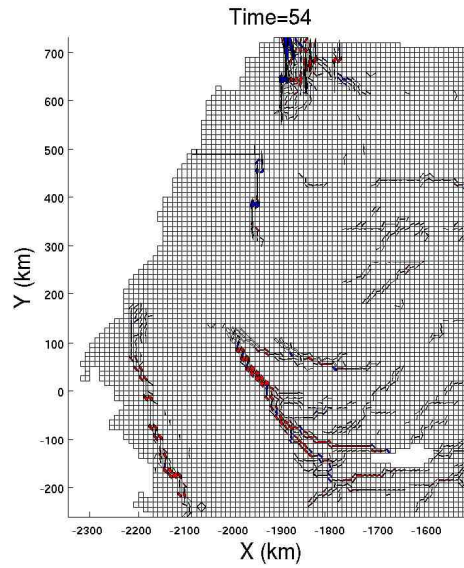Figure 6.22: Kinematic results for Beaufort region day 70 (a) cracks (b) determinant **F**.
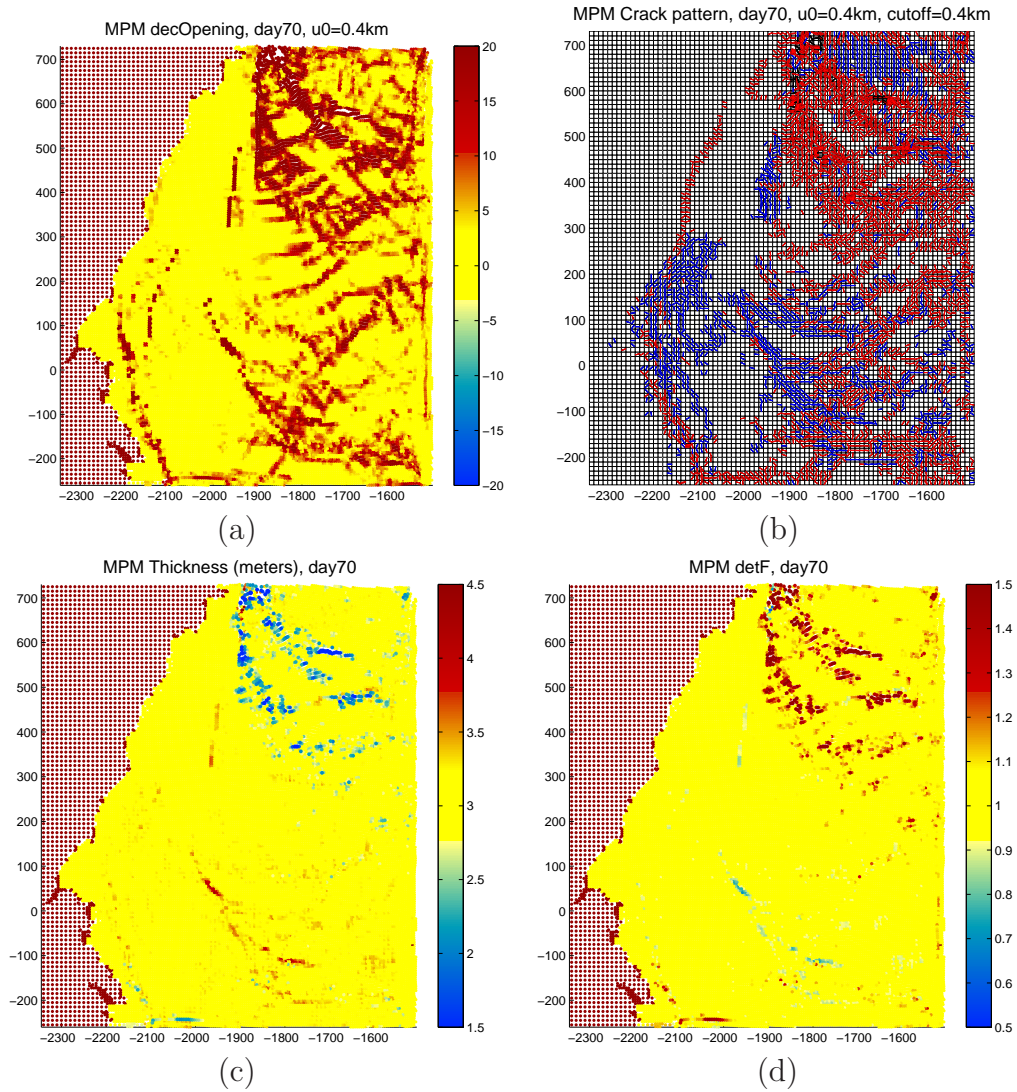

Figure 6.23: Initial cracks for Beaufort calculation.

Figure 6.24: Beaufort calculation with initialization day 70 (a) decohesion opening (b) cracks (c) ice thickness (d) determinant of **F**
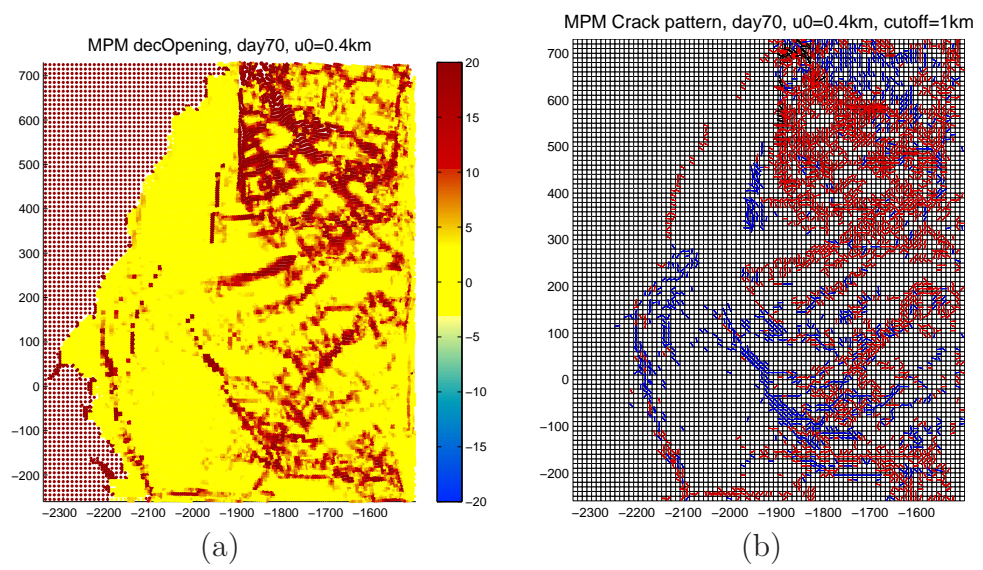
Figure 6.25: Beaufort calculation with initialization and no ITD or thermodynamics day 70 (a) decohesion opening (b) cracks

Chapter 7

Conclusions

Sea ice is an important indicator of global warming and an important component of the global climate balance. Therefore, there is considerable motivation to develop updated models that address some of the limitations of the standard models. To this end, a new model for sea ice has been presented that attempts to address several of these limitations. First, this model explicitly accounts for leads in the ice through the elastic-decohesive constitutive relation, which is anisotropic once failure has been initiated. Second, the model naturally calculates the transport of ice thickness category fractional areas and volumes by using Lagrangian material points in the Material-Point Method.

The assumptions needed to obtain the simplified governing equations used for this model from the full three-dimensional mass, momentum, and energy conservation equations have been highlighted. Clarifying the assumptions inherent in the form of the ice governing equations is important for understanding the limitations of the model and for giving the model a firm theoretical basis. In particular, the connection between the ice thickness distribution and the conservation of mass equation with incompressibility was shown through the derivation. Also, the two-dimensional momentum equation was derived from the full three-dimensional momentum equation and a thermodynamically consistent derivation of the elastic-decohesive constitutive model was given in a finite strain setting. Finally, the one-dimensional heat equation for a column of ice was derived from the energy equation.

The two-dimensional momentum equation, elastic-decohesive rheology, ice thickness distribution, and one-dimensional heat equation were combined in the Material-Point Method to create a full sea ice model. In the Material-Point Method, the momentum equation is solved on a background grid, while the constitutive model, ice thickness distribution, and heat equation are solved at each material point.

Preliminary calculations indicate that this model produces reasonable results for a variety of test problems. Additionally, results from the Beaufort Sea calculation

demonstrate that the model is effective for large-scale calculations and can be reasonably considered for climate modeling applications.

Future work on this sea ice model would include modifications to allow it to connect to active ocean and atmosphere codes, which is a critical step for incorporation into a global climate model. Additionally, more calculations can be done to compare directly with current models and test problems with longer time scales can be done to see more of the effects of the ice thickness and thermodynamic components.

References

[1] In F. Nansen, editor, *The Norwegian North Polar Expedition 1893-1896. Scientific Results*, 1902.

[2] T. L. Amundrud, H. Melling, and R.G. Ingram. Geometrical constraints on the evolution of ridged sea ice. *Journal of Geophysical Research*, 109:doi:10.1029/2003JC002251, 2004.

[3] F. Armero. Large-scale modeling of localized dissipative mechanisms in a local continuum: applications to the numerical simulation of strain localization in rate-dependent inelastic solids. *Mechanics of Cohesive-Frictional Materials*, 4:101–131, 1999.

[4] F. Armero and K. Garikipati. An analysis of strong discontinuities in multiplicative finite strain plasticity and their relation with the numerical simulation of strain localization in solids. *International Journal of Solids and Structures*, 33:2863–2885, 1996.

[5] T. Belytschko, W. Liu, and B. Moran. *Nonlinear Finite Elements for Continua and Structures*. John Wiley and Sons, Chichester, 2000.

[6] C. M. Bitz, M. M. Holland, A. J. Weaver, and M. Eby. Simulating the ice-thickness distribution in a coupled climate model. *Journal of Geophysical Research*, 106:2441–2463, 2001.

[7] C. M. Bitz and W. H. Lipscomb. An energy-conserving thermodynamic model of sea ice. *Journal of Geophysical Research*, 104(C7):15669–15677, 1999.

[8] W. J. Campbell. The wind-driven circulation of ice and water in a polar ocean. *Journal of Geophysical Research*, 70(14), 1965.

[9] M.D. Coon. A review of AIDJEX modeling. In R. S. Prichard, editor, *Sea Ice Processes and Models*, pages 12–27, 1980.

References

[10] G. M. Flato. A particle-in-cell sea-ice model. *Atmosphere-Ocean*, 31(3):339–358, 1993.

[11] K. Garikipati. *On Strong Discontinuities in Inelastic Solids and their Numerical Simulation*. Doctoral dissertation, Stanford University, 1996.

[12] C. A. Geiger, W. D. Hibler, and S. F. Ackley. Large-scale sea ice drift and deformation: Comparison between models and observations in the western weddel sea during 1992. *Journal of Geophysical Research*, 103:21893–21913, 1998.

[13] Golub and Van Loan. *Matrix Computations*. The Johns Hopkins University Press, London, 1996.

[14] J. M. N. T. Gray and P. D. Killworth. Stability of the viscous-plastic sea ice rheology. *Journal of Physical Oceanography*, 25:971–978, 1995.

[15] J. M. N. T. Gray and L. W. Morland. A two-dimensional model for the dynamics of sea ice. *Philosophical Transactions: Physical Sciences and Engineering*, 347(1682):219–290, 1994.

[16] W. D. Hibler. A viscous sea ice law as a stochastic average of plasticity. *Journal of Geophysical Research*, 82(27):3932–3938, 1977.

[17] W. D. Hibler. A dynamic thermodynamic sea ice model. *Journal of Physical Oceanography*, 9:815–845, 1979.

[18] W. D. Hibler. Modeling a variable thickness sea ice cover. *Monthly Weather Review*, 108:1943–1973, 1980.

[19] E. C. Hunke and J. K. Dukowicz. An elastic-viscous-plastic model for sea ice dynamics. *Journal of Physical Oceanography*, 27:1849–1867, 1997.

[20] J. K. Hunter and B. Nachtergaele. *Applied Analysis*. World Scientific, 2001.

[21] C. F. Ip, W. D. Hibler, and G. M Flato. On the effect of rheology on seasonal sea-ice simulations. *Annals of Glaciology*, 15:17–25, 1991.

[22] I. Kubat, M. Sayed, S. Savage, and T. Carrieres. Flow of ice through converging channels. In J. Chung, S. W. Hong, P. W. Marshall, T. Komai, and W. Koterayama, editors, *The Proceedings of the Sixteenth International Offshore and Polar Engineering Conference*, pages 577–583, 2006.

[23] R. Kwok and G. F. Cunningham. Radarsat geophysical processor system data user's handbook. *JPL Report*, JPL D-19149, 2000.

References

[24] R. Kwok, J.C. Curlander, R. McConnell, and S.S. Pang. An ice-motion tracking system at the Alaska SAR facility. *IEEE Journal of Oceanic Engineering*, 15:44–54, 1990.

[25] R. Kwok, D. A. Rothrock, H. L. Stern, and G.F. Cunningham. Determination of ice age using lagrangian observations of ice motion. *IEEE Trans. Geosci. Remote Sens.*, 33(2):392–400, 1995.

[26] W. Lipscomb. *Modeling the Thickness Distibution of Arctic Sea Ice*. Doctoral dissertation, University of Washington, 1998.

[27] W. H. Lipscomb. Remapping the thickness distribution in sea ice models. *Journal of Geophysical Research*, 106:13989–14,000, 2001.

[28] W. H. Lipscomb, E. C. Hunke, W. Maslowski, and J. Jakacki. Ridging, strength, and stability in high-resolution sea ice models. *Journal of Geophysical Research*, 112:doi:10.1029/2005JC003355, 2007.

[29] L. Malvern. *Introduction to the Mechanics of a Continuous Medium*, volume Series in Engineering of the Physical Sciences. Prentice-Hall, Englewood Cliffs, N.J., 1969.

[30] G. A. Maykut and N. Untersteiner. Some results from a time-dependent thermodynamic model of sea ice. *Journal of Geophysical Research*, 76(6):1550–1575, 1971.

[31] L. W. Morland and R. Staroszczyk. A material coordinate treatment of the seaice dynamics. *Proceedings of the Royal Society of London A*, 454:2819–2857, 1998.

[32] F. Nansen. *Farthest North*. New York, 1897.

[33] J. Oliver, A.E. Huespe, M.D.G Pulido, and E. Samaniego. On the strong discontinuity approach in finite deformation settings. *International Journal for Numerical Methods in Engineering*, 56:1051–1082, 2003.

[34] J. Pedlosky. *Geophysical Fluid Dynamics*. Springer, New York, 1987.

[35] D. A. Rothrock. The energetics of the plastic deformation of pack ice by ridging. *Journal of Geophysical Research*, 80:4514–4519, 1975.

[36] S. B. Savage. Two component sea-ice thickness redistribution model. *Cold regions science and technology*, 51:20–37, 2008.

References

[37] H. Schreyer, L. Monday, D. Sulsky, M. Coon, and R. Kwok. Elastic-decohesive constitutive model for sea ice. *Journal of Geophysical Research*, 111:C11S26,doi:10.1029/2005JC003334, 2006.

[38] H. Schreyer, D. Sulsky, and S. Zhou. Modeling delamination as a strong discontinuity with the material-point method. *Comput. Methods Appl. Mech. Eng.*, 191:2483–2508, 2002.

[39] R. M. S. M Schulkes, L. W. Morland, and R. Staroszczyk. A finite element treatment of sea ice dynamics for different ice rheologies. *International Journal for Numerical and Analytical Methods in Geomechanics*, 22:153–174, 1998.

[40] E. M. Schulson. Compressive shear faults within arctic sea ice: Fracture on scales large and small. *Journal of Geophysical Research-Oceans*, 109, 2004.

[41] A. J. Semtner. A model for the thermodynamic growth of sea ice in numerical investigations of climate. *Journal of Physical Oceanography*, 6:379–389, 1976.

[42] J. C. Simo and T. J. R. Hughes. *Computational Inelasticity*. Springer, 1998.

[43] J. C. Simo, J. Oliver, and F. Armero. An analysis of strong discontinuities induced by strain-softening in rate-independent inelastic solids. *Computational Mechanics*, 12:277–296, 1993.

[44] I. Stakgold. *Green's Functions and Boundary Value Problems*. John Wiley and Sons, Inc., 1979.

[45] D. Sulsky, Z. Chen, and H. Schreyer. A particle method for history-dependent materials. *Computer Methods in Applied Mechanics and Engineering*, 118:179–196, 1994.

[46] D. Sulsky, K. Peterson, H. Schreyer, R. Kwok, and M. Coon. On the evaluation of ice models. In J.P. Dempsey, editor, *POAC 05 Conference Proceedings*, volume 2, pages 765–774, 2005.

[47] D. Sulsky, H. Schreyer, K. Peterson, M. Coon, and R. Kwok. Using the material-point method to model sea ice dynamics. *Journal of Geophysical Research*, 112:C02S90,doi:10.1029/2005JC003329, 2007.

[48] D. Sulsky, S. Zhou, and H. Schreyer. Application of a particle-in-cell method to solid mechanics. *Computer Physics Communications*, 87:236–252, 1995.

[49] H. U. Sverdrup. Physical oceanography of the north polar sea. *Arctic*, 3(3):178–186, 1950.

References

[50] A. S. Thorndike and G. A. Maykut. On the thickness distribution of sea ice. *AIDJEX Bulletin*, 21:31–48, 1973.

[51] A.S. Thorndike, D.A. Rothrock, G.A. Maykut, and R. Colony. The thickness distribution of seaice. *Journal of Geophysical Research*, 80(33):4501–4513, November 1975.

[52] N. Untersteiner. On the mass and heat budget of arctic sea ice. *Arch. Meteorol. Geophys, Bioklimatol. A.*, 12:151–182, 1961.

[53] N. Untersteiner, A. S. Thorndike, D. A. Rothrock, and K. L. Hunkins. AIDJEX revisited: A look back at the U.S.-Canadian arctic ice dynamics joint experiment 1970-78. *Arctic*, 60(3):327–336, 2007.

[54] M. Winton. A reformulated three-layer sea ice model. *Journal of Atmospheric and Ocean Technology*, 17:525–531, 2000.

[55] Q. Yang, L. Stainier, and M. Ortiz. A variational formulation of the coupled thermo-mechanical boundary-value problem for general dissipative solids. *Journal of the Mechanics and Physics of Solids*, 54:401–424, 2006.

[56] J. Zhang and D. Rothrock. A thickness and enthalpy distribution sea-ice model. *Journal of Physical Oceanography*, 31:2986–3001, 2001.